



Science Arts & Métiers (SAM)

is an open access repository that collects the work of Arts et Métiers Institute of Technology researchers and makes it freely available over the web where possible.

This is an author-deposited version published in: <https://sam.ensam.eu>
Handle ID: <http://hdl.handle.net/10985/8420>

To cite this version :

Maurine MONTAGNAT, Olivier CASTELNAU, P.D BONS, S.H FARIA, O GAGLIARDINI, F GILLET-CHAULET, Fanny GRENNERAT, A GRIERA, R.A. LEBENSOHN, Hervé MOULINEC, J. ROESSIGER, Pierre SUQUET - Multiscale modeling of ice deformation behavior - Journal of Structural Geology - Vol. 61, p.78–108 - 2013

Any correspondence concerning this service should be sent to the repository

Administrator : scienceouverte@ensam.eu



Multiscale modeling of ice deformation behavior

M. Montagnat^{a,*}, O. Castelnau^b, P.D. Bons^c, S.H. Faria^{d,e}, O. Gagliardini^{a,i},
F. Gillet-Chaulet^a, F. Grennerat^a, A. Griera^f, R.A. Lebensohn^g, H. Moulinec^h, J. Roessiger^c,
P. Suquet^h

^aLaboratoire de Glaciologie et Géophysique de l'Environnement, CNRS, UJF – Grenoble I, 38402 Saint-Martin d'Hères, France

^bProcédés et Ingénierie en Mécanique et Matériaux, CNRS, Arts & Métiers ParisTech, 151 Bd de l'hôpital, 75013 Paris, France

^cDepartment of Geosciences, Eberhard Karls University Tübingen, Wilhelmstr. 56, 72074 Tübingen, Germany

^dBasque Centre for Climate Change (BC3), Alameda Urquijo 4, 48008 Bilbao, Spain

^eIKERBASQUE, Basque Foundation for Science, Alameda Urquijo 36, 48011 Bilbao, Spain

^fDepartament de Geologia, Universitat Autònoma de Barcelona, 08193 Bellaterra (Cerdanyola del V.), Spain

^gLos Alamos National Laboratory, MS G755, Los Alamos, NM 87545, USA

^hLaboratoire de Mécanique et d'Acoustique, CNRS, UPR 7051, 13402 Marseille cedex 20, France

ⁱInstitut Universitaire de France (IUF), Paris, France

A B S T R A C T

Understanding the flow of ice in glaciers and polar ice sheets is of increasing relevance in a time of potentially significant climate change. The flow of ice has hitherto received relatively little attention from the structural geological community. This paper aims to provide an overview of methods and results of ice deformation modeling from the single crystal to the polycrystal scale, and beyond to the scale of polar ice sheets. All through these scales, various models have been developed to understand, describe and predict the processes that operate during deformation of ice, with the aim to correctly represent ice rheology and self-induced anisotropy. Most of the modeling tools presented in this paper originate from the material science community, and are currently used and further developed for other materials and environments. We will show that this community has deeply integrated ice as a very useful “model” material to develop and validate approaches in conditions of a highly anisotropic behavior. This review, by no means exhaustive, aims at providing an overview of methods at different scales and levels of complexity.

Keywords:

Ice mechanical behavior
Multiscale modeling
Viscoplastic anisotropy
Fabric development

1. Introduction

Ice is a common mineral on the Earth's surface, where it occurs as ice Ih. As ice is relatively close to its melting temperature, glaciers and polar ice sheets deform by ductile dislocation creep at strain rates in the order of 10^{-12} to 10^{-6} s⁻¹. Research on the flow of ice is of direct importance to society as it is needed to understand and predict the effects that global warming could have on sea level rise, glacier retreat, etc. There is also an increasing awareness that ice is a valuable analogue for other minerals and crystalline materials, as it is the only common mineral where this creep can be readily observed in nature and in the laboratory. Numerical modeling has become a key method to link the mechanics of ice from the dislocation scale to that of flowing ice masses.

Most of the efforts made to simulate the ductile mechanical behavior of polycrystalline ice are related to the modeling of ice flow and fabric evolution in the conditions of polar ice sheets or glaciers. Ice is increasingly considered as a model material to validate micro-macro mechanical approaches for materials with a high viscoplastic anisotropy. Most of the modeling techniques presented in this paper are currently used or further developed for other materials. For geological applications, one main limitation could be related to the “one phase” approach for most of these techniques, well adapted to ice. The reader will find, at the end of the paper, a table summarizing the main aspects of each techniques, with application ranges and limitations.

1.1. Mechanical properties of ductile ice

Ice Ih has a hexagonal crystal structure with a c/a ratio of 1.628. This c/a ratio is very close to the 1.633 value for a closely packed structure, but ice is not closely packed (see Schulson and Duval

* Corresponding author.

E-mail address: montagnat@lgge.obs.ujf-grenoble.fr (M. Montagnat).

URL: <http://lgge.osug.fr/montagnat-rentier-maurine>

(2009) for a recent review). The elastic anisotropy of ice single crystals is small. The Young modulus E only varies by about 30%, depending on the direction of the loading axis with respect to the c -axis. The highest value is along the c -axis with $E = 11.8$ GPa at -16 °C (Gammon et al., 1983).

Single crystals deform plastically essentially by glide of dislocations on the basal plane. There are three equivalent $\langle 1\bar{2}10 \rangle$ directions for the Burgers vector, but slip on the basal plane is almost isotropic. In conditions where basal slip is favored, the stress-strain rate relationship after a strain of about 5% can be expressed by a power law with a stress exponent $n = 2 \pm 0.3$ (Higashi et al., 1965; Jones and Glen, 1969; Mellor and Testa, 1969). At similar strain rates, the equivalent stress requested for non-basal slip is about 60 times larger than for basal slip (Duval et al., 1983).

For ice polycrystals deformed under the laboratory conditions (strain rate between 10^{-8} s $^{-1}$ and 10^{-6} s $^{-1}$ and temperature generally higher than -30 °C), strain is essentially due to intracrystalline dislocation glide. The transient creep regime is characterized by a strong directional hardening until the strain-rate minimum is reached for an overall strain of 1% (Duval et al., 1983). This strain-rate decrease can reach three orders of magnitude. It is associated to the development of a strong internal stress field due to plastic incompatibility between grains (Ashby and Duval, 1985; Duval et al., 1983; Castelnau et al., 2008b). A significant part of the transient creep is recoverable, *i.e.*, on unloading a creep specimen, a reverse creep is observed, with reverse strain which can be more than ten times the initial elastic strain (Duval, 1976; Duval et al., 1983). In the secondary creep regime, isotropic polycrystals deform (at similar stress levels) a 100 times slower than a single crystal optimally oriented for basal slip. In this regime, the minimum strain rate and the stress are linked by a power law, referred to as Glen's law in glaciology (Glen, 1955), expressed through a relationship of the form (1) for temperatures lower than -10 °C.

$$\dot{\epsilon}_{\min} = A\bar{\sigma}^n \exp(-E_p/k_B T) \quad (1)$$

with $\bar{\sigma}$ the applied stress, $E_p = 0.72$ eV and the stress exponent $n = 3$ (Barnes et al., 1971; Budd and Jacka, 1989). A is a constant, k_B the Boltzmann constant and T the temperature. Above -10 °C, $\dot{\epsilon}_{\min}$ rises more rapidly with increasing temperature and cannot be described by this equation (Morgan, 1991). No grain-size effect is expected for power-law secondary creep at laboratory conditions (see (Duval and Le Gac, 1980; Jacka, 1994) for instance). But a grain size effect was, however, measured during transient creep (Duval and Le Gac, 1980).

At strains larger than 1–2% (tertiary creep regime), dynamic recrystallization is predominant, and new grain microstructures and crystal orientations are generated (Jacka and Maccagnan, 1984; Duval et al., 2000).

At stresses lower than 0.1 MPa, relevant to deformation conditions in glaciers, ice sheets or planetary bodies, there is a clear indication of a creep regime with a stress exponent lower than two. This indication results from both the analysis of field data and laboratory tests, although the difficulty of obtaining reliable data at strain rates lower than 10^{-10} s $^{-1}$ is at the origin of contradictory results (Mellor and Testa, 1969; Barnes et al., 1971; Dahl-Jensen and Gundestrup, 1987; Pimienta et al., 1987; Lipenkov et al., 1997; Goldsby and Kohlstedt, 1997). In particular, Goldsby and Kohlstedt (1997) suggest a grain-size dependence of the ice viscosity associated with this low stress regime, based on laboratory experiments performed on very small grain-size samples. This grain-size effect would be associated with a grain boundary-sliding dominated creep. Its extrapolation to polar ice-core deformation conditions remains controversial (Duval and Montagnat, 2002). Diffusional creep, commonly associated with such conditions in many

materials yields a viscosity much higher than that deduced from field data (Lliboutry and Duval, 1985). For a review on ice behavior, see (Duval et al., 2010).

Ice as a model material exhibits a challenging viscoplastic anisotropy owing to the presence of only two independent easy slip systems for the dislocations (basal plane). While five independent systems are required to accommodate an arbitrary deformation in a single crystal (Taylor, 1938), Hutchinson (1977) showed that four systems are required for allowing a hexagonal polycrystal such as ice to deform. Being able to represent and to take into account this anisotropy in micro-macro models which aim at linking the single crystal scale to the polycrystal scale, is of primary interest to the material science community. This anisotropy needs to be accounted for at the dislocation scale in order to build physically-based model for the activation of (poorly known) secondary slip systems. The impact of dislocation induced internal stress fields, but also the characterization and development of highly heterogeneous strain and stress fields within polycrystals, and their impact on fabric development turn out to be of strong importance (Castelnau et al., 1996a; de la Chapelle et al., 1998).

During gravity-driven flow of glaciers and ice sheets, the macroscopic behavior of ice becomes progressively anisotropic with the development of fabrics (or textures, c -axis preferred orientations). This anisotropy and its development depends on the flow conditions, but strongly influences the response of ice layers to imposed stress (see Gundestrup and Hansen (1984); Van der Veen and Whillans (1990); Mangeney et al. (1997) for pioneer field work and modeling on the subject). Indeed, a polycrystal of ice with most of its c -axes oriented in the same direction deforms at least ten times faster than an isotropic polycrystal, when sheared parallel to the basal planes.

Fabrics basically develop as the result of lattice rotation by intracrystalline slip (Azuma and Higashi, 1985; Alley, 1988, 1992). Dynamic recrystallization can have a major impact on fabric development, especially at temperatures above -10 °C close to bedrocks or within temperate glaciers (Alley, 1992; Duval and Castelnau, 1995; de la Chapelle et al., 1998; Montagnat et al., 2009), see Section 5. Questions, however, remain to what extent different recrystallization processes operate as a function of depth in polar ice sheets (Kipfstuhl et al., 2006, 2009; Weikusat et al., 2009).

1.2. Main objectives

Accurate modeling of ice flow under natural conditions is relevant for many scientific objectives, such as the response of ice sheet to climate changes (Seddik et al., 2012), the interpretation of climate signals extracted from ice cores (Faria et al., 2010), the energy balance in extraterrestrial satellites (Sotin et al., 2009), and since a few years, the accurate prediction of sea-level rise that is linked to the behavior of fast-moving coastal glaciers (Gillet and Durand, 2010). In this context, challenges are mainly (i) to establish an ice flow law adapted to low stress conditions, changes in temperatures and impurity content, (ii) to consider the macroscopic anisotropy due to fabric development at the given conditions, (iii) to be able to integrate processes such as dynamic recrystallization that can strongly influence fabric development and the flow law.

The aim of this paper is to present a general overview of the main modeling techniques adapted to ice, and the main modeling results obtained from the single crystal scale to the large scale that is relevant to ice sheet flow modeling. Techniques are highly diverse, from dislocation dynamics (micron scale) to Finite Element methods that are adapted to the whole ice sheet (km scale), via mean-field and full-field micro-macro approaches and coupling with a microstructure evolution models (cm to m scale, limited to a

2D configuration, see 5.2). We will mostly focus on recent advances and topics that are still under development.

2. Modeling ice single crystal behavior

Owing to its high viscoplastic anisotropy, with dislocations gliding mostly on the basal plane, studying and modeling ice single crystal behavior is a challenge for regular approaches.

Recent efforts focused on three main objectives; (i) understanding, representing and taking into account the dislocation dynamics, (ii) improving our knowledge about secondary slip systems in ice, (iii) providing an accurate crystal plasticity constitutive law that can be implemented in mean-field and full-field approaches for micro-macro polycrystal models. For the two first objectives, Dislocation Dynamic models (DD) were used at the scale of the interaction between dislocation populations (Section 2.1). At a larger scale, the Field Dislocation Mechanic modeling approach (FDM) was applied to ice to evaluate the role of internal stresses associated with dislocation fields and arrangements (Section 2.2). Section 2.3 presents a crystal-plasticity model adapted to the transient creep behavior of ice single crystals.

2.1. Dislocation dynamics modeling

Dislocation dynamics in ice was shown to be scale free and intermittent, thanks to dislocation avalanche measurements via acoustic emissions (Weiss and Grasso, 1997; Weiss et al., 2001; Weiss and Marsan, 2003; Weiss and Montagnat, 2007). Ice was used as a model material for the following reasons: (i) transparency allows direct verification that acoustic emission activity is not related to microcracking, (ii) with the range of stress and temperature considered, diffusion creep is not a significant mechanism, and deformation occurs by dislocation glide only. DD modeling tools were used to better understand and characterize this scale free and intermittent behavior (see for example Miguel et al. (2001); Weiss and Miguel (2004)).

Miguel et al. (2001) made use of a discrete dislocation dynamics model with a two-dimensional cross-section of the crystal. This 2D space is randomly filled with edge dislocations gliding along a single slip direction parallel to their respective Burgers vector. This simplification is an effective way to describe materials like ice crystals owing to their strong plastic anisotropy with a single slip system dominating. A basic feature common to most DD models is that dislocations interact with each other through the long-range elastic stress field they produce in the host material. In (Miguel et al., 2001), dislocation velocity depends linearly on this effective stress, and the Peierls stress is set to zero. Mechanisms for dislocation annihilation and multiplication are classically taken into account.

Within this simplified scheme the authors found that dislocations generate a slowly evolving configuration landscape which coexists with rapid collective rearrangements. These arrangements involve a comparatively small fraction of dislocations and lead to an intermittent behavior of the net plastic response. The model was therefore able to reproduce the fact that dislocations themselves, through the various structures such as dipoles and walls, generate a pinning force landscape that is virtually frozen into a slow state. Creation and annihilation mechanisms allow the system to jump between slow dynamics states through bursts of activity.

More recently, Chevy et al. (2007, 2012) used DD simulations to analyze torsion tests performed on ice single crystals. The tests were performed with the ice-crystal *c*-axis oriented parallel to the torsion axis so that basal screw dislocations were mainly activated. With synchrotron topography analyses of the deformed samples, it was possible to show that dislocation arrangements were highly

heterogeneous, with a scale-invariant character and long-range correlations (Montagnat et al., 2006; Weiss and Montagnat, 2007; Chevy et al., 2010). Although these tests were performed in a way that highly favored basal glide, the double-cross slip mechanisms was invoked to explain this scale invariant dislocation arrangement.

Three-dimensional DD simulations, based on the TRIDIS code (Verdier et al., 1998), were adapted to these torsion tests on ice and the hexagonal structure. Screw dislocation sources were positioned within one slip plane at the periphery of a cylinder submitted to a constant torque. Cross-slip on prismatic planes was made possible thanks to the internal stress induced by the pile-up of basal dislocations in the center of the cylinder (where $\sigma_{app} = 0$), which produces the out-of-plane component needed (see Fig. 1). Simulation results allowed to test this hypothesis, and explain the power law relationship between stress and strain rate (Chevy et al., 2012).

2.2. Field dislocation mechanics (FDM)

Field dislocation theory is a mesoscale approach, which aims at taking into account the inhomogeneous distribution of dislocations in plasticity modeling. Therefore, FDM modeling makes it possible to represent and consider the internal stress field created by the dislocation arrangements within the crystal. FDM is a continuous approach able to deal simultaneously with long-range correlations associated with distortion fields, internal stresses due to dislocation arrangements, and short-range correlations (Acharya, 2001). The reader is referred to (Acharya and Roy, 2006; Varadhan et al., 2006; Fressengeas, 2010) for details.

The first application to ice samples was performed in the configuration of the torsion test presented in part 2.1 (Taupin et al., 2007). This test is by itself highly heterogeneous, and this heterogeneity was shown to induce unexpected non-basal slip. Taking into account the coupled dynamics of geometrically necessary screw dislocations gliding in the basal plane (also called “excess” dislocations) and statistical dislocations developed through cross slip in prismatic planes, the model was able to reproduce the creep curves during torsion, and the size effect measured experimentally (see Fig. 2). More recently, the model was used to reproduce the complex scale-invariant character of dislocation arrangements forming during torsion tests on ice single crystals (Chevy et al., 2010). In particular, the fact that the model takes into account both the long-range elastic interactions due to the presence of

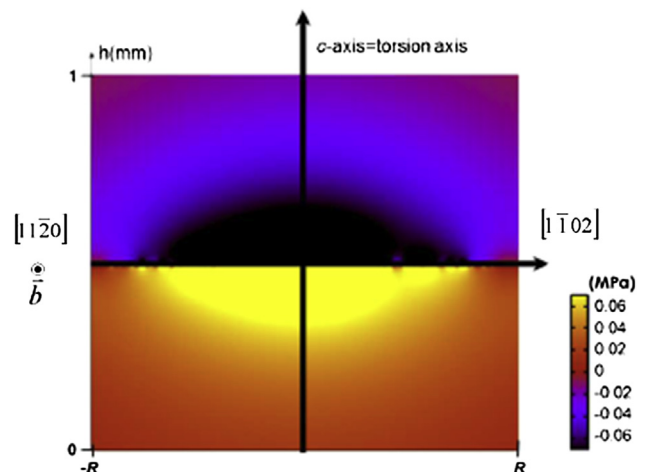


Fig. 1. Map of the resolved shear stress in the prismatic system for a torsion boundary made of basal screw dislocations. The cylinder diameter is 1 mm, and the maximum applied stress is 0.1 MPa. From Chevy et al. (2012).

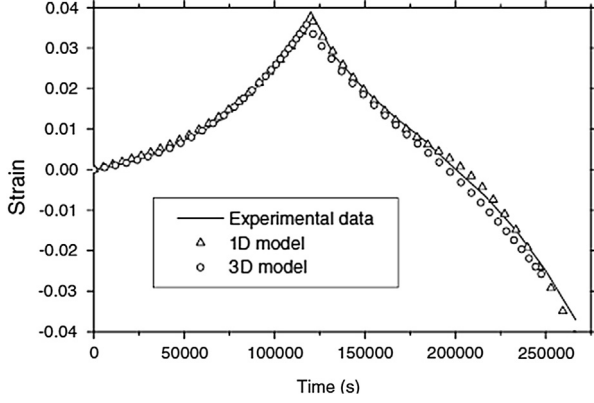


Fig. 2. Creep curves in forward and reverse torsion from experiments on single crystals, obtained by 1D and 3D FDM models. From Taupin et al. (2007).

dislocations and the short-range interactions inherent to the transport of dislocations (obstacles, cross-slip, etc.) allowed to reproduce the shift in control of the dislocation distribution by long-range correlations at low strain to a control by short-range correlations at strain as high as 50%. It was shown that non-basal dislocations activated by the internal stress fields induce a screening potential at large strain, through obstacles such as twist sub-boundaries. However, this screening was shown to be too small to hinder creep acceleration prevailing during torsion creep test on ice single crystals (Chevy et al., 2010).

2.3. Crystal plasticity modeling

Constitutive relations to describe the transient creep of ice single crystals have been proposed by Castelnau et al. (2008b) and then used in a modified version in Suquet et al. (2011). One of the difficulty here is the description of the softening of basal slip in the transient regime, as discussed above. As is usual in crystal plasticity at infinitesimal strains, the strain tensor is decomposed into the sum of an elastic ϵ^e and a viscoplastic ϵ^{vp} part

$$\epsilon = \epsilon^e + \epsilon^{vp}. \quad (2)$$

The elastic strain is related to the local stress tensor σ with the local compliance tensor S , and the viscoplastic strain results from slips on a total of M different slip systems:

$$\epsilon^e = S : \sigma, \quad \epsilon^{vp} = \sum_{k=1}^M \gamma^{(k)} \mu^{(k)}. \quad (3)$$

Here, $\mu^{(k)} = \frac{1}{2}(n^{(k)} \otimes b^{(k)} + b^{(k)} \otimes n^{(k)})$ is the (purely geometric) Schmid tensor depending on the orientation of the slip system (k), \mathbf{n} being the slip plane normal and \mathbf{b} the slip direction (parallel to the Burgers vector and orthogonal to \mathbf{n}) in that plane, with \otimes the dyadic product.

Ice crystals, which have a hexagonal symmetry, deform easily by shear on the basal plane, on the three systems $\{0001\}\langle 11\bar{2}0 \rangle$ which provide only two independent systems. The three prismatic systems $\{1\bar{1}00\}\langle 11\bar{2}0 \rangle$ provide two more independent systems. An additional independent slip system is thus required to attain any isochoric deformation at the single crystal level and this is achieved by adding the six $\langle c+a \rangle$ pyramidal systems $\{11\bar{2}2\}\langle 11\bar{2}3 \rangle$. In total, $M = 12$ slip systems are taken into account in the present analysis.

In the constitutive relations originally proposed by Castelnau et al. (2008b), the slip rate on the k -th system is related to the resolved shear stress $\tau^{(k)}$ on that system through:

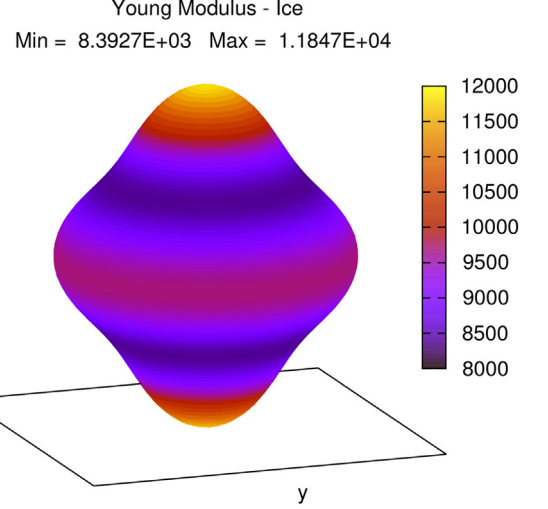


Fig. 3. Young's modulus in [MPa] of an ice single crystal with its c-axis aligned with z, at -16°C .

$$\dot{\gamma}^{(k)} = \dot{\gamma}_0^{(k)} \left(\frac{|\tau^{(k)}|}{\tau_0^{(k)}} \right)^{n^{(k)}} \text{sgn}(\tau^{(k)}), \quad \tau^{(k)} = \sigma : \mu^{(k)}, \quad (4)$$

where $\tau_0^{(k)}$, the reference resolved shear stress on system k , depends on the activity of the other systems through:

$$\dot{\tau}_0^{(k)} = \sum_{\ell=1}^M H^{(k,\ell)} \frac{\tau_{sta}^{(\ell)} - \tau_0^{(\ell)}}{\tau_{sta}^{(\ell)} - \tau_{ini}^{(\ell)}} |\dot{\gamma}^{(\ell)}|. \quad (5)$$

The two material parameters $\tau_{ini}^{(k)}$ and $\tau_{sta}^{(k)}$ refer, respectively, to the initial value of $\tau_0^{(k)}$ at the onset of plasticity (when the $\gamma^{(k)}$'s are small) and to the stationary value of $\tau_0^{(k)}$ at saturation when the plasticity is fully developed (i.e. when the $\gamma^{(k)}$'s are large). Therefore the contribution of system ℓ in the hardening (or softening) of system k vanishes when $\tau_0^{(\ell)}$ is close to $\tau_{sta}^{(\ell)}$. The hardening matrix $H^{(k,\ell)}$ expresses the influence of the plastic activity of system ℓ on the hardening of system k and is taken to be symmetric. Material data for this model are given in Castelnau et al. (2008b).

In (Suquet et al., 2011), Eqs (4) and (5) are improved in two ways:

1. Kinematic hardening is introduced in (4) through a back stress $X^{(k)}$:

$$\dot{\gamma}^{(k)} = \dot{\gamma}_0^{(k)} \left(\frac{|\tau^{(k)} - X^{(k)}|}{\tau_0^{(k)}} \right)^{n^{(k)}} \text{sgn}(\tau^{(k)} - X^{(k)}), \quad (6)$$

where the back stress evolves with the plastic activity according to an Armstrong-Frederick type law (Chaboche, 2008):

$$\dot{X}^{(k)} = c^{(k)} \dot{\gamma}^{(k)} - d^{(k)} X^{(k)} |\dot{\gamma}^{(k)}| - e^{(k)} X^{(k)}, \quad (7)$$

including static recovery through coefficient $e^{(k)}$. The introduction of a back stress on each slip system is motivated by the experimental observation of recovery strain developing in single crystals when specimens are subjected to recovery tests (see Section 2.3.2 and Fig. 4).

2. The equation governing the reference resolved shear stress $\tau_0^{(k)}$ is modified into

$$\dot{\tau}_0^{(k)} = (\tau_{sta}^{(k)} - \tau_0^{(k)})\dot{p}^{(k)}, \quad \dot{p}^{(k)} = \sum_{\ell=1}^M H^{(k,\ell)} |\dot{\gamma}^{(\ell)}|. \quad (8)$$

The motivation for the change in the evolution rule for the reference resolved shear stresses $\tau_0^{(k)}$ is that with the original rule (5) they never reach their stationary value, unless all systems do so at the same time, a condition which cannot be met in a polycrystal (see details in (Suquet et al., 2011)). By contrast, the law (8) ensures convergence of $\tau_0^{(k)}$ toward its stationary value, provided all coefficients $H^{(k,\ell)}$ are positive. Indeed, in this case, $\dot{p}^{(k)}$ is always positive and $p^{(k)}$ is increasing with time, acting on system k in a similar way as the classical cumulated plastic strain of von Mises plasticity. The differential Eq. (8) can be integrated into

$$\tau_0^{(k)}(p^{(k)}) = \tau_{sta}^{(k)} + (\tau_{ini}^{(k)} - \tau_{sta}^{(k)}) \exp(-p^{(k)}), \quad (9)$$

which shows that $\tau_0^{(k)} - \tau_{sta}^{(k)}$ has the same sign as $\tau_{ini}^{(k)} - \tau_{sta}^{(k)}$. Furthermore $\tau_0^{(k)}$ tends to $\tau_{sta}^{(k)}$ when $p^{(k)}$ becomes large.

2.3.1. Data for elasticity

As mentioned in Section 1, ice crystals exhibit a low elastic anisotropy, the largest stiffness ($E \sim 11.8$ GPa) being along the c -axis (Fig. 3). The tensor of elastic moduli (in Kelvin's notations) at -16°C is given by (10) (Gammon et al., 1983),

$$\begin{pmatrix} \sigma_{11} \\ \sigma_{22} \\ \sigma_{33} \\ \sqrt{2}\sigma_{23} \\ \sqrt{2}\sigma_{13} \\ \sqrt{2}\sigma_{12} \end{pmatrix} = \begin{pmatrix} 13930. & 7082. & 5765. & 0. & 0. & 0. \\ 7082. & 13930. & 5765. & 0. & 0. & 0. \\ 5765. & 5765. & 15010. & 0. & 0. & 0. \\ 0. & 0. & 0. & 6028. & 0. & 0. \\ 0. & 0. & 0. & 0. & 6028. & 0. \\ 0. & 0. & 0. & 0. & 0. & 6848. \end{pmatrix} \times \begin{pmatrix} \epsilon_{11}^e \\ \epsilon_{22}^e \\ \epsilon_{33}^e \\ \sqrt{2}\epsilon_{23}^e \\ \sqrt{2}\epsilon_{13}^e \\ \sqrt{2}\epsilon_{12}^e \end{pmatrix}, \quad (10)$$

where all entries are in MPa and 3 is the axis of transverse isotropy (c -axis of the hexagonal crystalline structure). For conditions prevailing in ice sheets and glaciers, elastic constants vary little with

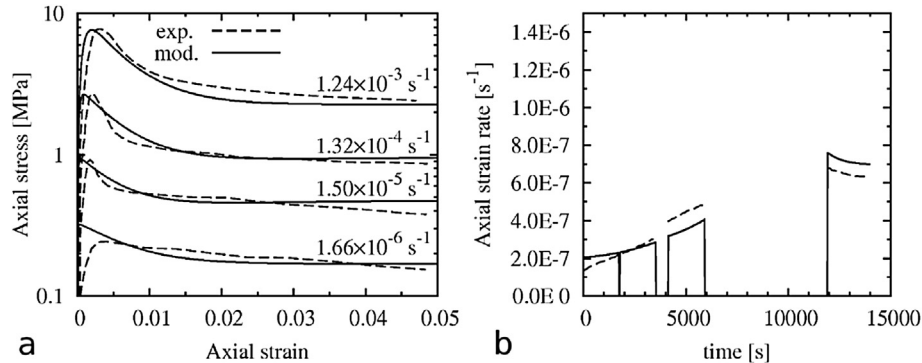


Fig. 4. Behavior of an ice single crystal deformed by basal slip. a) Predictions of the model, based on Eq. (6) and with parameters given in Table 1, in comparison with the experimental data of Weertman (1973). Axial strain rates are indicated. b) Prediction of the model in comparison with the results of the recovery tests of Taupin et al. (2008). Temperature is -10°C . From Suquet et al. (2011).

Table 1

Material parameters used in the full-field simulations for single crystals of ice at -10°C . Units are MPa and s^{-1} .

| | τ_{ini} | τ_{sta} | $\dot{\gamma}_0$ | n | c | d | e |
|-----------|--------------|--------------|------------------|------|-----|-----|--------|
| Basal | 0.1 | 0.022 | 10^{-6} | 2 | 9 | 60 | 0.0003 |
| Prismatic | 0.13 | 1.5 | 10^{-6} | 2.85 | 9 | 60 | 0.0003 |
| Pyramidal | 3.875 | 3.875 | 10^{-6} | 4 | 9 | 60 | 0.0003 |

| Hardening matrix: | | | |
|-------------------|-------|-----------|-----------|
| | Basal | Prismatic | Pyramidal |
| Basal | 70 | 125 | 0 |
| Prismatic | 125 | 110 | 0 |
| Pyramidal | 0 | 0 | 0 |

temperature: a temperature change of 5°C only modifies the elastic constants by about 1.5%.

2.3.2. Data for basal slip

The literature provides a number of experimental data for the behavior of ice crystals deformed in such a way that only basal slip is activated. Due to the very large viscoplastic anisotropy of ice single crystals, it is stressed that mechanical tests have to be carried out very carefully to avoid any heterogeneity of the stress field within the specimen (Boehler et al., 1987).

Mechanical tests on single crystals where solely non-basal systems are activated have not been reported so far. This would require straining the crystal along or perpendicular to the c -axis, but unfortunately any unavoidable deviation from perfect alignment activates basal slip. Duval et al. (1983) has given upper bounds for the flow stress on non-basal systems.

Consequently, only the material parameters of Eq. (6) relevant for basal slip can be identified with confidence from experimental data on single crystals:

- First, data compiled by Duval et al. (1983) were used to determine the stationary flow stress and the stress-sensitivity exponent $n^{(k)}$ of basal slip. There is quite a large spread in these experimental results from different authors. Despite these uncertainties, the stress-sensitivity exponent for basal slip can be directly identified from these experimental data (numerical values are reported in Table 1), whereas the stationary flow stress depends on both the stationary reference stress $\tau_{sta}^{(k)}$ and the stationary backstress $X^{(k)}$.
- Next, data from Weertman (1973) were used for the identification of the transient creep regime of basal systems. Single crystals were deformed under uniaxial compression at different strain rates, with c -axis oriented at 45° from the

loading direction (Fig. 4). The observed stress peak is associated with the increase in density of mobile dislocations (Duval et al., 1983), a behavior typical for material with very low initial dislocation density (see Sauter and Leclercq (2003); Cochard et al. (2010)). These tests shed light on the softening of basal slip in the transient regime. The static recovery term $e^{(k)}$ in the constitutive law (7) helps achieving the correct stationary stress at very small strain rates (since $X^{(k)}$ tends to a constant value $c^{(k)}/d^{(k)}$ at large shear $\gamma^{(k)}$ if static recovery is not introduced).

- Finally, the recovery test of Taupin et al. (2008) performed on single crystals under uniaxial compression was considered. Here the c -axis orientation was not precisely defined experimentally, but it made an angle “less than 10° ” with the compression direction. The single crystal was submitted to four creep loadings for 30 min separated by unloading stages for respectively 1 min, 10 min, and 100 min (Fig. 4). Upon reloading, the strain rate is larger than just before the last unloading, indicating that dislocations are rearranging during the time intervals where the specimen is unloaded. This is accounted for in the model by the back stress $X^{(k)}$, and by $e^{(k)}$.

Fig. 4 shows the good match between the model (constitutive Eq. (6)) with the set of parameters given in Table 1 and these experimental results.

3. Mean field approaches for the mechanical response of ice polycrystals

3.1. Microstructure characterization

From the mechanical point of view, polycrystalline materials have to be considered as a specific class of composites. They are composed of many grains, with grain size in the range of mm to cm for natural ice. Grains are assembled in a random way, *i.e.* their size, shape, and lattice orientation do generally not depend on the size, shape, and orientation of the surrounding grains (Fig. 5). Therefore, the microstructure of ice polycrystals can hardly be described exactly in 3-D, unless one makes use of tomography techniques (Rolland du Roscoat et al., 2011). From (2-D) thin sections, one can at best access a statistical characterization of the 3-D grain arrangement *e.g.* with the help of cross-correlation functions, although the description is generally limited to a few parameters, such as the average grain size and grain shape (aspect ratio). In the Euler orientation space, microstructure description is based on the distribution of crystal lattice orientations (Orientation Distribution Function, ODF, or crystallographic texture, often denoted “fabric” in the

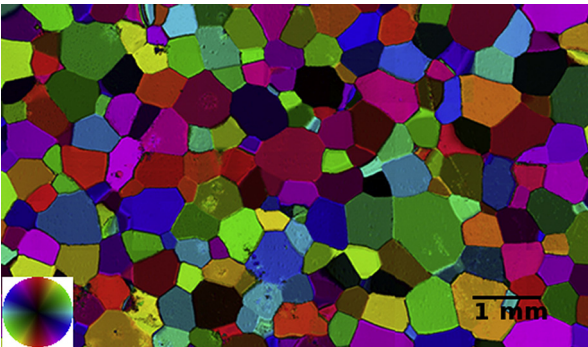


Fig. 5. Typical 2D microstructure of an ice polycrystal grown in the laboratory. The color wheel gives the color-code for the c -axis orientation.

geophysical community). The complex behavior of polycrystalline materials comes from the anisotropic behavior at the grain scale, closely related to the symmetry of the crystal lattice. This is true for all quantities of interest here, such as elasticity, viscoplasticity and thermal dilation. Grains with different lattice orientations react differently to a given stress level. As far as grain boundaries maintain the cohesion of the material, the *local* stress (*i.e.* inside a grain) differs from the *overall* one (the applied stress), leading to a heterogeneous distribution of stress and strain fields within the polycrystal.

Most research efforts in the past years have focussed on the understanding of the build-up of these heterogeneities, in relation with the microstructure and local (grain) behavior, since they greatly influence the overall behavior (for ice, see Grennerat et al. (2012) for instance). For instance, plasticity in a polycrystal can start far below the macroscopic yield stress, as it is sufficient that the local stress reaches the local yield stress somewhere in the structure where stress concentration is large enough, such as along grain boundaries (Brenner et al., 2009).

There are basically two strategies to get the mechanical response: mean-field (this section) and full-field (next section) approaches. For both of them, the key issue is the estimation of the stress or strain localization (or heterogeneities), in relation to the microstructure and local behavior of grains. Basically, the problem to be solved is to find an equilibrated stress field, related to a compatible strain field with the local constitutive relation, both fields fulfilling the applied boundary conditions. In the following, we review (not in an exhaustive way) some homogenization techniques used for the investigation of the mechanical behavior of ice polycrystals.

3.2. Linear thermo-elasticity

For reasons that will become evident below, let us consider the case of thermo-elastic ice polycrystals. The local constitutive relation at point (\mathbf{x}) reads

$$\boldsymbol{\epsilon}(\mathbf{x}) = \mathbf{S}(\mathbf{x}) : \boldsymbol{\sigma}(\mathbf{x}) + \boldsymbol{\epsilon}_0(\mathbf{x}), \quad (11)$$

with $\boldsymbol{\epsilon}_0$ a stress-free thermal strain (*e.g.* a dilation), due to temperature changes. The local stress $\boldsymbol{\sigma}(\mathbf{x})$ can be related to the overall stress (applied at the polycrystal scale) by means of the stress-concentration tensor $\mathbf{B}(\mathbf{x})$ for the purely elastic problem

$$\boldsymbol{\sigma}(\mathbf{x}) = \mathbf{B}(\mathbf{x}) : \bar{\boldsymbol{\sigma}} + \boldsymbol{\sigma}_{\text{res}}(\mathbf{x}), \quad (12)$$

with $\boldsymbol{\sigma}_{\text{res}}$ the residual stress, *i.e.* the stress field remaining locally when the overall load is suppressed ($\bar{\boldsymbol{\sigma}} = 0$). It can be shown that the overall polycrystal behavior takes a similar form as Eq. (11)

$$\bar{\boldsymbol{\epsilon}} = \tilde{\mathbf{S}} : \bar{\boldsymbol{\sigma}} + \bar{\boldsymbol{\epsilon}}_0, \quad (13)$$

with symbols $\tilde{\cdot}$ and $\bar{\cdot}$ denoting the homogenized (or effective) property and the volume average over the whole polycrystal volume (also denoted $\langle \cdot \rangle$), respectively. Therefore, one has $\bar{\boldsymbol{\sigma}} = \langle \boldsymbol{\sigma}(\mathbf{x}) \rangle$ and $\bar{\boldsymbol{\epsilon}} = \langle \boldsymbol{\epsilon}(\mathbf{x}) \rangle$, and it can be shown that the effective compliance $\tilde{\mathbf{S}}$ and the effective thermal strain $\bar{\boldsymbol{\epsilon}}_0$ are given by (Laws, 1973).

$$\tilde{\mathbf{S}} = \langle \mathbf{S}(\mathbf{x}) : \mathbf{B}(\mathbf{x}) \rangle, \quad \bar{\boldsymbol{\epsilon}}_0 = \langle \boldsymbol{\epsilon}_0(\mathbf{x}) : \mathbf{B}(\mathbf{x}) \rangle. \quad (14)$$

Since, for thermo-elastic polycrystals, the elastic compliance and the thermal dilation coefficients are uniform properties inside grains, the quantities $\mathbf{S}(\mathbf{x})$ and $\boldsymbol{\epsilon}_0(\mathbf{x})$ in Eq. (11) can be replaced by the corresponding homogeneous values $\mathbf{S}^{(r)}$ and $\boldsymbol{\epsilon}_0^{(r)}$ of the considered phase (r). A similar substitution can be made in Eq. (14), leading to

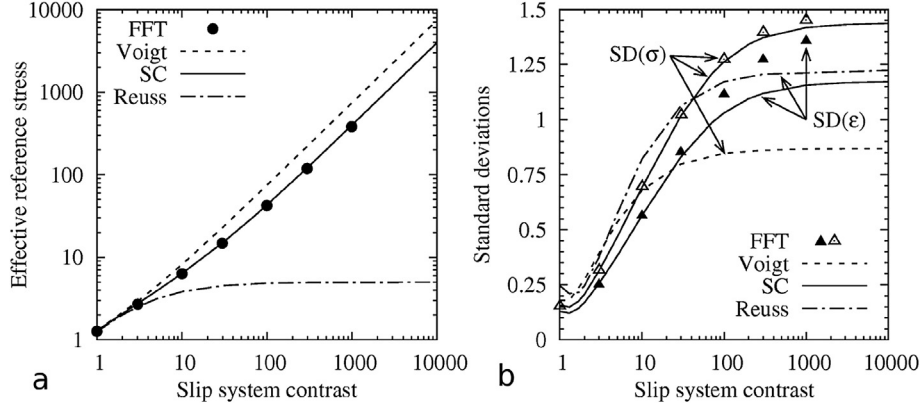


Fig. 6. Full-field vs. mean-field behavior for ice polycrystals with random fabric, for a linear viscous behavior ($n = 1$) and various viscoplastic anisotropy (or slip system contrasts) at the grains level. a) Effective flow stress $\bar{\sigma}_0$. b) Standard deviation of equivalent stress and strain rate, normalized by $\bar{\sigma}_{eq}$ and $\bar{\epsilon}_{eq}$, respectively, characterizing field heterogeneities at the polycrystal scale. Results from the linear SC scheme are compared to reference numerical solutions provided by the FFT approach. Reuss and Voigt bounds are also indicated. Note that, for these bounds, standard deviations of stress and strain rate, respectively, do vanish.

$$\bar{\mathbf{S}} = \sum_r c^{(r)} S^{(r)} : \bar{\mathbf{B}}^{(r)}, \quad \bar{\boldsymbol{\epsilon}}_0 = \sum_r c^{(r)} \boldsymbol{\epsilon}_0^{(r)} : \bar{\mathbf{B}}^{(r)} \quad (15)$$

with $\bar{\cdot}^{(r)}$ indicating the average over the volume of phase (r), e.g. $\bar{\mathbf{B}}^{(r)} = \langle \mathbf{B}(\mathbf{x}) \rangle^{(r)}$, and $c^{(r)}$ the volume fraction of phase (r). Here, a *mechanical phase* (r) denotes the set of all grains of the polycrystal having the same crystal orientation; those grains have different shape and environment but their elastic and thermal properties are identical. From (15), it can be observed that the sole knowledge of the mean (phase average) values $\bar{\mathbf{B}}^{(r)}$ is sufficient to estimate the overall polycrystal behavior. It can be anticipated that, if the quantities $\bar{\mathbf{B}}^{(r)}$ can be calculated without having to know the complete field of $\mathbf{B}(\mathbf{x})$, computation will be way faster. Hence the name of “mean-field” approaches presented here.

With the effective behavior (Eq. (14)) in hand, statistical averages over crystal orientations (r) can be estimated. Basically, two quantities can be obtained from mean-field approaches:

1. The phase average stress (or first moment) $\bar{\boldsymbol{\sigma}}^{(r)} = \langle \boldsymbol{\sigma}(\mathbf{x}) \rangle^{(r)}$

$$\bar{\boldsymbol{\sigma}}^{(r)} = \bar{\mathbf{B}}^{(r)} : \bar{\boldsymbol{\sigma}} + \bar{\boldsymbol{\sigma}}_{res}^{(r)}, \quad (16)$$

with $\bar{\boldsymbol{\sigma}}_{res}^{(r)}$ the average residual stress of phase (r). The knowledge of $\bar{\boldsymbol{\sigma}}^{(r)}$ for all phases (r) allows investigating the so-called *interphase* heterogeneities, i.e. the variation of the phase average stress with respect to the crystal orientation.

2. Deeper insight into the stress distribution can be obtained from the second moment $\langle \boldsymbol{\sigma} \otimes \boldsymbol{\sigma} \rangle^{(r)}$ of the stress. This second moment can be obtained by a derivation of the effective energy with respect to local compliances, see (Bobeth and Diener, 1987; Kreher, 1990; Ponte-Castañeda and Suquet, 1998; Brenner et al., 2004).

The standard deviation of the stress distribution within a given crystal orientation (r) can be estimated from these two moments as the square root of $\langle \boldsymbol{\sigma} \otimes \boldsymbol{\sigma} \rangle^{(r)} - \langle \boldsymbol{\sigma} \rangle^{(r)} \otimes \langle \boldsymbol{\sigma} \rangle^{(r)}$ (i.e. the mean of the square of the stress minus the square of the mean); it is related to the width of the stress distribution in crystal orientation (r), and accounts for both the heterogeneity of stress distribution *inside* grains but also for the heterogeneity *between* grains of identical orientation but exhibiting different shapes and having different neighborhood. Similar relations can be derived for the strain statistics.

3.3. Reuss and Voigt approximations

First, two very basic models can be derived, namely *Reuss* (also called *static* in the viscoplastic context) and *Voigt* (or *Taylor*) models. The Reuss model is constructed by considering a uniform stress throughout the polycrystal, i.e. $\boldsymbol{\sigma}(\mathbf{x}) = \bar{\boldsymbol{\sigma}} \forall \mathbf{x}$, or equivalently $\mathbf{B}(\mathbf{x}) = \mathbf{I}$ (with \mathbf{I} the identity tensor), and leads to vanishing intra- and inter-granular stress heterogeneities, and uniform strain within grains. The Voigt model considers uniform strain, i.e. $\boldsymbol{\epsilon}(\mathbf{x}) = \bar{\boldsymbol{\epsilon}} \forall \mathbf{x}$, i.e. no intra- and inter-granular strain heterogeneities, and uniform stress within grains. These models violate strain compatibility and stress equilibrium, respectively, and are of limited accuracy when the local behavior is highly nonlinear and/or highly anisotropic, as will be illustrated in the next section. Besides simplicity, the main interest of Reuss and Voigt models is based on their bounding character, since they provide, respectively, a lower and an upper bound for the effective stress potential.

3.4. The Self-Consistent (SC) scheme

Unlike full-field approaches detailed in the Section 4, mean-field methods are based on a statistical description of the microstructure, e.g. based on few n -points correlation functions, so that the exact position and shape of a specific grain with respect to its neighbors is not known. However, as already introduced, all grains exhibiting the same crystallographic orientation are treated as a single mechanical phase. Owing to the random character of the microstructure with all grains playing geometrically similar roles, the Self-Consistent (SC) scheme (Hershey, 1954; Kröner, 1958; Willis, 1981) is especially well suited for polycrystals. This model, which provides a relatively simple expression for $\bar{\mathbf{B}}^{(r)}$, relies on specific microstructures exhibiting perfect disorder and infinite size graduation (Kröner, 1978). The SC scheme has often been described as if the interaction between each grain and its surrounding could be approximated by the interaction between one ellipsoidal grain with the same lattice orientation as the original grain and a homogeneous equivalent medium whose behavior represents that of the polycrystal, taking thus advantage of the analytical solution of Eshelby (1957) for the inclusion/matrix interaction. This reasoning led to the conclusion that the SC scheme implicitly considers uniform stress and strain rate inside grains. This interpretation turns out to be incorrect, since intraphase stress and strain heterogeneities do not vanish as explained above, see (Ponte-Castañeda and Suquet, 1998) for a review.

The ability of the SC scheme to estimate polycrystal behavior is shown in Fig. 6. Numerical reference solutions from the full-field FFT method (see Section 4) have been generated for many randomly generated Voronoi microstructures, and ensemble average over these random microstructures has been calculated in order to attain results that are representative for a Representative Volume Element, *i.e.* a volume sufficiently large to be statistically representative of the material (Kanit et al., 2003; Lebensohn et al., 2004b). In Fig. 6, we provide results for the effective behavior, that is entirely defined by the effective reference stress $\bar{\sigma}_0$ which enters in the effective constitutive relation

$$\frac{\bar{\epsilon}_{\text{eq}}}{\dot{\epsilon}_0} = \frac{\bar{\sigma}'_{\text{eq}}}{\bar{\sigma}_0} \quad (17)$$

with $\dot{\epsilon}_0$ a reference strain rate (taken here equal to $\dot{\gamma}_0$), and $\bar{\sigma}'_{\text{eq}}$ and $\bar{\epsilon}_{\text{eq}}$ the effective equivalent stress and strain rate respectively ($\bar{\sigma}'_{\text{eq}} = \sqrt{3\bar{\sigma} : \bar{\sigma}/2}$, $\bar{\epsilon}_{\text{eq}} = \sqrt{2\bar{\epsilon} : \bar{\epsilon}/3}$). Calculations are performed for various viscoplastic anisotropy contrasts (or slip system contrasts) at the grain level, defined by the ratio between non-basal and basal reference shear stresses, *i.e.* $\tau_0^{(\text{Pr})}/\tau_0^{(\text{Ba})}$ for $\tau_0^{(\text{Pr})} = \tau_0^{(\text{Pr})}$. It can be observed that the SC model perfectly reproduces the reference full-field (FFT) results. Note also that the Reuss bound, often used for highly anisotropic materials like ice, predicts a much too soft overall behavior. This simple approach does not allow to make a realistic link between local and overall rheologies. We also report in this figure the standard deviations (or overall heterogeneities) of equivalent stress and strain rate. These standard deviations have been calculated over the whole polycrystal. Recall that they account for both intra- and inter-granular field heterogeneities for both SC and FFT approaches. It can be observed that the increase of standard deviation with the slip system contrast is well reproduced by the SC scheme, although some discrepancies with FFT results arise at very large contrasts (mostly for the strain-rate fluctuation). Note again that Reuss and Voigt bound do not reproduce these results, even in a qualitative way, since they predict, by construction, vanishing fluctuation of stress and strain rate, respectively. Unlike these simple approaches, the SC scheme not only predicts the correct effective stress, but also accurately captures the field heterogeneities within the polycrystal. Similar agreement have been obtained for Voronoi and EBSD 2-D microstructures under antiplane shear by Lebensohn et al. (2005).

3.5. Nonlinear viscoplasticity

The mean-field estimate of *nonlinear materials* is significantly more complex than the thermo-elastic case treated above. We consider the case of a viscoplastic polycrystal of ice in which grains are deforming by glide of dislocations on specific slip planes, as discussed above, with slip rates given by Eq. (4), so that the local strain rate reads, since elastic deformations are neglected:

$$\dot{\epsilon}(\mathbf{x}) = \sum_k \mu_{(k)}^{(r)} \dot{\gamma}_{(k)}(\mathbf{x}). \quad (18)$$

Here, reference stresses τ_0 and stress sensitivities n are supposed to be constant. The constitutive Eq. (18) can also be written

$$\dot{\epsilon}(\mathbf{x}) = M(\mathbf{x}) : \boldsymbol{\sigma}(\mathbf{x}) \quad (19)$$

with

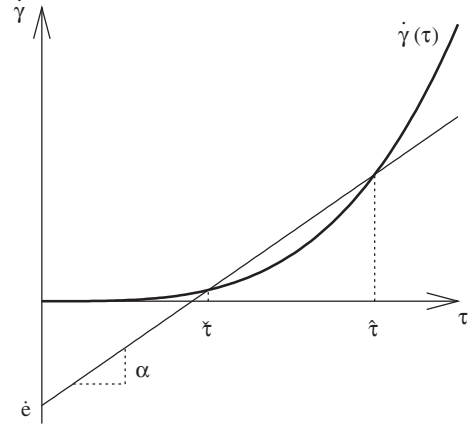


Fig. 7. Schematic representation of the linearization between the shear rate ($\dot{\gamma}$) and the stress (τ), to illustrate Eq. (21).

$$M(\mathbf{x}) = \sum_k \frac{\dot{\gamma}_0^{(k)}}{\tau_0^{(k)}} \left| \frac{\boldsymbol{\mu}^{(k)}(\mathbf{x}) : \boldsymbol{\sigma}(\mathbf{x})}{\tau_0^{(k)}} \right|^{n^{(k)}-1} \boldsymbol{\mu}^{(k)}(\mathbf{x}) \otimes \boldsymbol{\mu}^{(k)}(\mathbf{x}). \quad (20)$$

Obviously, the viscous compliance \mathbf{M} relating $\dot{\epsilon}(\mathbf{x})$ and $\boldsymbol{\sigma}(\mathbf{x})$ – which plays a similar role as \mathbf{S} in Eq. (11) – is not uniform within a phase, owing to the stress sensitivities $n \neq 1$ and the heterogeneity of $\boldsymbol{\sigma}$ in the phases. Consequently, (14) cannot be replaced by (15) for nonlinear behavior. The basic method to deal with such nonlinear behavior is to define a *Linear Comparison Polycrystal* (LCP) having the same microstructure as the real nonlinear polycrystal, and to which the linear homogenization scheme applies (Ponte-Castañeda and Suquet, 1998). Of course, the effective behavior estimated this way remains nonlinear, since the definition of the LCP depends on the applied macroscopic stress. The difficult part of the problem consists of finding the best *linearization* procedure leading to the optimal selection of the LCP. Since decades, there has been quite a number of propositions in the literature dealing with this issue, leading to a *generalization* of the SC scheme for nonlinear behavior. The local constitutive relation given by Eqs (18–20) has to be linearized in a suitable way to obtain a form similar to (11), with \mathbf{S} and $\dot{\epsilon}_0$ uniform per phase (and where ϵ is replaced everywhere by $\dot{\epsilon}$). Generally speaking, the linearization can be expressed in the form depicted in Fig. 7, (Liu and Ponte Castañeda, 2004).

$$\dot{\gamma}_{(k)}(\mathbf{x}) = \alpha_{(k)}^{(r)} \tau_{(k)}(\mathbf{x}) + \dot{\epsilon}_{(k)}^{(r)}, \quad (21)$$

thus leading to the following expressions for $\mathbf{S}^{(r)}$ and $\dot{\epsilon}_0^{(r)}$

$$\mathbf{S}^{(r)} = \sum_k \alpha_{(k)}^{(r)} \boldsymbol{\mu}_{(k)}^{(r)} \otimes \boldsymbol{\mu}_{(k)}^{(r)}, \quad \dot{\epsilon}_0^{(r)} = \sum_k \dot{\epsilon}_{(k)}^{(r)} \boldsymbol{\mu}_{(k)}^{(r)}, \quad (22)$$

where the shear compliance $\alpha_{(k)}^{(r)}$ and stress-free slip-rate $\dot{\epsilon}_{(k)}^{(r)}$ can be

easily expressed with respect to two reference shear stresses $\bar{\tau}_{(k)}^{(r)}$ and $\hat{\tau}_{(k)}^{(r)}$, see Fig. 7. The optimal choice (from the point of view of the variational mechanical problem) of those reference stresses is not straightforward; this is the main reason why several extensions of the SC scheme have been proposed in the literature. Obviously, all of them reduce to the same SC model in the linear case $n = 1$.

Following Ponte Castañeda (1996), Masson et al. (2000) proposed the so-called “affine” (AFF) linearization scheme which is

based on the simple idea of a linear behavior (21) tangent to the nonlinear one (4) at the mean shear stress, leading to

$$\dot{\tau}_{(k)}^{(r)} = \hat{\tau}_{(k)}^{(r)} = \langle \tau_{(k)} \rangle^{(r)}, \quad \alpha_{(k)}^{(r)} = \left. \frac{\partial \dot{\gamma}}{\partial \tau} \right|_{\tau = \hat{\tau}_{(k)}^{(r)}}. \quad (23)$$

The main limitations of this procedure are discussed in detail in (Masson et al., 2000) and (Bornert and Ponte Castañeda, 1998). One of them is the violation of rigorous upper bounds for the effective behavior. More generally, the affine extension is known to over-estimate the overall viscosity, *i.e.* to predict an effective behavior that is too stiff. This negative feature can be alleviated by means of the energy formulation originally proposed by Ponte Castañeda (1996) (see Bornert et al. (2001)).

Alternative, more sophisticated ways to generalize the SC scheme, have been proposed by Ponte Castañeda and co-workers during the last decades. The basic idea of these methods is to guide the choice of the properties of the LCP by a suitably designed variational principle. An “optimal” solution has been obtained in the context of the so-called “variational” procedure (VAR) (Ponte Castañeda, 1991), which was extended to polycrystals by De Botton and Ponte Castañeda (1995), leading to the choice

$$\dot{\tau}_{(k)}^{(r)} = \mathbf{0}, \quad \hat{\tau}_{(k)}^{(r)} = \left[\langle \tau_{(k)}^2 \rangle^{(r)} \right]^{1/2}. \quad (24)$$

The main advantage of this procedure is to provide a rigorous bound, sharper than the Voigt bound, for the effective potential. More recently, the “second-order” (SO) method of Ponte Castañeda (2002), extended to polycrystals in (Liu and Ponte Castañeda, 2004) has been proposed. It leads to reference shear stresses reading

$$\dot{\tau}_{(k)}^{(r)} = \langle \tau_{(k)} \rangle^{(r)}, \quad \hat{\tau}_{(k)}^{(r)} = \dot{\tau}_{(k)}^{(r)} \pm \left[\left\langle \left(\tau_{(k)} - \dot{\tau}_{(k)}^{(r)} \right)^2 \right\rangle^{(r)} \right]^{1/2}. \quad (25)$$

The main differences between AFF, VAR, and SO models may be summarized as follows. The AFF estimate can be regarded as a relatively simple model, allowing rapid computations which can even be rather accurate for polycrystals with weak grain anisotropy and small stress sensitivity. However, its predictions can become unrealistic (*e.g.* bound violation) at a strong anisotropy or nonlinearity. Contrary to AFF, for which linearization only accounts for the phase average stress, VAR accounts for the second moments of the stress, whereas the SO procedure accounts for both the phase average stress *and* intraphase standard deviation (first and second moments) to build the LCP. They can therefore provide better estimates in cases of highly heterogeneous stress distributions, such as for strongly nonlinear or anisotropic polycrystals. Applications of the VAR procedure to polycrystals with grains having cubic or hexagonal crystallographic structures can be found in (Nebozhyn et al., 2001; Liu et al., 2003).

Finally, the “tangent” (TGT) extension of the SC scheme (Molinari et al., 1987; Lebensohn and Tomé, 1993), often referred to as the “VPSC model” in the literature, is based on the same tangent linearization (23) as the AFF method. However, unlike the AFF extension, this procedure takes advantage of the fact that, for power-law polycrystals with a single stress exponent n for all slip systems, the tangent behavior (21) can be replaced by a secant-like relation, with $\dot{\epsilon}_{(k)}^{(r)} = 0$ and $\alpha_{(k)}^{(r)}$ replaced by $\alpha_{(k)}^{(r)}/n$. The same procedure is further applied at the macroscopic level, leading to an inconsistent definition for the stress localization tensor $\mathbf{B}^{(r)}$ that combines a secant description for the local and global behaviors but a tangent analysis for the inclusion/matrix interaction (Masson et al., 2000). When expressed in the form of tangent expressions, it can be shown that $\dot{\epsilon}_0$ differs from the exact relation given in (15).

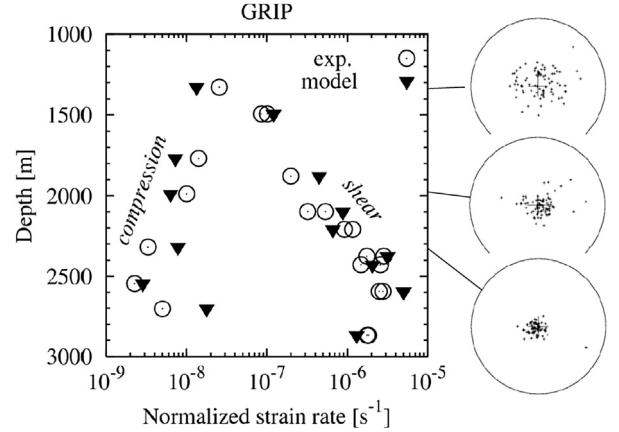


Fig. 8. Stationary creep behavior at -10 °C calculated by the affine SC model, and compared to experimental data obtained on anisotropic specimens from the GRIP ice core. The c -axis pole figures on the right show an increasing concentration of c -axes toward the *in situ* vertical direction from the surface of the ice sheet down to ~ 2600 m depth. Experimental data from Castelnau et al. (1998) are expressed for a stress of 1 MPa using a stress sensitivity $n = 3$. Points on the left hand side reflect the (hard) behavior under vertical compression, whereas data on the right correspond to (soft) horizontal shear.

3.5.1. Application to natural ices: effective behavior

Application of homogenization techniques to natural ices aims at understanding (and predicting) the anisotropic behavior of strongly textured specimens, as encountered at depth in natural ice sheets. As will be seen in Section 6, the viscoplastic anisotropy of polycrystals significantly influences ice flow at large scales (Mangeny et al., 1996; Gillet-Chaulet et al., 2006; Pettit et al., 2007; Martín et al., 2009). Castelnau et al. (1998) reported mechanical tests performed on specimens from the GRIP ice core (Central Greenland). Along the ice core, the ice microstructure, and in particular the crystallographic fabric, is evolving; with increasing depth, randomly oriented c -axis at the surface of the ice sheet tend to concentrate toward the *in situ* vertical direction down to a depth of ~ 2600 m. Beneath this depth, less pronounced textures are observed due to the initiation of migration recrystallization (Thorsteinsson et al., 1997). In (Castelnau et al., 1998), the experimental stationary creep behavior of those ices have been obtained for two loading conditions (Fig. 8). The first one corresponds to an *in situ* vertical compression, showing an increasing flow stress (decreasing strain rate for a constant applied stress) with increasing depth, since the activation of non-basal slip systems is necessary for pronounced fabrics. The second loading condition corresponds to *in situ* horizontal shear, promoting basal slip and resulting in a softening of the ice with increasing fabric strength. It can be seen that for a given applied stress, strain rates can vary by more than two orders of magnitude depending on the orientation of the applied stress with respect to the specimen fabric, reflecting the very strong viscoplastic anisotropy of ice specimens.

The effective behavior predicted by the affine (AFF) SC model is compared to the experimental data in Fig. 8. It can be observed that the agreement is excellent, meaning that the relation between fabric and effective rheology is very well captured by the model. The model captures correctly the increasing anisotropy from the surface down to ~ 2600 m depth, and the decrease below. The difference by more than two orders of magnitude between the vertical and shear strain-rates at ~ 2600 m is also well reproduced, although this was a challenging feature for the model. To get these results, the reference shear stress $\tau_0^{(k)}$ entering the local constitutive relation, and also the stress sensitivity $n^{(k)}$, for each slip system (k), had to be identified from comparison with a database that included single-crystal experimental tests, and polycrystal ones on many

different crystallographic textures (Castelnaud et al., 2008b). The resulting single-crystal rheology, used as input in the SC model to get the effective behavior described above, is shown in Fig. 9. For basal slip, agreement with experimental data from the literature is almost perfect. Non-basal systems are much stiffer than the basal systems, and pyramidal slip is found to be much more difficult than prismatic slip. These results are in good agreement with the available data on single crystals, and in qualitative agreement with the known dislocation structure in ice. Therefore, it can be anticipated that the affine SC model does a good job in making the link between the grain and the polycrystal scales, and provides an accurate estimate of the mechanical interaction between deforming grains. In other words, one can anticipate that results shown in Fig. 8 are based on a realistic description of the mechanical interaction between grains and physical deformation processes (dislocation glide) at the (sub)grain level. It can also be seen on Fig. 9 that this identification procedure leads to different stress sensitivities for the different slip system families. A value $n^{(k)} = 2$ was imposed for basal slip in accordance with experimental data, but values for prismatic and pyramidal systems were considered as adjustable parameters. It is also worth noting that the affine model perfectly reproduces an effective stress sensitivity (i.e. at the polycrystal scale) $\bar{n} = 3$ in agreement with experimental data, although the two major slip systems, basal and prismatic slip, have stress sensitivities smaller than 3 ($n^{(bas)} = 2$, $n^{(pr)} = 2.85$). A larger value was considered only for pyramidal slip ($n^{(py)} = 4.0$), but it is worth mentioning that the contribution of pyramidal slip is only very minor (<2%). It can be concluded that, in ice, although basal slip is by far the most active deformation mechanism, secondary slip systems are of great importance for explaining the polycrystal behavior. Basal slip alone does not allow for plastic deformation of ice polycrystals, since it only provides two independent slip systems. Secondary slip systems, here prismatic and pyramidal slip, must therefore be activated to add two more independent slip systems. The strength of these stiffer mechanisms determines the viscoplastic anisotropy at the grain scale, and therefore they also

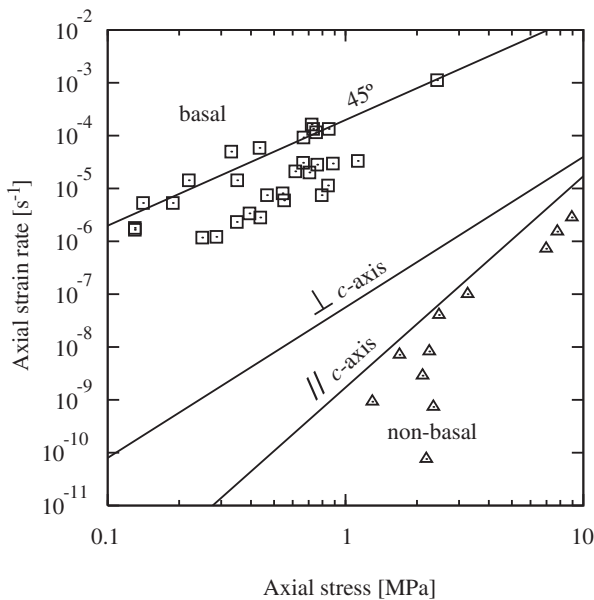


Fig. 9. Stationary creep behavior of single crystals at $-10\text{ }^{\circ}\text{C}$ input in the AFF SC model to get results of Fig. 8 (lines), compared to the data set compiled by Duval et al. (1983) (symbols). Results are indicated for uniaxial compression at 45° from the c -axis (activation of basal slip), as well as for compression perpendicular (activation of prismatic slip) and parallel (activation of pyramidal systems) to the c -axis. From Castelnaud et al. (2008b).

control the level of inter- and intra-granular heterogeneities of stress and strain(-rate), and therefore the effective polycrystal rheology. Similar conclusions have been drawn for olivine, a mineral with only three independent slip systems (Castelnaud et al., 2008a, 2009, 2010a,b). We therefore anticipate that the strong effect of secondary deformation mechanisms observed here might be a general feature for all polycrystalline materials with less than four independent slip systems. The corollary of these results is that simple or *ad hoc* polycrystal models, such as the Reuss (uniform stress) model, in which ice polycrystals can deform with only basal slip, cannot be accurate. This has been shown for example in (Castelnaud et al., 1997): whatever the strength used for prismatic and pyramidal systems, the Reuss model is not able to reproduce the very large anisotropy of GRIP specimens shown in Fig. 8. This comes from the fact that internal stresses, that have a large influence on the material behavior, are ignored.

Finally, it is also worth mentioning that the TGT SC approach, used in earlier studies, e.g. (Castelnaud et al., 1997), does not provide as good a match to experimental data as the AFF SC extension. There can be two reasons for that: (i) first of all, it is now known that the inconsistency in the formulation of the TGT SC version leads to an underestimation of the internal stress level, predicting a too soft polycrystal behavior (Gilormini, 1995; Masson et al., 2000); (ii) second, by construction, the TGT model is limited to grain behavior for which all slip systems exhibit the same stress sensitivity $n^{(k)}$. When applied to ice, one must thus consider $n^{(k)} = 3$ for all systems, including basal slip, in order to get an effective $\bar{n} = 3$. The fact that the AFF extension does not have this limitation might also explain a better consistency with experimental data.

3.5.2. Application to natural ices: texture development

Using the Reuss approximation, Van der Veen and Whillans (1994) and Castelnaud and Duval (1994) described the fabric evolution under compression, tension, simple and pure shear. Van der Veen and Whillans (1994) needed to impose a kind of “recrystallization” criterion (see Section 5.1) to be able to correctly represent the single-maximum fabric (with c -axis oriented along one direction) in ice deforming in pure shear. Nevertheless, the Reuss approximation faces inconsistency to describe the fabric evolution at the polycrystal scale, as it requires additional kinematical constraints to link the grain rotation-rate with the polycrystal rotation-rate. In most of the “Reuss” type models, these two rates are supposed to be equal, although the velocity field is not continuous.

Models that modify this homogeneous stress assumption were proposed by Azuma (1994) and Thorsteinsson (2002). They introduce some redistribution of stress through neighborhood interaction to define the crystal strain at a given bulk equivalent strain. In particular, Thorsteinsson (2002) defines a crystal arrangement on a three-dimensional cubic grid, where each crystal has six nearest neighbors. The nearest neighbor interaction (NNI) is taken into account by defining a local softness parameter for each crystal which modifies the stress acting on the central crystal compared to the macroscopic stress. This softness parameter further influences the rotation rate of the crystal lattice compared to the bulk. For uniaxial compression tests, the fabrics obtained with the NNI formulation are less concentrated than the ones where no NNI is considered. The reason for this is that the NNI formulation allows all crystals to deform to some extent, while only “soft” crystals would deform in the no-NNI formulation. The fabric obtained after 50% shortening strain compares qualitatively well with the one measured along the GRIP ice core at a depth where the strain is similar (1293 m) (Thorsteinsson et al., 1997).

The VPSC model in its “tangent” version was applied to simulate the fabric development along ice cores (Castelnaud et al., 1996b,a; 1998). In (Castelnaud et al., 1996a), a comparison was made with

bound estimates (Reuss and Voigt). Fabrics simulated in uniaxial compression and extension were found to be qualitatively similar for all models. However, large differences in the rate of fabric development were found. This was explained by the different interaction stiffness between grain and matrix for the three approaches. The fabrics obtained with the VPSC model for uniaxial deformation were in close agreement with the one measured along the ice core (see Fig. 10). In particular, this model well reproduced the fabric evolution along the GRIP ice core within the upper 650 m where dynamic recrystallization is not supposed to strongly impact this evolution (Castelnaud et al., 1996b). Lower down, the modeled fabric concentration is too high. Although (Castelnaud et al., 1996b) attributed this discrepancy to the effects of rotation recrystallization along the core, it was later shown that the tangent approximation overestimates the lattice rotation. In simple shear, the single-maximum fabric found along the ice cores or experimentally could not be reproduced with the VPSC scheme. To get close to this fabric, an extensive (and probably unrealistic) activity of non-basal slip systems was required. More recently, the “second order” (SO) mean field method of Ponte Castañeda (2002) was used to simulate the fabric development along the Talos Dome ice core (Montagnat et al., 2012). Although no recrystallization mechanisms were implemented in this version, the fabric development was astonishingly well reproduced, under the crude assumption of uniaxial compression with a constant strain rate (see Fig. 11). In particular, a good match was obtained when the initial fabric is non isotropic and similar to the one measured in the top firn, at 18 m depth. The cumulated compressive strain along the core was derived from the thinning function provided by the TALDICE-1 chronology (Buiron et al., 2011). The good prediction performed by the VP-SO scheme is probably due to the fact that this SO approach provides a better estimate of the effective behavior than the classical tangent “VPSC” model does in the case of strongly anisotropic materials such as ice (see Section 3.5). Nevertheless, the modeled fabric evolution could not capture the strengthening rate associated with the Glacial to Interglacial climatic transition. At these transition, a change in ice viscosity is expected. It induces a higher sensitivity to the impact of shear stress increasing with depth, that the modeling approach did not considered.

It is also recalled that the heterogeneity of shear on slip systems at the grain level gives rise to heterogeneities of lattice rotation, and therefore generates intragranular misorientations that somehow spread crystal orientations. It is however worth mentioning that *all* models presented above do not consider this strain heterogeneity for estimating fabric evolutions at finite strain. Even in VAR and SO procedures, intraphase strain heterogeneities are considered for defining the LCP, but so far not for estimating microstructure evolutions. As a consequence, mean-field approaches generally predict too sharp textures. The same applies to the prediction of strain hardening, associated with dislocation processes such as storage

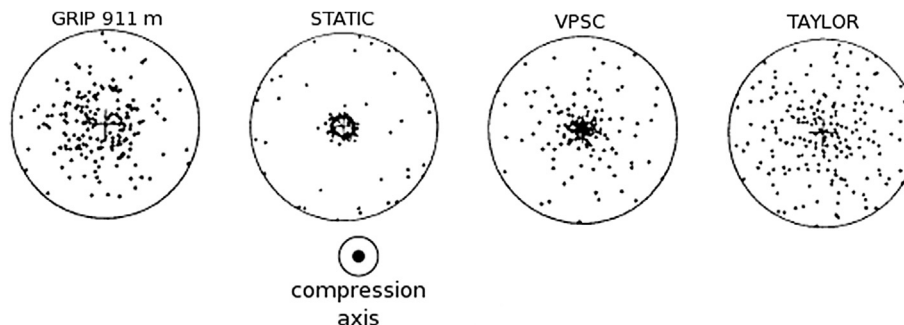


Fig. 10. Comparison between fabrics measured along the GRIP ice core (911 m depth), simulated by the static (Reuss), VPSC-tangent, and Taylor (Voigt) approaches.

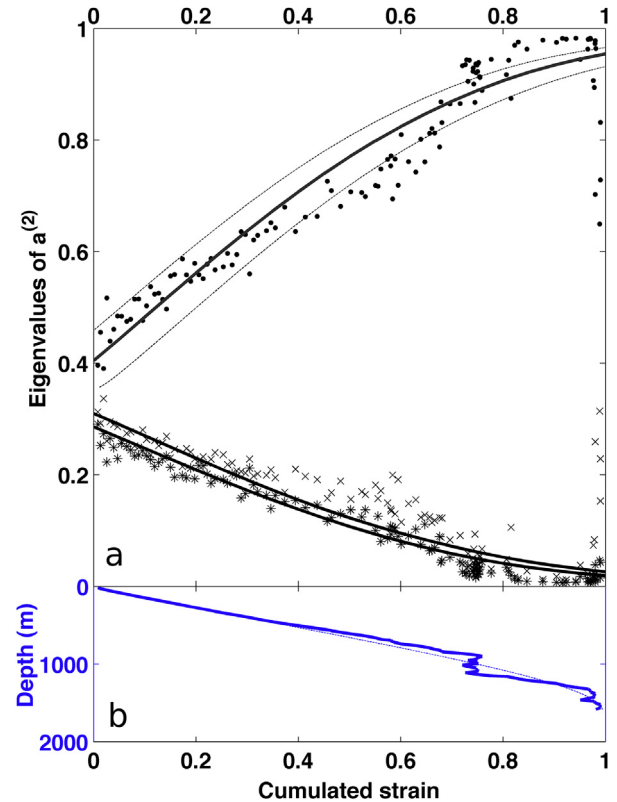


Fig. 11. a) Evolution of the eigenvalues of the orientation tensor $a^{(2)} = c \otimes c$ of the fabric along the Talos Dome ice core, as a function of the cumulated compressive strain. Lines = VP-SO model results, dashed line represents the range of fabric evolution modeled with variation of the initial orientation tensor eigenvalue from isotropic (bottom line), as measured at 18 m (central line), more concentrated than measured (top line). Dots, crosses and plus = measurements performed with the Automatic Ice Texture Analyzer (Russell-Head and Wilson, 2001). b) Cumulated in-situ compressive strain as a function of depth as model by the TALDICE-1 chronology (full line) (Buiron et al., 2011).

and annealing. A quantitative study, based on comparisons with reference results obtained by an FFT full-field approach, can be found in (Castelnaud et al., 2006).

Most of the efforts to simulate the fabric development in ice, and especially along ice cores, had to face the fact that recrystallization mechanisms could impact this fabric development. This was, most of the time, the analysis made for the observed discrepancies between simulated and measured fabrics (Van der Veen and Whillans, 1994; Wenk et al., 1997; Castelnaud et al., 1996b; Thorsteinsson, 2002). Some efforts to implement recrystallization mechanisms in mean-field approaches will be described in Section 5.1.

3.6. Modeling the elasto-viscoplastic behavior

Transient creep is typically encountered when ice flow changes direction, such as in glaciers flowing above irregular bedrock or submitted to tide forcing close to the sea-shore or in icy satellites. During laboratory experiments, transient creep is characterized by a strain-rate drop of more than two orders of magnitude before reaching the secondary creep close to 1% strain, following Andrade's law (Duval, 1978). This decrease is associated with the development of large internal stress fields due to intergranular interactions and a strong kinematic hardening (Duval et al., 1983; Ashby and Duval, 1985; Castelnaud et al., 2008b). To reproduce this transient behavior, one has to consider the coupling between elasticity and viscoplasticity that gives rise to the so-called "long-term memory effect", as explained below.

The application of homogenization schemes to the *elasto-viscoplasticity* of polycrystals is more complicated than for viscoplasticity, see for instance (Laws and McLaughlin, 1978). In short, it can be shown that, even in the simple case of a polycrystal comprising grains whose behavior exhibits a single relaxation time (so-called "short-term memory"), the effective behavior exhibits a continuous spectrum of relaxation time ("long-term memory effect") (Sanchez-Hubert and Sanchez-Palencia, 1978; Suquet, 1987). In other words, the overall behavior of a polycrystal is not of the Maxwell type (parallel association of a spring and a dashpot with constant viscosity), even though the individual grains do exhibit local Maxwell type behavior. The basic difference between elasto-viscoplasticity and viscoplasticity is that, for elasto-viscoplasticity, the local strain rate depends on both the stress (viscous part) and the stress-rate (elastic part), whereas it only depends on the stress for viscoplasticity. Therefore, the local strain rate not only depends on the actual local stress, but also on the whole stress history from the initial specimen loading at $t = 0$ up to the current time. To obtain the exact effective mechanical response at time t , it is thus required to keep track of all information (or internal variables) corresponding to the strains at all previous times, and therefore the problem is not simple. Within mean-field approaches, some approximations (with hopefully limited effects on the accuracy of the solution) are thus necessary.

Basically, two approaches have been proposed to deal with this issue. A promising method based on an incremental variational procedure has been proposed by Labeledlec and Suquet (2006, 2007). These authors have shown that the homogenization of a *linear visco-elastic* material (*i.e.* with $n = 1$) can be expressed in terms of a homogenization problem for a linear thermoelastic composite with non piecewise uniform eigenstrains. One advantage of this formulation is that it can make use of the intraphase heterogeneities of stress and strain (-rate), and it can therefore probably provide accurate results even at high stress sensitivity and/or local anisotropy. An alternative approach, which provides a good compromise between accuracy of the solution and simplicity of the formalism, is the so-called "affine" Self-Consistent method of Masson and Zaoui (1999). It is based on the correspondence principle (Mandel, 1966), which states that the elasto-viscoplastic problem can be reduced to a simpler homogenization problem (in fact similar to a standard thermo-elastic problem) if solved in Laplace space. One difficulty of this approach is the calculation of the inverse Laplace transforms, that has to be carried out numerically. An approximate inversion procedure, adapted for creep, has been proposed by Brenner et al. (2002b). It has provided promising results for the creep behavior of Zirconium alloys (Letouzé et al., 2002; Brenner et al., 2002a), since it retains the long-term memory effect associated with the elasto-viscoplastic coupling. Recent developments (Ricaud and Masson, 2009) have shown that an internal variable formulation arises naturally from this affine method,

providing results in perfect match with reference FFT solutions in the case of linear viscoelasticity (Vu et al., 2012).

To the best of our knowledge, this affine method is the only mean-field approach that has been applied to simulate the transient creep of ice (Castelnaud et al., 2008b). Applications make use of the crystal plasticity model for single crystals detailed in Section 2.3. It was shown that the strong hardening *amplitude* during the transient creep (*i.e.* the decrease of the overall strain rate by several orders of magnitude) is explained by the stress redistribution within the specimen: when the overall stress is applied instantaneously, the instantaneous polycrystal response is purely elastic, and since the elastic anisotropy is small, stress distribution within and between grains is almost uniform. But plastic deformation comes into play rapidly to cause a strong redistribution of stress (with large interphase and intraphase heterogeneities) due to the strong viscoplastic anisotropy at the grain scale. This significantly reduces the overall strain rate. On the other hand, the experimental hardening rate (*i.e.* the time necessary to reach the secondary creep regime) is much too slow to be explained by the same process, and is attributed to the hardening of hard-glide slip systems (prismatic slip) in the transient regime, associated with dislocation processes (Fig. 12).

4. Full field approaches for the polycrystal

Mean-field approaches have been extensively used to predict the mechanical behavior of ice polycrystals, and the fabric development as measured along ice cores. Due to its high viscoplastic anisotropy, deformation in ice is expected to be strongly heterogeneous, with a strong impact of grain interactions and kinematic hardening (Duval et al., 1983; Hamman et al., 2007; Montagnat et al., 2011; Grennerat et al., 2012). The mean-field approaches described above are based on the statistical characterization of the intragranular mechanical fields (in terms of average grain stresses and strain rates, and, in the most advanced formulations, also through the determination of the intracrystalline average field fluctuations), but the actual micromechanical fields remain inaccessible to these homogenization approaches. Modeling the full

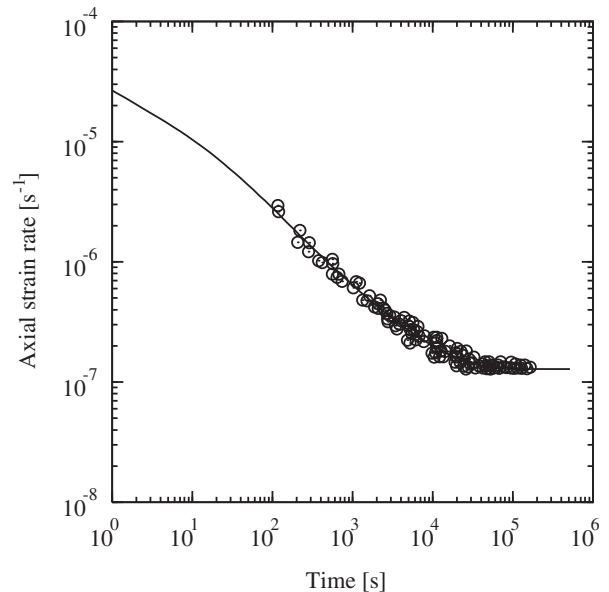


Fig. 12. Transient creep response of isotropic ice under an uniaxial compressive stress of 1 MPa predicted with the affine elasto-viscoplastic extension of the self-consistent scheme (line). Model results are compared to the data of Ashby and Duval (1985), expressed for the same loading conditions (points). Strain hardening of prismatic and pyramidal slip systems is taken into account. From Castelnaud et al. (2008b).

intracrystalline heterogeneity that develops in ice polycrystals requires the use of full-field approaches. This part will concentrate on full-field approaches that are using the Fast Fourier Transform method to solve the constitutive equations in a discretized polycrystal. It aims at studying the correlation between the heterogeneous deformation patterns that appear inside the constituent single-crystal grains of an ice aggregate and their corresponding crystallographic orientations, along with the influence of other factors, such as orientation and size of neighboring grains. Both viscoplastic and elasto-viscoplastic behavior were investigated, and are presented in the two following sections.

4.1. Viscoplastic approach – FFT

4.1.1. Viscoplastic FFT-based formulation

The intracrystalline states that are developed during creep of polycrystalline ice can be obtained using an extension of an iterative method based on FFT, originally proposed by [Moulinec and Suquet \(1998\)](#) and [Michel et al. \(2001\)](#) for linear and non-linear composites. This formulation was later adapted to polycrystals and applied to the prediction of texture development of fcc materials ([Lebensohn, 2001](#)), and in turn used for the computation of field statistics and effective properties of power-law 2D polycrystals ([Lebensohn et al., 2004a, 2005](#)) and 3D cubic, hexagonal ([Lebensohn et al., 2004b](#)) and orthorhombic ([Castelnau et al., 2008a](#)) materials. The FFT-based formulation was also applied to compute the development of local misorientations in polycrystalline copper, with direct input from orientation images ([Lebensohn et al., 2008](#)). As will be detailed in Section 4.2 it was further extended to transient behavior with an elasto-viscoplastic formulation ([Idiart et al., 2006](#); [Suquet et al., 2011](#); [Lebensohn et al., 2012](#)). The FFT-based full-field formulation for viscoplastic polycrystals is conceived for a periodic unit cell, provides an exact solution of the governing equations, and has better numerical performance than an FE calculation for the same purpose and resolution. The viscoplastic FFT-based formulation consists in finding a strain-rate field, associated with a kinematically-admissible velocity field, which minimizes the average of local work-rate, under the compatibility and equilibrium constraints. The method is based on the fact that the local mechanical response of a periodic heterogeneous medium can be calculated as a convolution integral between the Green function of a linear reference homogeneous medium and the actual heterogeneity field. Such type of integrals reduce to a simple product in Fourier space, therefore the FFT algorithm can be used to transform the heterogeneity field into Fourier space and, in turn, to get the mechanical fields by antitransforming that product back to real space. However, since the actual heterogeneity field depends precisely on the a priori unknown mechanical fields, an iterative scheme should be implemented to obtain, upon convergence, a compatible strain-rate field and a stress field in equilibrium.

The periodic unit cell representing the polycrystal is discretized by means of a regular grid $\{\mathbf{x}^d\}$, which in turn determines a corresponding grid of the same dimensions in Fourier space $\{\xi^d\}$. Velocities and tractions along the boundary of the unit cell are left undetermined under the sole condition of periodicity. An average velocity gradient $V_{i,j}$ is imposed to the unit cell, which gives an average strain rate $\dot{\tilde{\epsilon}}_{ij} = \frac{1}{2}(V_{i,j} + V_{j,i})$. The local strain-rate field is a function of the local velocity field, i.e. $\dot{\epsilon}_{ij}(v_k(\mathbf{x}))$, and can be split into its average and a fluctuation term: $\dot{\epsilon}_{ij}(v_k(\mathbf{x})) = \dot{\tilde{\epsilon}}_{ij} + \tilde{\dot{\epsilon}}_{ij}(\tilde{\mathbf{v}}_k(\mathbf{x}))$, where $v_i(\mathbf{x}) = \tilde{\epsilon}_{ij}x_j + \tilde{v}_i(\mathbf{x})$. By imposing periodic boundary conditions, the velocity fluctuation field $\tilde{\mathbf{v}}_k(\mathbf{x})$ is assumed to be periodic across the boundary of the unit cell, while the traction field is

antiperiodic, to meet equilibrium on the boundary between contiguous unit cells. The local constitutive equation that relates the deviatoric stress $\boldsymbol{\sigma}'(\mathbf{x})$ and the strain rate $\dot{\epsilon}(\mathbf{x})$ at point \mathbf{x} is obtained from Eqs (18) to (20).

If $p(\mathbf{x})$ is the unknown pressure field introduced by the incompressibility constraint, the Cauchy stress field can be written as:

$$\boldsymbol{\sigma}(\mathbf{x}) = \mathbf{L}^0 : \dot{\epsilon}(\mathbf{x}) + \boldsymbol{\varphi}(\mathbf{x}) - p(\mathbf{x})\mathbf{I} \quad (26)$$

where the polarization field $\boldsymbol{\varphi}(\mathbf{x})$ is given by:

$$\boldsymbol{\varphi}(\mathbf{x}) = \boldsymbol{\sigma}'(\mathbf{x}) - \mathbf{L}^0 : \dot{\epsilon}(\mathbf{x}) \quad (27)$$

where \mathbf{L}^0 is the stiffness (viscosity) of a linear reference medium. Eqs. (26) and (27) amount to transform the actual heterogeneity problem into an equivalent one, corresponding to a homogenous medium with eigen-strain-rates. Note, however, that the above defined polarization field depends on the unknown $\dot{\epsilon}(\mathbf{x})$. Combining Eq. (27) with the equilibrium and the incompressibility conditions gives:

$$\mathbf{L}^0_{ijkl}v_{k,j}(\mathbf{x}) + \boldsymbol{\varphi}_{ij,j}(\mathbf{x}) - p_{,i}(\mathbf{x}) = 0, v_{k,k}(\mathbf{x}) = 0 \quad (28)$$

Assuming for a moment that the polarization field $\boldsymbol{\varphi}(\mathbf{x})$ is known, the system of partial differential Equation (28), with periodic boundary conditions across the unit cell boundary, can be solved by means of the Green function method.

If G_{km} and H_m are the periodic Green functions associated with the velocity and hydrostatic pressure fields, the solutions of system (28) are convolution integrals between those Green functions and the actual polarization term.

The velocity gradient, after some manipulation is given by:

$$\tilde{v}_{i,j}(\mathbf{x}) = \int_{R^3} G_{ik,jl}(\mathbf{x} - \mathbf{x}')\boldsymbol{\varphi}_{kl}(\mathbf{x}')d\mathbf{x}' \quad (29)$$

Convolution integrals in direct space are simply products in Fourier space. Hence:

$$\widehat{\tilde{\epsilon}}_{ij}(\xi) = \widehat{\Gamma}_{ijkl}^{\text{sym}}(\xi)\widehat{\boldsymbol{\varphi}}_{kl}(\xi), \quad (30)$$

where $\widehat{\Gamma}_{ijkl}^{\text{sym}} = \text{sym}(\widehat{G}_{ik,jl})$. The tensors $\widehat{G}_{ik}(\xi)$ and $\widehat{\Gamma}_{ijkl}^{\text{sym}}(\xi)$ are only functions of \mathbf{L}^0 and can be readily obtained for every point belonging to $\{\xi^d\}$ (for details, see [Lebensohn et al. \(2008\)](#)). Now, taking into account the definition (27) of $\boldsymbol{\varphi}(\mathbf{x})$, Eq. (29) is an integral equation where the velocity gradient appears in both sides, and, thus, it can be solved iteratively. Assigning initial guess values to the strain-rate field in the regular grid (e.g. $\tilde{\epsilon}(\mathbf{x}^d) = 0 \Rightarrow \dot{\epsilon}^{(0)}(\mathbf{x}^d) = \dot{\tilde{\epsilon}}$), and computing the corresponding stress field $\boldsymbol{\sigma}^{(0)}(\mathbf{x}^d)$ from the local constitutive relation (18) allows to obtain an initial guess for the polarization field in direct space $\boldsymbol{\varphi}^{(0)}(\mathbf{x}^d)$ (27), which in turn can be Fourier-transformed to obtain $\widehat{\boldsymbol{\varphi}}^{(0)}(\xi^d)$.

The rate of convergence of this fixed point technique is rather poor for nonlinear constitutive relations such as power-law relations between the stress and the strain-rate. Accelerated schemes based on augmented Lagrangians have been proposed to improve this rate of convergence originally by [Michel et al. \(2000, 2001\)](#) for composites, and later adapted by [Lebensohn \(2001\)](#) for polycrystals to which the interested reader is referred for details. Upon convergence, the stress at each material point can be used to calculate the shear rates associated with each slip system (Eq. (4)), from which fields of relative activity of the basal, prismatic and pyramidal slip modes can be obtained, as well. While it is certainly possible to use the FFT-based formulation for the prediction of

microstructure evolution, in this section we have restricted our analysis to the local fields that are obtained for a fixed configuration. In this sense, the high strain-rate regions predicted by the model (see below) should be regarded as precursors of localization bands. Evidently, microstructural changes that are not considered under this approximation, like the eventual grain's and subgrain's morphologic evolution and rotation, as well as the possible occurrence of local strain hardening, may modify some of the trends observed in the initial micromechanical fields. In order to account for these microstructural changes, the FFT-based formulation has been coupled with the front-tracking numerical platform Elle (Bons et al., 2001). Results of this coupled model are reported in Section 5.2.2.

4.1.2. Application to columnar ice deforming in the secondary creep regime

Lebensohn et al. (2009) and Montagnat et al. (2011) applied this FFT method to simulate strain rate and stress fields, and local lattice misorientations obtained at secondary creep in columnar ice polycrystals. Lebensohn et al. (2009) compared the simulated fields to a series of compression creep experiments performed by Mansuy et al. (2000, 2002) on laboratory-grown columnar ice samples characterized by multicrystals of controlled shape and orientations. The specimen used for this comparison (see Fig. 13) was a plate of 210×140 mm with a relatively thick (8 mm) section, consisting of a multicrystalline cluster, located in the center of the plate, with c -axes lying on the plane of the plate, and embedded in a matrix of fine-grained ice. This specimen was deformed under a compressive stress of 0.75 MPa exerted vertically in the plane at -10°C under plane strain conditions. Fig. 13 shows, after 0.07 strain, three types of localization bands: basal shear bands, kink bands and sub-boundaries, that change orientation to follow crystallographic directions when they cross from one grain to another.

In this configuration, kink band boundaries are seen mainly inside grains oriented close to 45° from the imposed compression

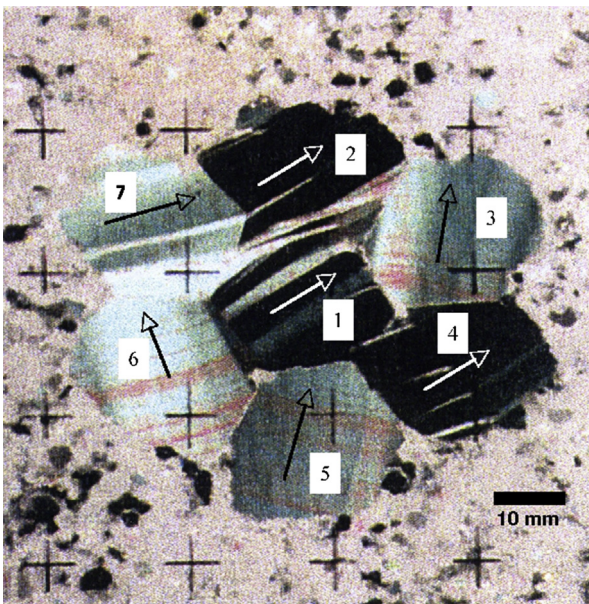


Fig. 13. Photograph of a compression creep specimen (after Mansuy et al. (2000)) between crossed polarizers, after a deformation of 6.6×10^{-2} at -10°C . The corresponding strain rate was $6.0 \times 10^{-8} \text{ s}^{-1}$. The compression direction is vertical in the plane of the photograph. The mean size of each hexagonal grain was 20 mm. Black and white arrows indicate the initial c -axis orientations. Kink bands appear as abrupt changes in color parallel to the c -axis, shear bands are perpendicular to the c -axis direction.

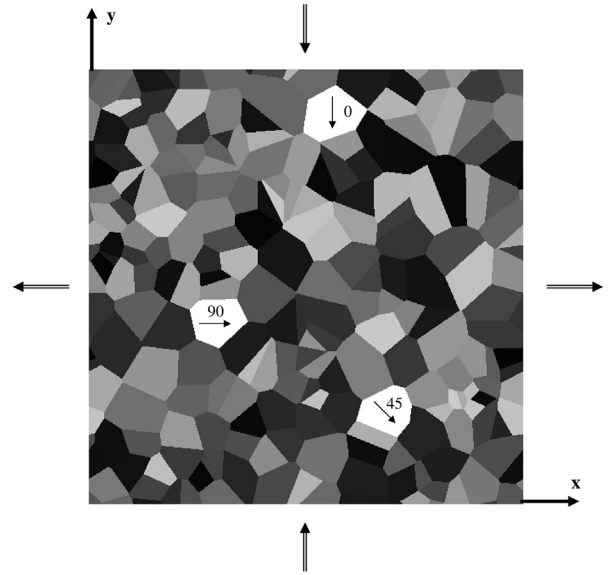


Fig. 14. Unit cell containing the cross-sections of 200 columnar grains generated by Voronoi tessellation. The three hand-picked orientations: $(0^\circ, 90^\circ, 0^\circ)$, $(45^\circ, 90^\circ, 0^\circ)$ and $(90^\circ, 90^\circ, 0^\circ)$, and the extension and shorting directions are also indicated.

direction. Kink bands, described as a sharp or discontinuous change in orientation of the active slip surface, had been reported in experimental studies conducted on 2-D ice polycrystals (Wilson et al., 1986; Wilson and Zhang, 1994; Montagnat et al., 2011). Sub-boundaries parallel to the c -axis were also observed.

The FFT-based calculation as described in the previous section, was run to obtain the overall and local mechanical response of the above-described unit cell representing a columnar ice polycrystal, to the following imposed strain-rate tensor (see also Fig. 14):

$$\dot{\bar{\epsilon}}_{ij} = \begin{bmatrix} 1 \times 10^{-8} & 0 & 0 \\ 0 & -1 \times 10^{-8} & 0 \\ 0 & 0 & 0 \end{bmatrix} \text{ s}^{-1} \quad (31)$$

The crystallographic texture of the 2-D ice polycrystal consisting of columnar grains with c -axes perpendicular to the axial (vertical) direction x_3 was described in terms of a collection of Euler-angle triplets of the form $(\phi_1, 90^\circ, \phi_2)$ (Bunge convention). The application of the FFT method required the generation of a periodic unit cell or representative volume Element (RVE), by repetition along x_1 and x_2 of a square domain. This square domain was constructed in such a way that it contained the cross-sections of 200 columnar grains, generated by Voronoi tessellation (see Fig. 14). This square domain is the cross-section of the unit cell, consisting of columnar grains with axes along x_3 and sections in the x_1 - x_2 plane. This unit cell was discretized using a $1024 \times 1024 \times 1$ grid of regularly-spaced Fourier points, resulting in an average of around 5250 Fourier points per grain. Note that the periodic repetition of this unit cell along x_3 determines infinitely long grains along this direction. Three specific orientations with c -axis respectively at 0° , 45° , and 90° from the compression direction were forced to be among the set of 200 (otherwise random) orientations assigned to the grains. For a plane-strain state, such that x_1 is the tensile direction and x_2 is the compression direction, the grain with $\phi_1 = 45^\circ$ (45 deg grain in what follows) is theoretically favorably oriented to deform by soft basal slip, while in the 0 deg and 90 deg grains, the hard pyramidal systems are the only ones favorably oriented to accommodate deformation. It is worth noting that due to the above plane-strain condition and the in-plane orientation of

RVE - equivalent strain-rate

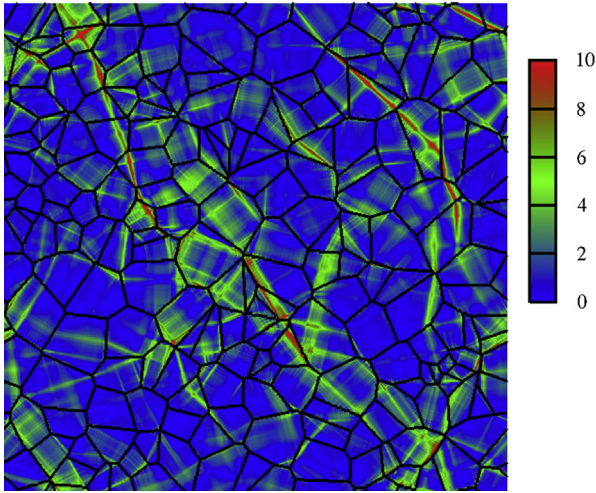


Fig. 15. Predicted equivalent strain-rate field over the entire unit cell of Fig. 14, normalized with respect to the average equivalent strain rate ($\bar{\dot{\epsilon}}_{eq} = 1.15 \times 10^{-8} s^{-1}$).

the c-axes, the prismatic slip systems are not well-oriented, for any φ_1 angle.

The computed effective response of this kind of isotropic columnar ice polycrystal deformed in-plane is twice softer compared to an isotropic 3-D polycrystalline ice (Lebensohn et al., 2007). The computed overall relative activities of the different slip modes (i.e. 90.7%, 7.6% and 1.7% for basal, pyramidal and prismatic slip, respectively) show a preeminence of basal slip, a minor contribution of pyramidal slip and a very low activity of prismatic

slip. Fig. 15 shows the computed equivalent strain-rate field for the entire unit cell, normalized with respect to the average equivalent strain rate ($\bar{\dot{\epsilon}}_{eq} = 1.15 \times 10^{-8} s^{-1}$). The main feature observed in this plot is a network of high strain-rate bands, precursors of localization bands (in what follows we will sometimes refer to them simply as “localization bands”). These bands are transmitted from grain to grain and are, in general, inclined with respect to the shortening and extension directions. They follow tortuous paths, sometimes with large deviations from $\pm 45^\circ$ (i.e. the macroscopic directions of maximum shear stress). They follow crystallographic directions (basal poles or basal planes) inside each grain. The predicted bands parallel or perpendicular to the c-axis were reasonably assumed to be kink or shear bands, respectively (see Lebensohn et al. (2009) for details). Some segments of these bands also follow favorably-oriented grain boundaries and frequently go through triple or multiple points between grains, in good agreement with some of the observations of (Mansuy et al., 2002) (Fig. 13). Fig. 16 shows in more details the predicted fields of equivalent strain rate (normalized to $\bar{\dot{\epsilon}}_{eq}$), equivalent stress (in units of τ^{bas}) and relative basal activity, in the vicinities of the 45 deg grain. Two very intense (i.e. local strain rates higher than 10 times the macroscopic strain rate) and parallel kink bands are seen inside the 45 deg grain, connected by several less intense shear bands (orthogonal to the pair of kink bands, lying on to the basal plane), in good agreement with Mansuy’s experiments (see Fig. 13). The basal activity in the 45 deg grain is very high, although some regions of high non-basal activity can be observed between shear bands and immediately outside the kink bands. The latter is compatible with a low or even vanishing resolved shear stress on basal planes in those locations, which may be responsible for the formation of basal dislocation walls that are at the origin of a kink band (Mansuy et al., 2002). This correlation between kink band

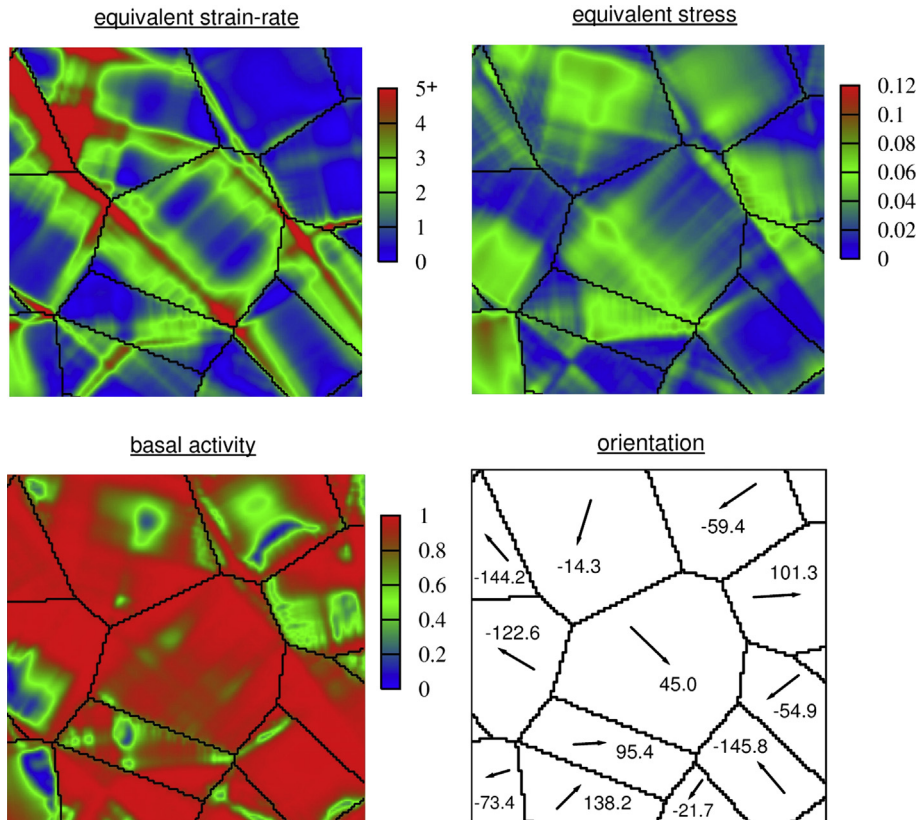


Fig. 16. Predicted fields of equivalent strain rate (normalized to $\bar{\dot{\epsilon}}_{eq}$), equivalent stress (in units of τ^{bas}), relative basal activity, and map of neighbor orientations, for the 45 deg grain and its surroundings.

precursors and nearby localized high non-basal activity is systematic in these results. From the same detailed analysis performed around the 0 and 90 deg grains, a good match was found with experimental observations.

In (Montagnat et al., 2011), the viscoplastic FFT-based approach was applied to the exact experimental microstructure of a compressive test performed on a 2D columnar sample. Samples (dimensions $\approx 100 \times 100 \times 15 \text{ mm}^3$) were grown in the laboratory under a uniaxial temperature gradient to reach a columnar microstructure with all c -axes lying parallel to the sample surface. In this work, the observed kink bands could be associated with misorientations between adjacent regions of a grain interior of more than 5° , and their exact nature in term of dislocation arrangements were confirmed by EBSD measurements. Although the boundary conditions of the modeling were slightly different from the experimental one, the model was able to predict the exact location of the localization bands. The bands were associated with stress concentration that could reach five times the applied macroscopic stress, and to high levels of local non basal activity (see Fig. 17). Nevertheless, the amplitude of the modeled lattice misorientations was always overestimated, and this was associated with the fact that very local grain boundary migration and new grain nucleation (dynamic recrystallization mechanisms) observed experimentally were not considered in the model (see Section 5.2.2).

4.2. Elasto-viscoplastic FFT approach

The full-field FFT approach described above has been extended very recently to the case of elasto-viscoplasticity, see (Idiart et al., 2006; Suquet et al., 2011; Lebensohn et al., 2012). As for purely viscoplastic behaviors, its application to highly anisotropic material like ice allows investigating the accuracy of elasto-viscoplastic mean-field models (see Section 3.6) since, as already mentioned, the FFT technique provides the “exact” (in a numerical sense) response of the specimen with the actual microstructure and local constitutive relations. Application to ice allows studying transient creep effects with more detail. Comparison with experimental strain field measured with an intragranular spatial resolution has been provided in (Grennerat et al., 2012) making use of the relative ease of producing samples with controlled 2-D microstructure, compared to other polycrystalline materials.

4.2.1. The mechanical problem

The method described in Suquet et al. (2011) considers the same microstructure description as in Section 4.1: a polycrystalline volume V composed of several grains of different orientations, each

grain obeying constitutive relations defined in Section 2.3. The volume V is subjected to a macroscopic loading path, which can be a prescribed history of average strain, or a history of average stress or a combination of both. For simplicity, the method is presented here assuming a prescribed history of macroscopic strain $\bar{\epsilon}(t)$, $t \in [0, T]$. Other types of loadings can be handled by different methods described in (Michel et al., 1999) for instance.

The local problem to be solved to determine the local stress and strain fields in the volume element V consists of the equilibrium equations, compatibility conditions, constitutive relations and periodic boundary conditions:

$$\begin{cases} (\dot{\sigma}, \dot{\tau}_0, \dot{\mathbf{X}}) = \mathbf{F}(\dot{\epsilon}, \sigma, \tau_0, \mathbf{X}, \mathbf{x}, t), & \text{for } (\mathbf{x}, t) \in V \times [0, T], \\ \epsilon(\mathbf{x}, t) = \frac{1}{2}(\nabla \mathbf{u}(\mathbf{x}, t) + {}^T \nabla \mathbf{u}(\mathbf{x}, t)), \\ \text{div } \sigma(\mathbf{x}, t) = 0 & \text{for } (\mathbf{x}, t) \in V \times [0, T], \\ \mathbf{u}(\mathbf{x}, t) - \bar{\epsilon}(t) \cdot \mathbf{x} \text{ periodic on } \partial V, & \text{for } t \in [0, T] \end{cases} \quad (32)$$

The data of interest are the effective response $\bar{\sigma}(t)$, $t \in [0, T]$ of the polycrystal, the history of the average strain $\bar{\epsilon}(t)$, $t \in [0, T]$, but also the local fields $\sigma(\mathbf{x}, t)$, $\epsilon(\mathbf{x}, t)$ and other significant fields (internal variables, thermodynamic forces etc...).

The extension of the simplest version of the FFT-based method, also called the *basic scheme*, to constitutive relations including crystalline elasto-viscoplasticity relies on two ingredients:

1. A time-integration scheme for the constitutive differential equations. The time interval of interest $[0, T]$ is split into time steps $[t_n, t_{n+1}]$. All quantities are assumed to be known at time t_n , and the quantities at time t_{n+1} are unknown. This time integration is performed at every point \mathbf{x}^d of the discretized polycrystal and the evolution problem is reduced to a problem for the stress and strain fields σ and ϵ at time t_{n+1} in the form

$$\sigma_{n+1}(\mathbf{x}^d) = \mathcal{F}_{n+1}(\mathbf{x}^d, \epsilon_{n+1}(\mathbf{x}^d)) \quad (33)$$

2. An FFT global scheme to solve the local problem for a nonlinear composite obeying Eq. (33).

The algorithm developed applies to a wide class of constitutive relations, see (Suquet et al., 2011). As before, it is limited to specimens submitted to periodic boundary conditions. Results presented

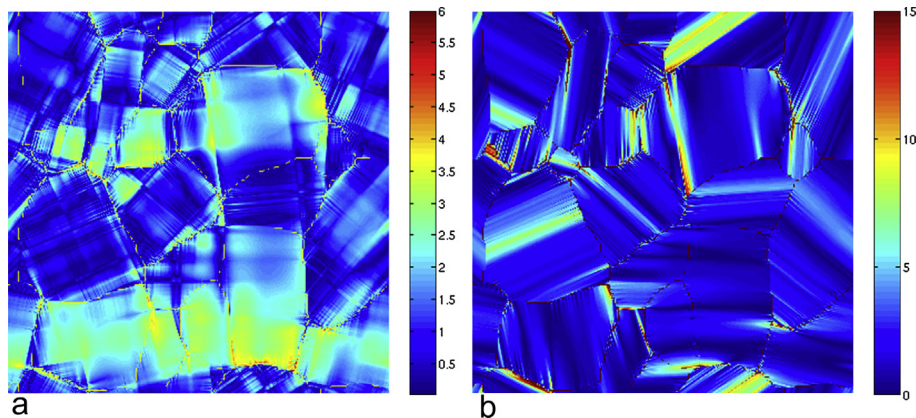


Fig. 17. a) Predicted equivalent stress field (in units of τ^{bas}), and b) misorientation, relative to initial orientation, obtained after 1% strain in a laboratory made microstructure. From Montagnat et al. (2011).

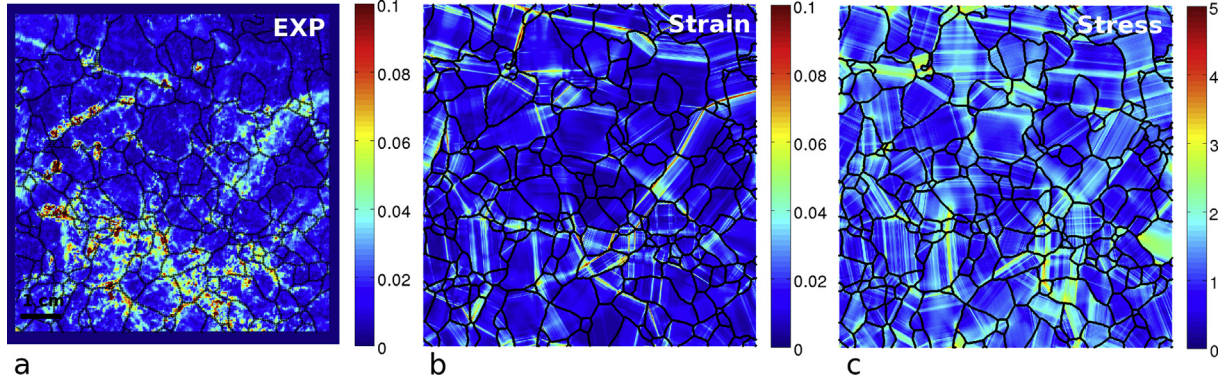


Fig. 18. a) Strain field measured experimentally, b) simulated, and c) stress field simulated, after 0.85% of axial compression. Experimental resolution is about 75×75 pixels, the modeling one is 1024×1024 pixels. From Grennerat et al. (2012).

below are performed with the FFT-based program Craft (freely available at <http://craft.lma.cnrs-mrs.fr>). For application to elasto-viscoplasticity in ice, the local constitutive relation is the one provided above, see Eqs (2, 3, 6, 7, 8). It can also be formulated via the following differential equation:

$$\dot{\mathbf{Y}} = \mathcal{F}(\dot{\boldsymbol{\epsilon}}, \mathbf{Y}, t), \quad (34)$$

where

$$\mathbf{Y} = \begin{pmatrix} \boldsymbol{\sigma} \\ \tau_0^{(k)}, k = 1, \dots, M \\ X^{(k)}, k = 1, \dots, M \end{pmatrix}, \quad \mathbf{F}(\dot{\boldsymbol{\epsilon}}, \mathbf{Y}, t) = \begin{pmatrix} \mathbf{C} : \dot{\boldsymbol{\epsilon}} - \sum_{k=1}^M \dot{\gamma}^{(k)}(\mathbf{Y}) \boldsymbol{\mu}^{(k)} \\ (\tau_{\text{sta}}^{(k)} - \tau_0^{(k)}) \sum_{\ell=1}^M h^{(k, \ell)} |\dot{\gamma}^{(\ell)}(\mathbf{Y})| \\ c^{(k)} \dot{\gamma}^{(k)}(\mathbf{Y}) - d^{(k)} X^{(k)} |\dot{\gamma}^{(k)}(\mathbf{Y})| - e^{(k)} |X^{(k)}|^m \text{sign}(X^{(k)}) \end{pmatrix} \quad (35)$$

with \mathbf{C} the elastic stiffness ($\mathbf{C} = \mathbf{S}^{-1}$). The set of parameters used are given in Table 1.

4.2.2. Application to strain field prediction in a 2D-1/2 configuration

The elasto-viscoplastic FFT approach was used to predict strain and stress field evolution during transient creep tests on ice polycrystals, in comparison with experimental measurements performed by Grennerat et al. (2012).

Samples were grown following (Montagnat et al., 2011) (see Section 4.1.2). This way, when compressed, (i) plastic deformation can be approximate as 2-D, and (ii) strain fields measured at the specimen surface are representative for the sample volume owing to the minimisation of in-depth microstructure gradients. Average grain size (section perpendicular to the column direction) was about 5 mm and most of the c-axes were oriented parallel to the surface ($\pm 15^\circ$). The microstructure and grain orientation were measured using an Automatic Ice Texture Analyzer (Russell-Head and Wilson, 2001) which provides orientation values with about $50 \mu\text{m}$ resolution, and 1° accuracy. A Digital Image Correlation technique (Vacher et al., 1999) was applied to measure the strain heterogeneities on the surface

perpendicular to the column direction. From displacement measurements performed during transient creep in ice, *i.e.* up to 1–2%, at -10°C , under 0.5 MPa, strain fields were evaluated with a resolution of about 0.2%, and at a spatial resolution of about 1 mm.

The experimental microstructures were implemented in the code using the fabric analyzer data of 2000×2000 pixels (but the model input does not need to be square). One pixel in the third dimension (column direction) is enough to reproduce

the 2D-1/2 geometry thanks to the periodic boundary conditions.

Fig. 18 presents the strain field measured experimentally at the end of the transient creep, and the simulated fields of strain and stress. Although simulated boundary conditions did not precisely match the experimental ones, the heterogeneities of the strain field that develop during transient creep of polycrystalline ice were reproduced well by the model (Grennerat et al., 2012). In particular, the model was able to reproduce the characteristic length of the heterogeneities being larger than the grain size, and scaling with the sample dimensions. Furthermore, both experimental and modeled results showed no correlation between the orientation of the c-axis and the strain intensity (see Fig. 19). This result casts doubt on the relevance of the distinction between “hard grains” and “soft grains” classically made for the analysis of ice mechanical behavior, and more generally for anisotropic materials.

Fig. 20 represents the evolution of the simulated equivalent strain field from 0.25 to 0.60% of compression during transient creep. As observed experimentally, the strain heterogeneities develop early during the transient creep and are reinforced up to about 10 times the imposed strain.

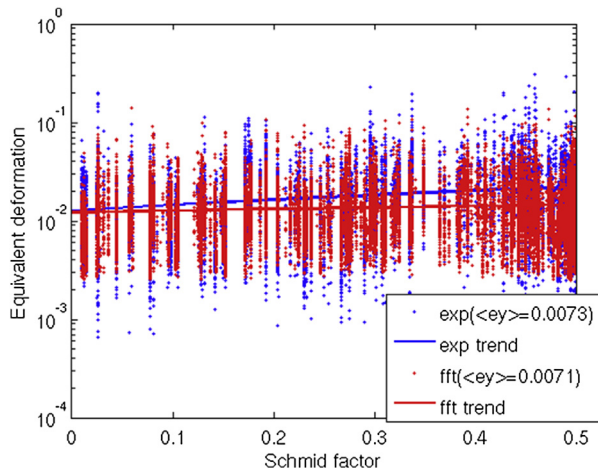


Fig. 19. Equivalent strain as a function of the Schmid factor (as a proxy of the orientation). Experimental results are in blue, modeling results in red. Each point is one pixel of the microstructure. The macroscopic strain was 0.7%. From Grennerat et al. (2012).

5. Modeling of dynamic recrystallization mechanisms

Under laboratory conditions (described in Section 1), dynamic recrystallization (DRX) dominates the changes of microstructures and fabrics in the tertiary creep regime, that is after about 1% macroscopic strain (Duval, 1981; Jacka and Maccagnan, 1984; Jacka and Li, 1994). During DRX, grain nucleation and grain boundary migration are two processes that contribute to the reduction of the dislocation density, therefore of the stored deformation energy (Humphreys and Hatherly, 2004). In the laboratory, tertiary creep is a continuous sequence of deformation and recrystallization that gradually results in a steady state. This steady state is associated with an equilibrium grain size (Jacka and Li, 1994) and a girdle-type fabric with *c*-axes at about 30° from the compression axis (Jacka and Maccagnan, 1984), or with two maxima in simple shear (Bouchez and Duval, 1982).

In polar ice sheets, DRX was identified from observations on ice thin sections along ice cores (Alley, 1992; Thorsteinsson et al., 1997; de la Chapelle et al., 1998; Kipfstuhl et al., 2006). Three regions are usually defined: (i) normal grain growth driven by the reduction of grain-boundary energy in the upper hundreds meters of the core, (ii) rotation recrystallization during which new grains are formed by the progressive lattice rotation of the subgrains, in the main part of the core and (iii) migration recrystallization similar to the one observed in the laboratory, in the bottom part where the temperature is above -10 °C (see Montagnat et al. (2009) and Faria et al. (2014) for a review).

Recrystallization and grain growth significantly influence the microstructure, the fabric and therefore the mechanical properties. To be able to integrate these mechanisms in the modeling of ice deformation is therefore crucial for an accurate prediction of its behavior.

5.1. Dynamic recrystallization within mean-field approaches

Several attempts were made to integrate dynamic recrystallization mechanisms into mean-field approaches as described in Section 3.

On the basis of the VPSC scheme (tangent version) described in Section 3 for the description of the mechanical behavior, Wenk et al. (1997) developed a nucleation and grain-growth model to represent DRX in anisotropic materials such as ice. The model is

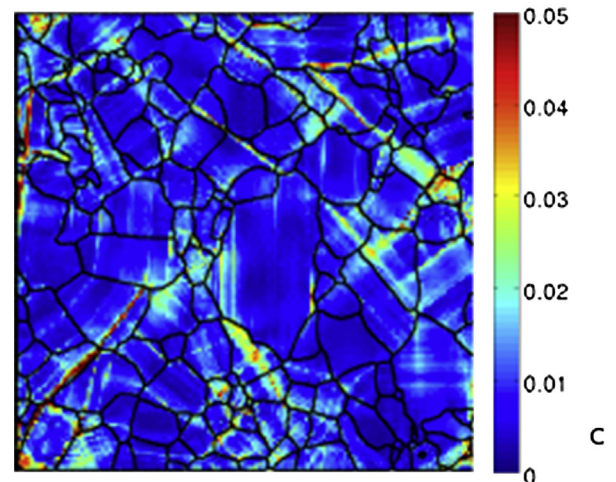
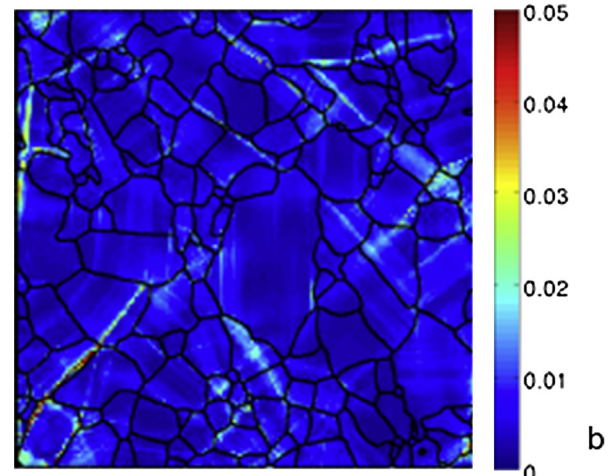
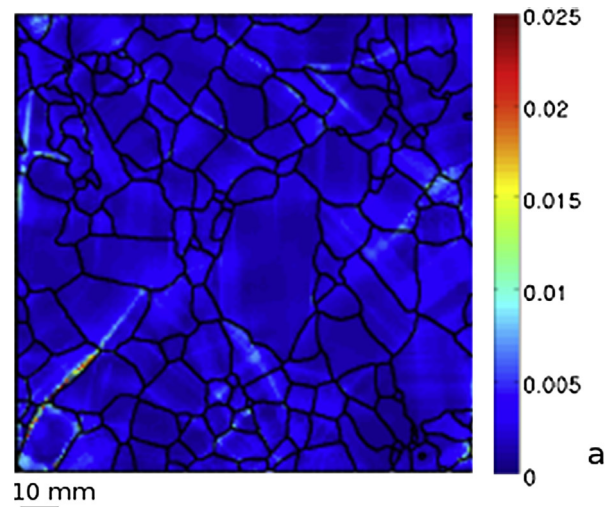


Fig. 20. Evolution of the FFT-simulated equivalent strain field during the transient creep of a “2D-1/2” sample of ice, after (a) 0.15%, (b) 0.35% and (c) 0.60% compressive strain (see Grennerat et al. (2012)).

based on the hypothesis that grains with a high stored energy (highly deformed) are likely to nucleate new grains and become dislocation-free. They may also be invaded by their neighbors which have a lower stored energy. Depending on the relative importance of nucleation and grain boundary migration processes, the recrystallization textures are expected to favor either highly deformed components or less deformed ones.

One must first remember that, in the VPSC scheme, grains are represented by inclusions in a homogenous equivalent medium (HEM). Grain interactions are therefore “averaged” through the interaction between the inclusion and the HEM.

In this model, nucleation is represented by a probability of nucleation P per time increment Δt for each deformation step:

$$P \propto \Delta t \times \exp(-A/E^2) \quad (36)$$

The constant A depends on the grain boundary energy and was taken as an adjustable parameter. E is a proxy of the stored energy, $E \propto \sum_s (\Delta \tau_0^s)$ with $\Delta \tau_0^s$ the variation of the critical resolved shear stress on the system s during the deformation step. This calculation supposes a hardening law for each slip system to be defined. An isotropic hardening law was chosen in the form $\tau_0^s = H \sum_s \dot{\gamma}^s$, with hardening matrix H being isotropic. A threshold was then defined for the minimum strain energy to nucleate, and the new grain completely replaced the old one (same size, same orientation), with a stored energy equal to zero.

The grain boundary migration rate was taken proportional to the difference in stored energy between the grain and the average, *i.e.*, the HEM. The development of the microstructure is therefore a balance between nucleation and growth. Adjustable parameters were varied arbitrarily for comparison purpose.

Applied to ice, this model resulted into weaker fabrics than the one obtained by the classical VPSC tangent approach, mostly because grains near the compression axis disappeared (high stored energy) and only a few girdle grains, and the few grains exactly aligned with the compression axis from the beginning, remained.

Thorsteinsson (2002) included some DRX in its Nearest-Neighbor Interaction (NNI) model described in Section 3. Polygonization associated with rotation (or continuous) recrystallization is accounted for by comparing the resolved shear stress in the crystal ($|\sum_s \tau_s \hat{\mathbf{b}}_s|$) to the applied stress (with τ_s the shear stress on system s , and $\hat{\mathbf{b}}_s$ a unit vector in the direction of the Burgers vector). If the ratio is smaller than a given value, and the dislocation density higher than a given value, then the crystal size is halved and both new grains are rotated by a fixed $\Delta\theta$ of 5° . Grain growth occurs by normal grain growth according to (Gow, 1969; Alley et al., 1986) parabolic law ($D^2 - D_0^2 = Kt$). The grain growth factor K follows an Arrhenius-type dependence on the temperature. To take into account the grain growth associated with the difference in dislocation-stored energy between the grain i and the average, this growth factor was modified into ($\tilde{K} = (E_{\text{disl}}^{av} - E_{\text{disl}}^i)K'$) with K' a constant depending on temperature and impurities.

Migration recrystallization is included in the model by considering the balance between grain-boundary energy, and stored energy associated with dislocations (the stored energy is calculated following (Wenk et al., 1997), as just described, and translated into dislocation density). A crystal recrystallizes (*i.e.* is replaced by a crystal with initial dislocation density ρ_0) when the dislocation energy is higher than the grain-boundary energy. This assumption relies on the hypothesis that stored energy is released by normal grain growth (driven by GB energy), and that dynamic recrystallization only occurs if this relaxation is not efficient enough to decrease the dislocation density. The size of the new crystal is

adjusted with the effective stress following (Guillopé and Poirier, 1979; Jacka and Li, 1994) and its orientation is chosen at random in the range of the “softest” orientations in the applied stress state.

Modeling results were obtained for comparison to a case similar to the GRIP ice core, with vertical compression, and rotation recrystallization dominating. The introduction of polygonization allows for the preferential removal of “hard” grains, which leads to a weaker fabric compared to the “no-recrystallization” case. In particular, when associated with the NNI formulation, the model is able to reproduce fabrics quite similar to those measured along the GRIP ice core at several depths. “Girdle-type” fabric similar to the experimental fabrics, results from the introduction of migration recrystallization. However, parametrization remains weak, in particular the estimation of the dislocation density, and of the recrystallized grain orientations.

The last example presented here is the cellular automaton model for fabric development by Ktitarev et al. (2002) and Faria et al. (2002). The application was mostly to reproduce the fabric measured along deep ice cores, with the assumption of deformation under uniaxial compression. The cellular automaton (CA) frame is especially suitable for simulation of systems represented by a certain number of cells, which are associated with generalized state variables and arranged in regular environment. The considered material is a thin horizontal layer of ice located along the ice core, thin enough so that it is considered homogeneous in the vertical dimension. To discretize the problem according to the CA method, the authors took a one-dimensional lattice of equal cells representing the grains, described by their size, and their orientation. The basic dynamical quantity of the algorithm is the dislocation density. This density increases with deformation and depends on the orientation of the grain. Recrystallization mechanisms proceed when a critical value is reached. Normal grain growth is accounted for following (Gow, 1969) and is the only growth mechanism associated with polygonization mechanisms. The increase in dislocation density is associated with the resolved shear stress on the basal system and the recrystallization model developed by Montagnat and Duval (2000) is used to estimate the evolution of the density in relation with grain size and polygonization mechanisms. Rotation of grains is ruled by a kinematic equation based on the inelastic spin, assuming a compressive stress proportional to the depth along the core, and a linear dependence between the shearing rate of sliding on the basal system and the resolved shear stress. The time evolution was related to the depth along the core using the Dansgaard et al. (1993) relation. Following Duval and Castelnau (1995), migration recrystallization was only applied below 2800 m depth. During migration recrystallization, new grains were allowed to grow much faster by consuming up to ten cells at every time step, until it is impinged by another growing grain, or until it reaches the critical size of the steady state.

The model was able to provide a good qualitative evolution of the grain size, by separating the influence of normal grain growth, polygonization and migration recrystallization similarly to what was suggested from the measurements along the GRIP ice core (Thorsteinsson et al., 1997; de la Chapelle et al., 1998). Concerning the fabric evolution, the model was able to predict the evolution toward a single maximum, but the kinetics is too strongly influenced by the polygonization, and further by migration recrystallization.

5.2. Dynamic recrystallization within full-field approaches

This section presents a coupling between a platform for structural change in materials (Elle) with the full-field FFT approach presented in Section 4.1, to predict the microstructure evolution of ice polycrystals during dynamic recrystallization. A critical step in

the development of generic models linking plastic deformation and recrystallization is the incorporation of the interaction between intra- and intergranular heterogeneities of the micromechanical fields (*i.e.* strain rate and stress) and the recrystallization processes. Because local rotations of the crystal lattice are controlled by local gradients of plastic deformation, heterogeneous distributions of lattice orientations are observed at the grain and subgrain scale, see Section 4. This has a strong influence on recrystallization as this is a process driven by the local gradients of energy (e.g. grain boundary or stored strain energy). Traditional mean-field models used to predict microstructure evolution during recrystallization are based on a simplified description of the medium and cannot fully describe intragranular heterogeneities (Section 5.1). Therefore, explicit full-field approaches are required for a better understanding of dynamic recrystallization and prediction of microstructure evolution at large strain.

5.2.1. The Elle modeling platform

Elle is a platform for the numerical simulation of processes in rocks and grain aggregates, with particular focus on (micro-) structural changes (Jessell et al., 2001; Jessell and Bons, 2002; Bons et al., 2008; Piazzolo et al., 2010). The simulations act on an actual 2D image of the microstructure (Fig. 21a). Elle is currently restricted to 2D cases although the underlying principles for 2D are equally valid in 3D (Becker et al., 2008), and therefore the approach could be converted for 3D simulations.

The central philosophy of Elle is to enable the coupling of processes that act on the material, recognizing that the effect of one process may significantly alter that of a concurrent process. Dynamic recrystallization, for example, can greatly change crystallographic preferred orientations in mineral aggregates deforming by dislocation creep (Jessell, 1988a,b). Coupling of processes is achieved in Elle using the principle of operator splitting, whereby individual processes successively act on the model in isolation, for a small time step. This approach greatly simplifies coding, as the coupling between processes needs not be programmed itself, but emerges from their alternating effect on the model.

Each process in Elle is an individual program or module. A shell-script takes the starting model and then passes it in a loop to the

individual processes, which each in turn modify the model slightly. Each loop represents one time step. The user can freely determine the mix of processes that operate by choosing which ones to include in the loop. The relative activity of individual processes is determined by the parameters passed on to each process.

The model is essentially defined by two types of nodes: boundary nodes (bnodes) and unconnected nodes (unodes) (Fig. 21b). Bnodes define the boundaries of a contiguous set of polygons (termed flynns). These flynns typically represent single grains, but can also represent regions within a material, for example rock layers (Llorens et al., 2012). The boundaries of the flynns are formed by straight segments that connect neighboring bnodes. One bnode can be connected by either two or three other bnodes. The use of bnodes and flynns makes the model suitable for a range of Finite Element and front-tracking models.

Unodes form a second layer of the model. These are nodes that do not necessarily have fixed neighborhood relationships and typically represent points within the material. Some processes are not amenable to be modeled with polygons, but are best simulated with a regular grid of unodes. The FFT code is an example. Nodes and flynns can have a range of attributes assigned to them, such as *c*-axis orientation, boundary properties, etc.

Elle uses fully wrapping boundaries. A flynn that touches one side of the model continues on the other side (Fig. 21a). The model is thus effectively a unit cell that is repeated infinitely in all directions. Although Elle typically uses a square model, deformation may change the unit cell into a parallelogram shape.

Elle now includes a large and ever growing number of process modules for a variety of processes that mostly relate to microstructural developments in mineral aggregates. Each process can essentially act on the model in only two ways: changing the position of a node (e.g. a bnode in case of grain boundary migration) or changing the value(s) of attributes of flynns or nodes (e.g. concentration at an unode in a diffusion simulation). Some of the most relevant current processes are:

- Normal grain growth driven by the reduction of surface energy, and hence curvature of grain boundaries. This process was used by Roessiger et al. (2011) to address the issue of the

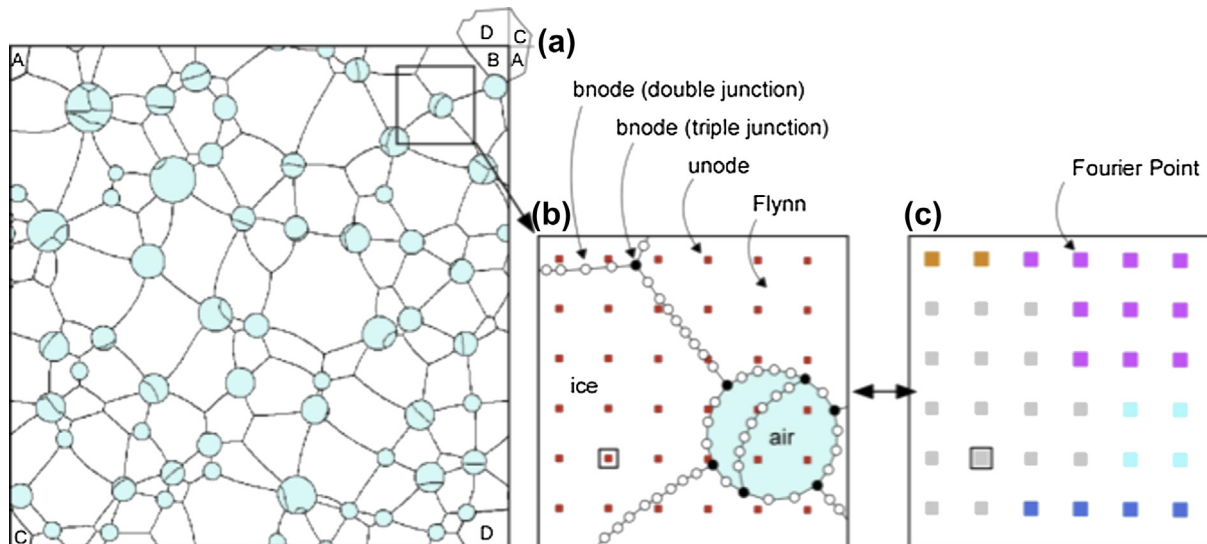


Fig. 21. (a) Example of an Elle model: Ice (white) with air bubbles (pale blue) (Roessiger et al., this volume). The Elle model has fully wrapping boundaries and grains A to D are in fact one single grain. (b) Close-up showing that grains are defined by flynns (polygons), themselves defined by straight segments that connect boundary nodes (bnodes). A second layer of unconnected nodes (unodes) can be added to keep track of material points. (c) For the FFT module, the microstructure is discretized into a periodic, regular mesh of Fourier points defined by a characteristic lattice orientation. A direct mapping between unodes layer and Fourier points is established between both codes.

competition between grain growth and grain size reduction in the upper levels of polar ice caps (Mathiesen et al., 2004). Surface energy can be anisotropic, *i.e.* depend on the lattice orientation of the grains on either side of the boundary (Bons et al., 2001). Two-phase grain growth has been applied to grain growth in rocks with a small proportion of melt (Becker et al., 2008) and to ice with air bubbles (Fig. 21) (Roessiger et al. this volume).

- The Finite Element module Basil is used for incompressible power-law viscous deformation (Barr and Houseman, 1996). Using viscosities that are assigned to flynns, it calculates the stress and velocity fields resulting from applied boundary conditions. It has been used to study the behavior of rigid inclusions in a deforming matrix (Bons et al., 1997), the behavior of deforming two-phase materials as a function of viscosity contrast and composition (Jessell et al., 2009) and for folding of layers (Llorens et al., 2012). The wrapping boundaries of the Elle model, in combination with continuous remeshing allows for arbitrarily high strains (Jessell et al., 2009). In combination with grain growth and dynamic viscosity, Jessell et al. (2005) studied strain localisation behavior. Durand et al. (2004) investigated the influence of uniaxial deformation on grain size evolution in polar ice cores and its influence on ice dating methods.
- Dynamic recrystallization includes grain boundary migration driven by strain energy (dislocation density) and the formation of new grain boundaries by progressive subgrain rotation or polygonisation (Urai et al., 1986). In the next section (5.2.2) we will describe how these processes, employing a front-tracking model for grain-boundary migration, are linked with the FFT approach (Griera et al., 2011, 2013; Piazzolo et al., 2012) to model the stress and strain-rate fields and the driving forces for recrystallization.
- A final Elle module of potential relevance to ice is that developed by Schmatz (2010) for the interaction between migrating grain boundaries and small particles (e.g. dust or clathrates). The particles are represented by unodes, which, when swept by a grain boundary, can latch onto that boundary. Particles can slow down grain boundary movement, but can also be dragged along and eventually be released by a grain boundary.

Summarizing, Elle provides a large number of routines to simulate grain-scale processes in minerals and rocks, and hence in ice. The open and versatile code allows for more process modules to be added or existing ones to be tailored for application to ice. A significant advantage of the code is that it enables the investigation of the complex microstructural and mechanical effects of multiple, concurrent and coupled processes.

5.2.2. Coupling Elle platform to FFT approach

Most of the numerical approaches used to simulate deformation and microstructural evolution of rocks and metals are based on combining deformation approaches based on the Finite Element Method with Monte Carlo, cellular automaton, phase field, network or level-set methods to simulate recrystallization (Jessell, 1988a, b; Raabe and Becker, 2000; Piazzolo et al., 2002, 2010, 2012; Solas et al., 2004; Battaile et al., 2007; Logé et al., 2008). An alternative to these methods is the numerical scheme used in this study based on the coupling between the crystal plasticity FFT-based code (Lebensohn, 2001) (Section 4.1) and the Elle modeling platform just described (Bons et al., 2008). Both codes have been previously explained and here we only concentrate on some particularities of the coupling between them. The FFT-based formulation is integrated within the Elle platform using a direct one-to-one mapping between data structures. The polycrystalline aggregate is discretized into a

periodic, regular array of spaced and unconnected nodes (Fourier Points in the FFT and “unconnected nodes”, unodes, in Elle; Fig. 21).

Numerical simulation is achieved by iterative application of small time steps of each process. After numerical convergence of the FFT model, data is transferred to Elle assuming that the micromechanical fields are constant in the incremental time step. The position and material information of unodes are directly updated because they are equivalent to the Fourier points, while position of boundary nodes (bnodes) are calculated using the velocity field. Based on the evolution of the predicted local lattice rotation field, the dislocation density can be estimated using strain gradient plasticity theory (e.g. Gao et al. (1999); Brinckmann et al. (2006)) or using the dislocation density tensor or Nye tensor (Nye, 1953; Arsenlis and Parks, 1999; Pantleon, 2008). With this approach, only geometrical necessary dislocations required to ensure strain compatibility are estimated. To simplify the problem, we use a scalar approach where all dislocations are assumed to be related to the basal plane. The lattice-orientation and dislocation-density fields provide the input parameters to predict recrystallization in the aggregate.

Recrystallization is simulated by means of three main processes: nucleation, subgrain rotation and grain boundary migration. Using the kinematic and thermodynamic instability criteria of classical recrystallization theory (Humphreys and Hatherly, 2004; Raabe and Becker, 2000), nucleation is simulated by the creation of a small new, dislocation-free flynn when the local misorientation or dislocation density exceeds a defined threshold. The lattice orientation of the new grain is set to that of the critical unode. When a cluster of unodes within a grain share the same orientation that is different from the rest of the unodes in that grain, a new grain boundary is created, while preserving the lattice orientations of the unodes. A technical limitation is that nucleation of grains and subgrains is only allowed along grain boundaries. Nucleation within grains are therefore not possible.

Grain boundary migration is described by a linear relationship between velocity (v) and driving force per unit area (Δf), by $v = M\Delta f$ where M corresponds to the grain boundary mobility, which has an Arrhenius-type dependency on temperature. Grain boundary curvature and stored strain energies are used as driving forces for grain boundary motion. For this situation, the driving force can be defined as

$$\Delta f = \Delta E - 2\gamma/r \quad (37)$$

where ΔE is the difference of stored strain energy across the boundary, γ is the boundary energy and r is the local radius of curvature of the grain boundary. Stored strain energy is the energy per unit volume associated with lattice distortions and depends on the dislocation density (ρ) and dislocation type. Grain boundary motion is simulated using the free-energy minimization front-tracking scheme of Becker et al. (2008). When an unode is swept by a moving grain boundary, it is assumed that dislocations are removed and the new lattice orientation is that of the nearest unode belonging to the growing grain.

Following the Elle philosophy, each process runs individually, following a pre-established sequence. After all Elle processes have run, the unodes layer is used to define the new input microstructure to be deformed viscoplastically by the FFT code. A drawback is that the unodes are not following a regular mesh, a requirement needed by the FFT approach. For this reason, as proposed by Lahellec et al. (2003), and later adapted in the context of Elle by Griera et al. (2011, 2013), a particle-in-cell method is used to remap all material and morphological information to a new regular computational mesh. In order to avoid unrealistic crystallographic orientations, these are not interpolated during remapping. The

crystallographic orientation of a new Fourier Point that belongs to a specific grain is that of the nearest node that belongs to the same grain. This allows to run numerical simulation up to large strains.

5.2.3. Application to creep experiments and natural ice

An example of numerical simulation using the FFT/Elle approach is shown in Fig. 22. The simulation is based on a creep experiment of polycrystalline columnar ice. Samples and experimental conditions are those of (Montagnat et al., 2011) described in Section 4.1.2. The specimen was deformed at $-10\text{ }^{\circ}\text{C}$ under uniaxial conditions with a constant load of 0.5 MPa up to an axial strain of 4%. A thin section of the initial and the final microstructure was analyzed using the Automatic Ice Texture Analyzer method to obtain the local c-axis orientations. After a 4% of shortening, the onset of local recrystallization is evident in the experiment (Fig. 22a), in the form of irregular and serrated grain boundaries and small new grains that are preferentially located at triple junctions and along grain boundaries. Localized variations in the orientation of the basal plane form sharp and straight subgrain boundaries that indicate intracrystalline deformation. The experimental c-axis map was used as input for the FFT/Elle simulation. The experimental starting microstructure was discretized into a grid of 256×256 Fourier points. As only the c-axis orientation is known, the other axes are given a random orientation. Crystal plasticity is described with an incompressible rate-dependent equation for basal, prismatic and pyramidal slip (see Section 3). Critical resolved shear stress for basal slip was set 20 times lower than for non-basal systems. The physical properties used for recrystallization are as follows: mobility $M = 1 \times 10^{-10} \text{ m}^2 \text{ Kg}^{-1} \text{ s}^{-1}$ (e.g. Nasello, 2005), isotropic boundary energy $\gamma = 0.065 \text{ J m}^{-2}$ (Ketcham and Hobbs, 1969), shear modulus $G = 3 \times 10^9 \text{ Pa}$ and critical dislocation density $\rho = 1 \times 10^{12} \text{ m}^{-2}$ (de la Chapelle et al., 1998). Pure shear boundary conditions were imposed with vertical constant strain rate of $-1 \times 10^{-8} \text{ s}^{-1}$ up to a 4% of strain in 1% increments.

The computed orientation map and grain boundary misorientation are shown in Fig. 22b. Several features of the experiment are seen in the numerical simulation, such as the

development of sharp misorientations or kink bands, bulging and serrated grain boundaries, and new grains at triple junction and grain boundaries. There is a good correlation between location of kink bands in the experiment and the simulation. However, the width of kink bands in the simulation is dependent on the numerical resolution. A relationship between grain boundary motion/nucleation and high dislocation-density regions is observed (Fig. 23). Variations in dislocation densities across grain boundaries lead to migration of these boundaries in the direction of the dislocation density gradient. However, some discrepancies are also seen, such as, for example, grain boundary motion (e.g. at the bottom-left part) that was not observed in the experiment. One explanation may be that low and high angle grain boundaries were not differentiated in the simulation and, therefore, both types had similar mobility.

A second example aims to show the strong effect recrystallization can have on the final microstructure. A $10 \times 10 \text{ cm}^2$ microstructure with 1600 grains with random c-axis orientations (Fig. 24a) was deformed to 40% shortening in plane-strain pure shear. The values of mechanical (slip systems, CRSS, etc) and recrystallization (mobility, surface energy, etc) properties are similar to those of the model described before, but adjusted to a natural strain rate of 10^{-12} s^{-1} at about $-30\text{ }^{\circ}\text{C}$. Fig. 24b shows the c-axis and relative misorientation maps for an extreme case with no recrystallization (FFT only). Dominant red and purple colors indicate that the c-axis of crystallites are preferentially oriented at low angles to the shortening direction. Elongated grains are oriented parallel to the stretching direction. Remarkable differences are observed when recrystallization is activated (Fig. 24c). Grain boundaries are smooth and grains larger and more equidimensional. Despite the significant difference in microstructure, both simulations show a single maximum c-axis distribution at low angle to the shortening direction. The strong resemblance of the simulated microstructure with that of natural ice (Thorsteinsson et al., 1997; de la Chapelle et al., 1998; Weikusat et al., 2009) shows the strong potential of modeling of ice deformation based on an actual map of the microstructure.

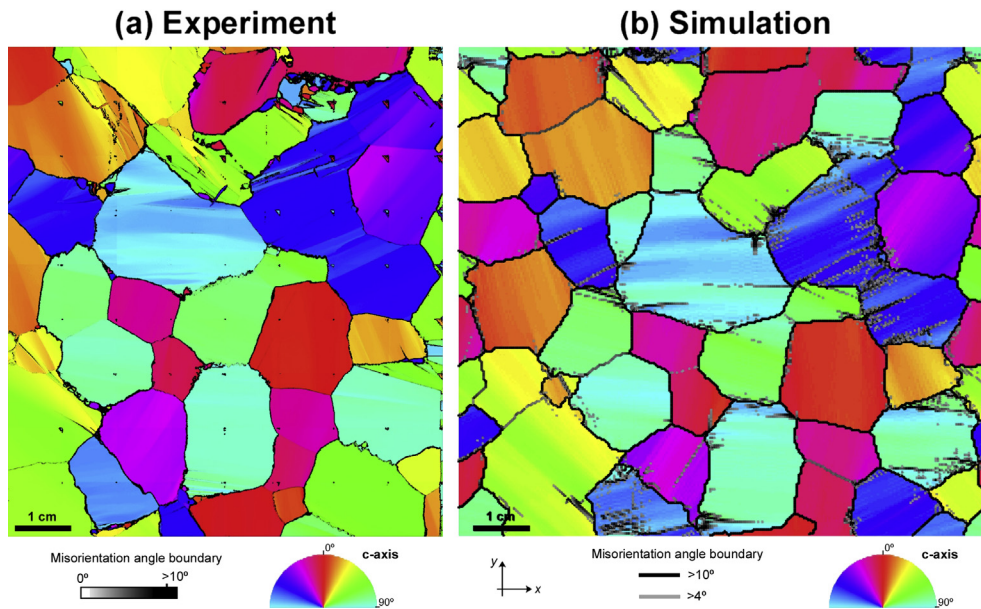


Fig. 22. Comparison of (a) physical experiment and (b) numerical simulation after a vertical shortening of 4%. A qualitative equivalence between experiment and simulation is observable, such as correspondence of kink-bands or discontinuous subgrain boundaries at sharp grain boundaries asperities. Colors indicate the orientation of the c-axis with respect to the sample reference. Misorientation angle between nodes are indicated in gray ($>4^{\circ}$) and black ($>10^{\circ}$). Triangular patches seen in the experiment are due to erroneous misfit during Automatic Ice Texture Analyzer acquisition.

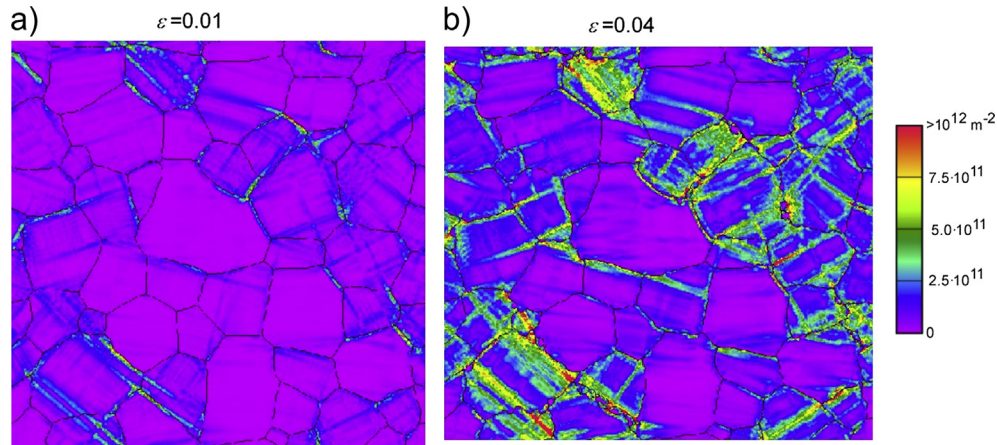


Fig. 23. Dislocation density maps after (a) 1% and (b) 4% of shortening. Grain microstructure is indicated by dark lines. Serrated and bulging grain boundaries develop due to grain boundary migration into regions of high dislocation density. New recrystallized grains develop preferentially at triple points and along grain boundaries. Low dislocation densities are typically observed at bulge areas and new grains.

6. Toward large scale ice flow modeling

A number of models have been developed in glaciology to simulate the flow of anisotropic ice and the strain-induced development of fabric within polar ice-sheets. Accounting for ice anisotropy in an ice-flow model implies to (i) build a macroscopic anisotropic flow law whose response will depend on the local fabric and (ii) have a proper description of the ice fabric at each node of the mesh domain and be able to model the fabric evolution as a function of the flow conditions. We hereafter present the main issues to address these two points.

Due to the scale of these large ice-masses, the implementation of a polycrystalline law must stay simple enough and numerically tractable. At present, full-field or even homogenization models presented previously are computationally too demanding and cannot realistically be used to estimate the mechanical response in an ice-sheet flow model. Here we present two approaches to build a

simple and efficient macroscopic law for polycrystalline ice. The first one is based on the concept of a scalar enhancement factor function so that the collinearity between the strain-rate and the deviatoric stress tensors is conserved (Placidi and Hutter, 2006), see Section 6.1. The second polycrystalline law is fully orthotropic and depends on six relative viscosities, function of the fabric (Gillet-Chaulet et al., 2005, 2006), see Section 6.2. Both models are phenomenological and must be calibrated using experimental or numerical results, as described below.

With regards to other materials, the advantage of the hexagonal symmetry of ice is that the crystal rheology can be assumed transversally isotropic (only true for a linear rheology). Under this assumption, only one unit vector suffices to describe the lattice orientation, thus simplifying the mathematical description of fabrics. With regards to other materials, the advantage of the hexagonal symmetry of ice is that only one unit vector suffices to describe the lattice orientation, thus simplifying the mathematical

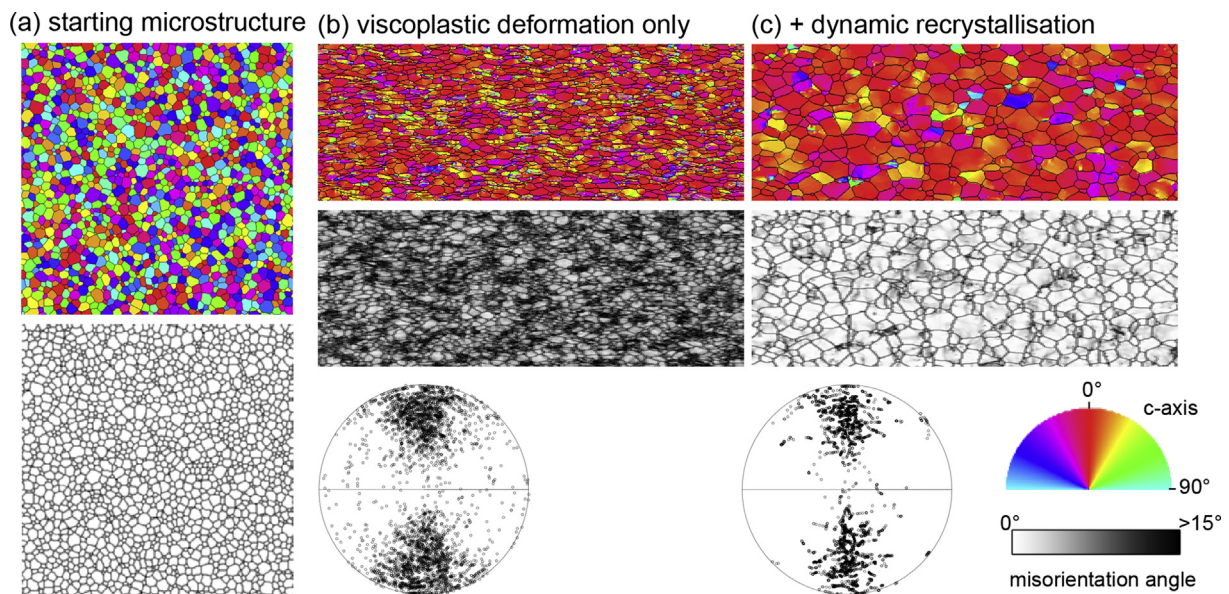


Fig. 24. Numerical simulation of polar ice microstructure using the FFT/Elle scheme. (a) Starting microstructure. (b) 40% vertical shortening with only viscoplastic deformation. (c) 40% shortening with viscoplastic deformation coupled with recrystallization. Top row shows c-axis orientations in color and local misorientation in gray. Bottom row shows local misorientation only. C-axis orientation distributions are shown in lower-hemisphere stereoplots.

description of fabrics. The discrete description of the fabric, *i.e.* a couple of angles for each crystal, would require too large a number of variables to be stored at each node of the domain mesh. Typical mesh size are hundreds of thousand nodes in 3D (Seddik et al., 2011) up to few millions for the most recent applications (Gillet-Chaulet et al., 2012). The use of a parameterized orientation distribution function (ODF) would decrease the number of parameters, but evolution equations for these parameters to describe the fabric evolution cannot be obtained in a general case (Gagliardini et al., 2009). The orientation tensors, which describe the fabric at the macroscopic scale in a condensed way are more suitable. Five parameters are needed to describe an orthotropic fabric (the two eigenvalues of the second-order orientation tensor and the three Euler angles to specify the position of the material symmetry basis), and an evolution equation for the second-order orientation tensor can be easily derived from the macroscopic stress and strain-rate fields.

6.1. Continuous diversity and the CAFFE model

The CAFFE model (Continuum-mechanical Anisotropic Flow model based on an anisotropic Flow Enhancement factor) results from a suitable combination of two basic concepts: a power law description of ice rheology resembling the well-known Glen's flow law Glen (1955); and a multiscale approach to model the evolution of the polycrystalline microstructure of ice based on the general theory of continuous diversity (Faria, 2001; Faria and Hutter, 2002; Faria et al., 2003).

The ideas leading to the CAFFE model have been elaborated in a series of works by Luca Placidi and his collaborators (Placidi, 2004, 2005; Placidi and Hutter, 2005, 2006; Placidi et al., 2004). These ideas culminated in the definitive CAFFE formulation, presented by Placidi et al. (2010), in which the so-called enhancement factor of Glen's flow law becomes a function of the material anisotropy (fabric), and the evolution of the latter is governed by an orientation-dependent mass balance equation derived from the theory of continuous diversity applied to glacier and ice-sheet dynamics (Faria, 2006a,b; Faria et al., 2006).

The greatest strength of the CAFFE model is its successful compromise between accuracy and flexibility, which allows one to upgrade existing computer models of isotropic ice-sheet dynamics based on Glen's flow law into efficient anisotropic models, without profound changes in the original code. In fact, due to its relative simplicity, the CAFFE model has already been implemented in several numerical ice-flow simulations. For instance, it has been used by Seddik et al. (2008) and Bargmann et al. (2011) to simulate the ice flow at the site of the EPICA-DML drill site at Kohnen Station, Dronning Maud Land, East Antarctica, while Seddik et al. (2011) used it to simulate the ice flow in the vicinity of the Dome Fuji drill site in central East Antarctica.

In the following, we review the CAFFE formulation presented by Placidi et al. (2010). The fundamental idea is to regard polycrystalline ice as a "mixture" of lattice orientations, following the philosophy of the theory of Mixtures with Continuous Diversity (MCD) proposed by Faria (2001, 2006a). Succinctly, a mixture with continuous diversity is a multicomponent medium made up of an infinite number of mutually interacting species, whose distinctive properties vary smoothly from one to another.

In the case of polycrystalline ice, species are distinguished by their *c*-axis orientations. Each point of the continuous body is interpreted as a representative volume element, which encompasses a large number of crystallites with their own *c*-axis orientations. Each of such orientations is mathematically identified with a point on the surface of the unit sphere S^2 and represented by a unit vector $\mathbf{n} \in S^2$. As a consequence, for each species one can

introduce a mass density field $\varrho^*(\mathbf{x}, t, \mathbf{n})$, given at a certain position \mathbf{x} within the polycrystal, and at time t , sometimes called orientational mass density, such that, when integrated over the whole unit sphere, the usual mass density field of the polycrystal (*i.e.* of the "mixture") results:

$$\varrho(\mathbf{x}, t) = \int_{S^2} \varrho^*(\mathbf{x}, t, \mathbf{n}) d^2n, \quad (38)$$

where $d^2n (= \sin\theta d\theta d\varphi$ in spherical coordinates) is the infinitesimal solid angle on the unit sphere S^2 . The product $\varrho^*(\mathbf{x}, t, \mathbf{n}) d^2n$ is the mass fraction of crystalline material in the volume element with *c*-axis directed toward \mathbf{n} within the solid angle d^2n . Therefore, assuming that the material is incompressible, the mass (or volume) fraction ϱ^*/ϱ can be interpreted as the usual orientation distribution function (ODF) in the context of materials science (Bunge, 1993; Zhang and Jenkins, 1993; Raabe and Roters, 2004). It should be remarked that in the glaciological literature the term "ODF" sometimes refers to the relative number, instead of the mass (or volume) fraction, of grains with a certain orientation.

The time evolution of ϱ^* is governed by the balance equation of species (orientational) mass

$$\frac{\partial \varrho^*}{\partial t} + \text{div}(\varrho^* \mathbf{v}) + \text{div}_{\mathbf{n}}(\varrho^* \mathbf{u}^*) = \varrho^* \Gamma^* \quad (39)$$

with

$$\text{div}_{\mathbf{n}}(\Phi^*) = \text{tr}[\text{grad}_{\mathbf{n}}(\Phi^*)], \quad \text{grad}_{\mathbf{n}}(\Phi^*) = \frac{\partial \Phi^*}{\partial \mathbf{n}} - \left(\frac{\partial \Phi^*}{\partial \mathbf{n}} \cdot \mathbf{n} \right) \mathbf{n} \quad (40)$$

for any scalar-, vector- or tensor-valued field $\Phi^*(\mathbf{x}, t, \mathbf{n})$. In (39), $\mathbf{u}^*(\mathbf{x}, t, \mathbf{n})$ denotes a sort of "velocity" on the unit sphere (with $\mathbf{u}^* \cdot \mathbf{n} = 0$), called orientational transition rate. Further, $\Gamma^*(\mathbf{x}, t, \mathbf{n})$ is the specific recrystallization rate, which describes the rate of change of mass (per unit mass) of one species into another one with different orientation. Integration of (39) over the unit sphere S^2 gives rise to the usual mass balance equation for the polycrystal (*i.e.* the "mixture")

$$\frac{\partial \varrho}{\partial t} + \text{div}(\varrho \mathbf{v}) = 0 \quad \text{with} \quad \int_{S^2} \varrho^* \Gamma^* d^2n = \int_{S^2} \text{div}_{\mathbf{n}}(\varrho^* \mathbf{u}^*) d^2n = 0, \quad (41)$$

Notice that the first integral in (41) is a consequence of mass conservation, while the second integral follows from Gauss' theorem.

As shown by Faria (2001, 2006a) and Faria and Hutter (2002), the transition rate \mathbf{u}^* is governed by its own balance equation, involving couple stresses and body couples. In the development of the CAFFE model, however, an abridged approach has been adopted by postulating a constitutive equation for the transition rate

$$\mathbf{u}^* = \mathbf{W} \mathbf{n} - \iota [\dot{\mathbf{e}} \mathbf{n} - (\mathbf{n} \cdot \dot{\mathbf{e}} \mathbf{n}) \mathbf{n}] - \frac{\lambda}{\varrho^*} \text{grad}_{\mathbf{n}}(\varrho^* H^*) \quad (42)$$

where

$$\mathbf{W} = \frac{1}{2} (\text{grad} \mathbf{v} - (\text{grad} \mathbf{v})^T), \quad \dot{\mathbf{e}} = \frac{1}{2} (\text{grad} \mathbf{v} + (\text{grad} \mathbf{v})^T) \quad (43)$$

are the tensors of rotation and strain rate, respectively. The first term on the right hand side of (42) represents a rigid-body

rotation, while the second term describes the process of strain-induced lattice rotation (Dafalias, 2001), with $\iota > 0$ denoting the so-called “shape factor” of the theory of rotational diffusion (Faria, 2001). According to Placidi et al. (2010), fabric evolution simulations of the GRIP and EPICA-DML ice cores suggest that best results are obtained for $0.6 > \iota > 0.4$. Finally, the third term on the right hand side of (42) models rotation recrystallization as a diffusive process, with $\lambda > 0$ being the orientational diffusivity and $H^*(\mathbf{x}, t, \mathbf{n})$ an orientational (“chemical”) potential, also called “hardness function” by Gödert (2003). In principle H^* should be a constitutive function, but, based on microstructural analyses of the NorthGRIP ice core (Durand et al., 2008), Placidi et al. (2010) suggest that one may simply set $H^* = 1$.

In the original application of the MCD theory to the flow of glaciers and ice sheets (Faria, 2006b), the specific recrystallization rate Γ^* is regarded as a dissipative variable. However, for simplicity, in the CAFFE model Placidi (2004, 2005) has proposed the following relation between Γ^* and the strain rate

$$\Gamma^* = G(D^* - D), \quad \text{with} \\ D^* = 5 \frac{(\dot{\mathbf{e}}\mathbf{n})^2 - (\mathbf{n} \cdot \dot{\mathbf{e}}\mathbf{n})^2}{\text{tr}(\dot{\mathbf{e}}^2)} \quad \text{and} \quad D = \frac{1}{\varrho} \int_{S^2} \varrho^* D^* d^2n, \quad (44)$$

where $G > 0$ is a material parameter, while $5/2 \geq D^* \geq 0$ and $5/2 \geq D \geq 0$ are called the species and polycrystal “deformability”, respectively.

As remarked by Placidi et al. (2010), owing to the difficulties in determining the values of the material parameters λ and G from experiments, they are usually determined by fitting numerical simulations of ice core fabrics and grain stereology. This concludes the description of the fabric evolution.

As for the flow law, in contrast to the full stress–strain rate relation with tensorial fluidity (viscosity) predicted by the theory of continuous diversity (Faria, 2006b), the CAFFE model adopts a much simplified generalization of Glen’s flow law:

$$\dot{\mathbf{e}} = E(D)A(T)\sigma_{\text{eq}}^{n-1}\boldsymbol{\sigma}', \quad (45)$$

where $\boldsymbol{\sigma}'$ is the deviatoric part of the Cauchy stress tensor $\boldsymbol{\sigma}$, σ_{eq} is the effective stress invariant, n is the power law exponent (usually set equal 3), T is the temperature, and $A(T)$ is a temperature-dependent rate factor. Clearly, (45) implies that all anisotropy effects are contained in the scalar-valued, deformability-dependent flow enhancement factor $E(D)$, such that stress and strain rate are collinear and (45) reduces to the classical form of Glen’s flow law when $E(D) \equiv \text{const}$.

A detailed functional form for the enhancement factor $E(D)$ has been proposed by Seddik et al. (2008) and Placidi et al. (2010), which is continuously differentiable at $D = 1$ and is compatible with the experimental results of Azuma (1995) and Miyamoto (1999)

$$E(D) = \begin{cases} (1 - E_{\min})D^\zeta + E_{\min} & 1 \geq D \geq 0, \\ \frac{4D^2(E_{\max} - 1) + 25 - 4E_{\max}}{21} & 5/2 \geq D > 1, \end{cases} \quad (46)$$

with

$$\zeta = \frac{8}{21} \left(\frac{E_{\max} - 1}{1 - E_{\min}} \right), \quad E_{\max} \approx 10, \quad E_{\min} \approx 0.1. \quad (47)$$

By introducing the orientation tensors (essentially equivalent to the dipole and quadrupole moments of ϱ^*/ϱ)

$$\mathbf{a}^{(2)} = \frac{1}{\varrho} \int_{S^2} \varrho^* \mathbf{n} \otimes \mathbf{n} d^2n, \quad \mathbf{a}^{(4)} = \frac{1}{\varrho} \int_{S^2} \varrho^* \mathbf{n} \otimes \mathbf{n} \otimes \mathbf{n} \otimes \mathbf{n} d^2n \quad (48)$$

Faria (2008) could show that the CAFFE model can be applied to all anisotropies (fabrics) that can satisfactorily be represented by a multipole expansion up to fourth order, as are most anisotropies observed in glaciers and ice sheets.

$$\dot{\mathbf{e}} = \widehat{E}(\boldsymbol{\sigma}')A(T)\sigma_{\text{eq}}^{n-1}\boldsymbol{\tau}, \quad (49)$$

6.2. GOLF law and Elmer/Ice

In this section, we present the anisotropic ice flow model developed at LGGE. This model has been used for various applications (Gillet-Chaulet et al., 2005, 2006; Durand et al., 2007; Martín et al., 2009; Ma et al., 2010). In this approach, the fabric is described using the second and fourth-order orientation tensors (48). In this continuum description of the fabric, the polycrystal represents the local behavior of a representative elementary ice volume. By assuming that the fourth-order orientation tensor $\mathbf{a}^{(4)}$ is given as a tensorial function of $\mathbf{a}^{(2)}$ (Gillet-Chaulet et al., 2005), the fabric can be described in a very condensed way using $\mathbf{a}^{(2)}$ solely. By definition, $\text{tr}\mathbf{a}^{(2)} = 1$, so that only the first two eigenvalues $a_1^{(2)}$ and $a_2^{(2)}$ and three Euler angles are needed to completely define the fabric. As a consequence, modeled fabrics are orthotropic, *i.e.* the c -axes distribution presents three orthogonal symmetry planes. Although orthotropy is a simple form of the most general anisotropy, it is thought to be a good compromise between physical adequateness and simplicity. The second-order orientation tensor allows to describe all the observed fabric patterns: for random c -axes distribution the diagonal entries of $\mathbf{a}^{(2)}$ are $a_{11}^{(2)} = a_{22}^{(2)} = a_{33}^{(2)} = 1/3$, for a single maximum fabric with its maximum in the third direction, $a_{33}^{(2)} > 1/3$ and $a_{11}^{(2)} \approx a_{22}^{(2)} < 1/3$, and for a girdle type fabric in the plane (x_1, x_2) , $a_{33}^{(2)} < 1/3$ and $a_{11}^{(2)} \approx a_{22}^{(2)} > 1/3$. When the material symmetry axes are those of the general reference frame, as for the three particular previous fabrics, the non-diagonal entries of $\mathbf{a}^{(2)}$ are zero.

The behavior of the polycrystal is described by the general orthotropic linear flow law GOLF (Gillet-Chaulet et al., 2005). In its initial form, ice was assumed to behave as a linearly viscous orthotropic material. In more recent works (Martín et al., 2009; Ma et al., 2010), the GOLF law has been extended to a nonlinear form by adding an invariant in the anisotropic linear law. The simple choice is either to add the second invariant of the strain rate (Martín et al., 2009) or the second invariant of the deviatoric stress (Pettit et al., 2007). No theoretical or experimental results are available today to discard one of these two solutions, and other solutions based on anisotropic invariants of the deviatoric stress and/or the strain rate are also possible. In (Ma et al., 2010) approach, the nonlinearity of the law is introduced through the second invariant of the deviatoric stress. With this definition, the anisotropy factors of the polycrystalline law for a given stress are identical in the linear and nonlinear cases. In other words, for a given fabric and a given state of stress, the corresponding strain rate relative to the isotropic response is the same for the linear and nonlinear cases. Using the strain-rate invariant in the same way as Martín et al. (2009) did, leads to different anisotropy factors (as defined here) in the linear and nonlinear

cases. Therefore, the proposed expression of the nonlinear GOLF law is as follows:

$$\sum_{r=1}^3 [\eta_r \text{tr}(\mathbf{M}_r \cdot \dot{\boldsymbol{\epsilon}}) \mathbf{M}'_r + \eta_{r+3} (\dot{\boldsymbol{\epsilon}} \cdot \mathbf{M}_r + \mathbf{M}_r \cdot \dot{\boldsymbol{\epsilon}})'] = 2A\sigma_{\text{eq}}^{n-1} \boldsymbol{\sigma}', \quad (50)$$

where A is the temperature-dependent Glen's law parameter for isotropic ice. The six dimensionless anisotropy viscosities $\eta_r(\mathbf{a}^{(2)})$ and $\eta_{r+3}(\mathbf{a}^{(2)})$ ($r = 1, 2, 3$) are functions of the eigenvalues of the second-order orientation tensor $\mathbf{a}^{(2)}$, which represent a measure of the anisotropy strength. The three structure tensors \mathbf{M}_r are given by the dyadic products of the three eigenvectors of $\mathbf{a}^{(2)}$, which then represent the material symmetry axes. In the method proposed by Gillet-Chaulet et al. (2005), the six dimensionless viscosities $\eta_r(\mathbf{a}^{(2)})$ are tabulated as a function of the fabric strength (i.e., the $a_i^{(2)}$) using a micro-macro model. When ice is isotropic, $\eta_r = 0$ and $\eta_{r+3} = 1$ ($r = 1, 2, 3$), and Eq. (50) reduces to the isotropic Glen's flow law.

Following Gillet-Chaulet et al. (2005), the six dimensionless viscosities $\eta_r(\mathbf{a}^{(2)})$ are tabulated using the visco-plastic self-consistent model (VPSC, Castelnau et al., 1996a, 1998), see Section 3. The two crystal parameters in the VPSC model used to tabulate the GOLF law were chosen so that the experimentally observed polycrystal anisotropy is reproduced. Gillet-Chaulet et al. (2005) use the shear-strain rates ratio for a polycrystal with a single maximum fabric and an isotropic polycrystal both experiencing the same shear stress. This anisotropy factor in shear is hereafter noted k_s and, according to the experimental results of Pimienta et al. (1987), its value is approximately $k_s = 10$. In other words, the VPSC parameters are chosen so that the response under simple shear of a polycrystal with a single maximum fabric is k_s times easier to deform than the corresponding isotropic polycrystal. The experimental results of Pimienta et al. (1987) also indicate that an isotropic polycrystal is much easier to deform than a single maximum fabric polycrystal experiencing the same uniaxial compressional stress. These experiments allow to define a second anisotropy factor for uniaxial compressional stress, which is noted k_c . A value $k_c = 0.4$ is in accordance with the experimental results of Pimienta et al. (1987). As discussed before, the anisotropy factors k_s and k_c are independent of Glen's flow law exponent n with the adopted nonlinear formulation.

Assuming that recrystallization processes do not occur and that the ice fabric is induced solely by deformation, the evolution of the second-order orientation tensor $\mathbf{a}^{(2)}$ can be written as

$$\frac{D\mathbf{a}^{(2)}}{Dt} = \mathbf{W} \cdot \mathbf{a}^{(2)} - \mathbf{a}^{(2)} \cdot \mathbf{W} - (\mathbf{C} \cdot \mathbf{a}^{(2)} + \mathbf{a}^{(2)} \cdot \mathbf{C}) + 2\mathbf{a}^{(4)} : \mathbf{C}, \quad (51)$$

where \mathbf{W} is the spin tensor defined as the antisymmetric part of the velocity gradient. The tensor \mathbf{C} is defined as

$$\mathbf{C} = (1 - \alpha)\dot{\boldsymbol{\epsilon}} + \alpha k_s A \sigma_{\text{eq}}^{n-1} \boldsymbol{\sigma}'. \quad (52)$$

The *interaction parameter* α controls the relative weighting of the strain rate $\dot{\boldsymbol{\epsilon}}$ and the deviatoric stress $\boldsymbol{\sigma}'$ in the fabric evolution Eq. (51). When $\alpha = 0$, the fabric evolution is solely controlled by the state of strain rate, whereas in the case where $\alpha = 1$ the fabric evolves under the influence of the deviatoric stress solely. In between, as for the VPSC approach, both the strain rate and deviatoric stress contribute to the fabric evolution. In what follows, the interaction parameter is $\alpha = 0.06$ in accordance with the crystal anisotropy and the VPSC model used to derive the polycrystal behavior (Gillet-Chaulet et al., 2005). In Eq. (51), the fourth-order orientation tensor is evaluated assuming a closure approximation giving $\mathbf{a}^{(4)}$ as a tensorial function of $\mathbf{a}^{(2)}$ (Gillet-Chaulet et al., 2005).

The anisotropic polycrystalline law described above and the associated fabric evolution equations have been implemented in the Finite Element code Elmer/Ice, the glaciological part of the open source Finite Element software Elmer developed by CSC (<http://www.elmerfem.org/>). Ice flow (velocity and isotropic pressure) are obtained solving the anisotropic Stokes equations and coupled with the fabric evolution Equation (51) and the upper free surface equation in the case of transient simulations. In Gillet-Chaulet et al. (2006), the model was applied to synthetic geometries in order to show the influence of coupling the Stokes and fabric evolution equations on the flow of ice over a bumpy bedrock. In Durand et al. (2007), the model was used to explain the fabric evolution in the Dome C ice core, in the framework of the EPICA project. The authors showed that to explain the fabric evolution at Dome C, shear stress must be invoked. The model was also applied to evaluate the value of the ad-hoc enhancement factor that should be incorporated in large-scale isotropic ice-sheet flow model in Ma et al. (2010). In Martín et al. (2009), the anisotropic ice flow model was applied to explain observed shapes of isochrones below ridges or domes.

7. Synthesis and perspectives

Applications of ice mechanical behavior modeling extend from below the single-crystal scale to the ice sheet scale. This scale range far exceeds that of engineering material sciences but is similar to the geological one. Within this scale range, many physical processes come into play, some of which are not yet very well described. Furthermore, there exist strong interactions between these processes that create bridges between the different levels of complexity. Modeling of ice has strongly benefited from advances in materials science. In return, as shown by the results presented in this paper, the contribution of the ice community to the theoretical understanding and modeling of the mechanical behavior of anisotropic materials is significant. With the large viscoplastic anisotropy of the ice crystal, ice is now considered as a model material. The advances presented here may equally well be applied to, for example, mantle flow, where the anisotropy due to fabric (CPO) development in olivine is thought to play a significant role (Tommasi et al., 2009; Long and Becker, 2010).

The presented modeling methods are basically of two types; some that aim to precisely reproduce the physical mechanisms as observed experimentally, and some with a more phenomenological approach. Going through scales, it clearly appears that individual dislocation interactions cannot be taken into account at the scale of the polycrystal imbedded in a glacier environment. Nevertheless, modeling at the scale of dislocation interactions provides a better estimate of the interactions between slip systems at the single crystal scale, which, in turn, is essential to reproduce an accurate mechanical response of the polycrystal with mean-field and full-field approaches. Furthermore, full-field approaches are necessary to validate the approximations made using mean-field models, as they provide the "exact" (in a numerical sense) response of the specimen with a real microstructure, integrating the inter- and intra-granular interactions. Finally, large-scale flow models are now getting to a sufficient level of complexity to be able to take into account and represent the anisotropy associated with the fabrics induced by the flow conditions. To do so, they integrate mean-field approaches that correctly reproduce the viscoplastic anisotropy and a non-linear mechanical behavior.

A summary of the main domains of application, advantages, and limitations of the main modeling tools presented in the paper is given on Tables 2–4

Much progress has recently been made in the modeling of dynamic recrystallization processes and their interactions with flow anisotropy. Nevertheless, due to the complexity of the physical

Table 2
Summary of techniques application domains, interest and limitations. DD: Dislocation Dynamics, FDM: Field Dislocation Mechanics, VPSC: Homogenized Polycrystal Visco-Plasticity, EVPSC: Homogenized Polycrystal Elasto-Visco-Plasticity.

| Model | Scale | Type | Applications | Advantages | Limitations |
|-------|-----------------------------|---------------------|---|---|--|
| DD | Single crystal (mesoscopic) | Finite Element (FE) | Dislocation dynamics and interactions | Solve physics of plasticity at the dislocation scale – Provide slip system activities and interactions | Computing time-intensive. Small samples. Simplified configurations |
| FDM | Single to poly-crystal | Full-field (FE) | Plasticity modeling taking into account heterogeneous internal stress field associated with dislocations | Length scaling, makes the link between the complexity of the dislocation field dynamics and the macroscopic behavior – Provide intra-crystalline fields | Computing time-intensive – Limited number of grains |
| VPSC | Polycrystal | Mean-field | Provides effective visco-plastic behavior of polycrystals, based on a given single-crystal behavior | Texture-induced polycrystal anisotropy, texture evolution for secondary creep, can reach large strains | Very limited information on intra-crystalline fields, elasticity and recrystallization neglected |
| EVPSC | Polycrystal | Mean-field | Provides effective elasto-visco-plastic behavior at polycrystal level, based on known single-crystal behavior | Captures texture-induced anisotropy during transient creep regime | Very limited information on intra-crystalline fields, limited to small strains |

Table 3
Summary of techniques application domains, interest and limitations. DRX: dynamic recrystallization, VPFFT: FFT-based formulation for visco-plastic polycrystals, EVPFFT: FFT-based formulation for Elasto-visco-plastic polycrystals.

| Model | Scale | Type | Applications | Advantages | Limitations |
|--------------|-------------|------------|--|---|---|
| VPSC + DRX | Polycrystal | Mean-field | DRX mechanisms with phenomenological laws, fabric evolution | Fast to run for high strain – easily adaptable to various DRX laws | Too simplified description of DRX mechanisms. No account for intra-crystalline fields |
| VPFFT | Polycrystal | Full-field | Provides effective visco-plastic behavior and local intra- crystalline fields, 2D and 3D | Microstructural effects on local fields distribution in the secondary creep regime | Microstructure evolution at large strains can only be captured in a crude way. No elasticity and DRX |
| EVPFFT | Polycrystal | Full-field | Provides effective elasto-visco-plastic behavior and local intra-crystalline fields, 2D and 3D | Microstructural effects on local fields distribution and their evolution during transient creep | Limited to small strains, no microstructure evolution yet, no DRX |
| VPFFT – Elle | Polycrystal | Full-field | Provides local intra-crystalline fields and microstructure evolution in 2D | Couple local field predictions to DRX mechanisms in the secondary creep regime | No account for local field evolution during transient creep. Limited to 2D (Elle). Rough update of the dislocation field during DRX |

Table 4
Summary of techniques application domains, interest and limitations. DRX: dynamic recrystallization.

| Model | Scale | Type | Applications | Advantages | Limitations |
|---|-------------|---|--|--|--|
| Mixture with continuous diversity (MCD) | Large scale | General continuum theory | General overview of the interactions between microstructure evolution, DRX and ice flow | Effects of microstructure and its evolution via internal variables. Secondary and tertiary creep regimes. Thermodynamically consistent | Mathematically complex. Not implemented numerically yet |
| CAFFE | Large Scale | Continuum model | Provides effective visco-plastic behavior on the large scale, including fabric development | Captures the effects of fabric development in the secondary and tertiary creep regimes, easy to implement | Stress and strain rate are colinear (scalar effective viscosity). Limited to fabrics represented by a multipole expansion up to fourth order only. |
| GOLF law | Polycrystal | Phenomenological orthotropic non-linear law | Provides orthotropic viscous behavior and fabric development | Efficient, easy-to-use and able to reproduce the response of micro-macro models | Orthotropic fabric restricted to the assumed closure approximation. Non-linear case not validated against micro-macro models yet |
| Elmer/Ice | Large scale | FE code including GOLF and CAFFE law | Flow of anisotropic polar ice and its fabric evolution | Fabric evolution consistent with the stress field and strain-rate field | Cannot be used to simulate the localization of the deformation (diffusion of the fabric induced by interpolation) |

processes involved, to jump the gap between scales is a strong challenge. The field dislocation mechanics approach appears very promising to associate the internal stress field and dislocation arrangements to the nucleation and grain boundary migration mechanisms. However, field dislocation mechanics cannot yet be applied to scales larger than the polycrystal. Full-field models, including the FFT-Elle coupling, have the same scale limitation, but may play an important role in parameterizing small-scale processes (dislocation glide, grain boundary migration, etc.) for mean-field models. They are also important tools to test models of mechanical and microstructural evolution.

Compared to other minerals, ice shows a remarkably strong transient behavior (Duval et al., 1983; Castelnau et al., 2008b). Continuum flow models, such as Glen law (Glen, 1955) have so far not been able to incorporate the resulting mechanical complexity of polycrystalline ice deformation. Only recently have mechanical models reached a level of sophistication to address transient behavior. This development is promising and probably highly relevant in cases where ice flow changes at rates for where both elastic and viscoplastic behavior may interact. In particular, this concerns the very topical subject of ice shelves, ice streams or extra-terrestrial ice submitted to tide forcing. Which model will be able to correctly take into account these transient, and event cyclic behavior, and at which scale?

A next step will likely be the multi-scale coupling of models of increasing complexity. We can expect dislocation dynamics and field dislocation mechanics to provide the local criteria for slip system interactions, nucleation, grain boundary migration as local input to full-field approaches that will be further used in interaction with mean-field approaches to calibrate dynamic recrystallization variables influencing the mechanical response and fabric development.

An interesting example of such model interweaving is given by the large-scale flow modeling presented in this paper. Nevertheless, a strong effort is still required concerning the flow law of ice and its dependency on fabrics (CPO) and strain. Recent velocity measurements in Greenland (Gillet-Chaulet et al., 2011) questioned the relevance of a stress exponent equal to three as classically considered for large scale flow modeling (for instance Paterson (1994); Hooke (2005); Greve and Blatter (2009), ...). Owing to the variety of processes that accommodate strain along an ice core path, one could also expect several regimes to occur with depth, as suggested by some authors (see for instance Lipenkov et al. (1989); Faria et al. (2009); Pettit et al. (2011)). Such modeling – observation comparisons mainly raise the complexity of the physical processes involved that can probably not be summarized in a single universal law.

Acknowledgment

Financial support by the French “Agence Nationale de la Recherche” is acknowledged (project ELVIS, #ANR-08-BLAN-0138). Together with support from institutes INSIS and INSU of CNRS, and UJF – Grenoble 1, France. PDB and JR gratefully acknowledge funding by the German Research Foundation (DFG, project BO-1776/7). The authors gratefully acknowledge the ESF Research Networking Programme Micro-Dynamics of Ice (MicroDICE).

References

Acharya, A., 2001. A model of crystal plasticity based on the theory of continuously distributed dislocations. *J. Mech. Phys. Solids* 49 (4), 761–784.
 Acharya, A., Roy, A., 2006. Size effects and idealized dislocation microstructure at small scales: predictions of a phenomenological model of mesoscopic field dislocation mechanics: Part I. *J. Mech. Phys. Solids* 54 (8), 1687–1710.

Alley, R.B., 1988. Fabrics in polar ice sheets – development and prediction. *Science* 240, 493–495.
 Alley, R.B., 1992. Flow-law hypotheses for ice-sheet modeling. *J. Glaciol.* 38 (129), 245–255.
 Alley, R.B., Perepezko, J.H., Bentley, C.R., 1986. Grain growth in polar ice: I. theory. *J. Glaciol.* 32 (112), 415–424.
 Arsenlis, A., Parks, D.M., 1999. Crystallographic aspects of geometrically-necessary and statistically-stored dislocation density. *Acta Materialia* 47, 1597–1611.
 Ashby, M.F., Duval, P., 1985. The creep of polycrystalline ice. *Cold Reg. Sci. Tech.* 11, 285–300.
 Azuma, N., 1994. A flow law for anisotropic ice and its application to ice sheets. *Earth Planetary Sci. Lett.* 128 (3a–4), 601–614.
 Azuma, N., 1995. A flow law for anisotropic polycrystalline ice under uniaxial compressive deformation. *Cold Reg. Sci. Tech.* 23, 137–147.
 Azuma, N., Higashi, A., 1985. Formation processes of ice fabric pattern in ice sheets. *Ann. Glaciol.* 6, 130–134.
 Bargmann, S., Seddik, H., Greve, R., 2011. Computational modeling of flow-induced anisotropy of polar ice for the EDML deep drilling site, Antarctica: the effect of rotation recrystallization and grain boundary migration. *Int. J. Numer. Anal. Meth. Geomech.* <http://dx.doi.org/10.1002/nag.1034>.
 Barnes, P., Tabor, D., Walker, J., 1971. The friction and creep of polycrystalline ice. In: *Proceeding of the Royal Society of London Series A, Mathematical and Physical Sciences*, vol. 324 (1557), pp. 127–155.
 Barr, T., Houseman, G., 1996. Deformation fields around a fault embedded in a non-linear ductile medium. *Geophys. J. Int.* 125, 473–490.
 Battaile, C., Counts, W., Wellman, G., Buchheit, T., Holm, E., 2007. Simulating grain growth in a deformed polycrystal by coupled finite-element and microstructure evolution modeling. *Metallurgical Mater. Trans. A* 38, 2513–2522. <http://dx.doi.org/10.1007/s11661-007-9267-6>.
 Becker, J.K., Bons, P.D., Jessell, M.W., 2008. A new front-tracking method to model anisotropic grain and phase boundary motion in rocks. *Comput. Geosciences* 34, 201–212.
 Bobeth, M., Diener, G., 1987. Static and thermoelastic field fluctuations in multi-phase composites. *J. Mech. Phys. Solids* 35, 137–149.
 Boehler, J.P., Aoufi, L.E., Raclin, J., 1987. On experimental testing methods for anisotropic materials. *Res. Mech.* 21, 73–95.
 Bons, P.D., Barr, T.D., ten Brink, C.E., 1997. The development of delta-clasts in non-linear viscous materials: a numerical approach. *Tectonophysics* 270, 29–41.
 Bons, P.D., Jessell, M.W., Evans, L., Barr, T.D., Stüwe, K., 2001. Modelling of anisotropic grain growth in minerals. *Geol. Soc. America Memoir* 193, 39–49.
 Bons, P.D., Koehn, D., Jessell, M.W., 2008. Lecture notes in earth sciences. In: Bons, P., Koehn, D., Jessell, M. (Eds.), *Microdynamic Simulation*. Springer, Berlin, p. 405. number 106.
 Bornert, M., Ponte Castañeda, P., 1998. Second-order estimates of the self-consistent type for viscoplastic polycrystals. *Proc. R Soc. Lond. A454*, 3035–3045.
 Bornert, M., Masson, R., Ponte Castañeda, P., Zaoui, A., 2001. Second-order estimates for the effective behaviour of viscoplastic polycrystalline materials. *J. Mech. Phys. Solids* 49, 2737–2764.
 Bouchez, J.L., Duval, P., 1982. The fabric of polycrystalline ice deformed in simple shear: experiments in torsion, natural deformation and geometrical interpretation. *Textures Microstruct.* 5, 171–190.
 Brenner, R., Béchade, J.L., Castelnau, O., Bacroix, B., 2002a. Thermal creep of Zr–Nb1%–O alloys: experimental analysis and micromechanical modelling. *J. Nucl. Mater.* 305, 175–186.
 Brenner, R., Masson, R., Castelnau, O., Zaoui, A., 2002b. A “quasi-elastic” affine formulation for the homogenized behaviour of nonlinear viscoelastic polycrystals and composites. *Eur. J. Mech. A/Solids* 21, 943–960.
 Brenner, R., Castelnau, O., Badea, L., 2004. Mechanical field fluctuations in polycrystals estimated by homogenization techniques. *Proc. R Soc. Lond. A460* (2052), 3589–3612.
 Brenner, R., Lebensohn, R.A., Castelnau, O., 2009. Elastic anisotropy and yield surface estimates. *Int. J. Solids Struct.* 46, 3018–3026.
 Brinckmann, S., Siegmund, T., Huang, Y., 2006. A dislocation density based strain gradient model. *Int. J. Plasticity* 22, 1784–1797.
 Budd, W., Jacka, T., 1989. A review of ice rheology for ice sheet modelling. *Cold Reg. Sci. Technol.* 16, 107–144.
 Buiron, D., Chappellaz, J., Stenni, B., Frezzotti, M., Baumgartner, M., Capron, E., Landais, A., Lemieux-Dudon, B., Masson-Delmotte, V., Montagnat, M., Parrenin, F., Schilt, A., 2011. TALDICE-1 age scale of the Talos Dome deep ice core, East Antarctica. *Clim. Past* 7, 1–16.
 Bunge, H.J., 1993. *Texture Analysis in Materials Science*, third ed. Cuvillier, Goettingen.
 Castelnau, O., Duval, P., 1994. Simulations of anisotropy and fabric development in polar ices. *Ann. Glaciol.* 20, 277–282.
 Castelnau, O., Duval, P., Lebensohn, R.A., Canova, G., 1996a. Viscoplastic modeling of texture development in polycrystalline ice with a self-consistent approach: comparison with bound estimates. *J. Geophys. Res.* 101 (6), 13,851–13,868.
 Castelnau, O., Thorsteinsson, T., Kipfstuhl, J., Duval, P., Canova, G.R., 1996b. Modelling fabric development along the GRIP ice core, central Greenland. *Ann. Glaciol.* 23, 194–201.
 Castelnau, O., Canova, G.R., Lebensohn, R.A., Duval, P., 1997. Modelling viscoplastic behavior of anisotropic polycrystalline ice with a self-consistent approach. *Acta Mater.* 45 (11), 4823–4834.

- Castelnaud, O., Shoji, H., Mangeney, A., Milsch, H., Duval, P., Miyamoto, A., Kawada, K., Watanabe, O., 1998. Anisotropic behavior of GRIP ices and flow in Central Greenland. *Earth Planetary Sci. Lett.* 154 (1–4), 307–322.
- Castelnaud, O., Brenner, R., Lebensohn, R.A., 2006. The effect of strain heterogeneity on the work-hardening of polycrystals predicted by mean-field approaches. *Acta Mater.* 54, 2745–2756.
- Castelnaud, O., Blackman, D.K., Lebensohn, R.A., Ponte-Castañeda, P., 2008a. Micro-mechanical modeling of the viscoplastic behavior of olivine. *J. Geophys. Res.* 113, B09202.
- Castelnaud, O., Duval, P., Montagnat, M., Brenner, R., 2008b. Elastoviscoplastic micromechanical modeling of the transient creep of ice. *J. Geophys. Res. Solid Earth* 113, B11203.
- Castelnaud, O., Blackman, D.K., Becker, T.W., 2009. Numerical simulations of texture development and associated rheological anisotropy in regions of complex mantle flow. *Geophys. Res. Lett.* 36, L12304.
- Castelnaud, O., Cordier, P., Lebensohn, R.A., Merkel, S., Raterron, P., 2010a. Micro-structures and rheology of the earth's upper mantle inferred from a multiscale approach. *Comptes Rendus Physique*. 11 (3–4), 304–315. Computational metallurgy and scale transitions.
- Castelnaud, O., Lebensohn, R.A., Ponte Castañeda, P., Blackman, D., 2010b. Earth Mantle Rheology Inferred from Homogenization Theories; ISTE. p. 55–70.
- Chaboche, J.L., 2008. A review of some plasticity and viscoplasticity constitutive theories. *Int. J. Plasticity* 24, 1642–1693.
- Chevvy, J., Montagnat, M., Duval, P., Fivel, M., Weiss, J., 2007. Dislocation patterning and deformation processes in ice single crystal deformed by torsion. In: *Proc 11th Int Conf Phys & Chem of Ice*, pp. 142–146.
- Chevvy, J., Fressengeas, C., Lebyodkin, M., Taupin, V., Bastie, P., Duval, P., 2010. Characterizing short-range vs. long-range spatial correlations in dislocation distributions. *Acta Mater.* 58 (5), 1837–1849.
- Chevvy, J., Louchet, F., Duval, P., Fivel, M., 2012. Creep behaviour of ice single crystals loaded in torsion explained by dislocation cross-slip. *Phil Mag. Lett.* 92 (6), 262–269.
- Cochard, J., Yonenaga, I., Gouttebroze, S., MHamdi, M., Zhang, Z.L., 2010. Constitutive modeling of intrinsic silicon monocrystals in easy glide. *J. Appl. Phys.* 107 (3), 033512–033519.
- Dafalias, Y.F., 2001. Orientation distribution function in non-affine rotations. *J. Mech. Phys. Solids* 49, 2493–2516.
- Dahl-Jensen, D., Gundestrup, N.S., 1987. Constitutive properties of ice at dye 3, Greenland. In: *The Physical Basis of Ice Sheet Modelling*. Vancouver Symposium, vol. 170. IAHS, pp. 31–43.
- Dansgaard, W., Johnsen, S.J., Clausen, H.B., Dahl-Jensen, D., Gundestrup, N.S., Hammer, C.U., Hvidberg, C.S., Steffensen, J.P., Sveinbjörnsdóttir, A.E., Jouzel, J., Bond, G., 1993. Evidence for general instability of past climate from a 250 kyr ice-core record. *Nature* 364, 218–220.
- De Botton, G., Ponte Castañeda, P., 1995. Variational estimates for the creep behaviour of polycrystals. *Proc. R Soc. Lond. A* 448, 121–142.
- de la Chapelle, S., Castelnaud, O., Lipenkov, V., Duval, P., 1998. Dynamic recrystallization and texture development in ice as revealed by the study of deep ice cores in Antarctica and Greenland. *J. Geophys. Res.* 103 (B3), 5091–5105.
- Durand, G., Graner, F., Weiss, J., 2004. Deformation of grain boundaries in polar ice. *EPL (Europhysics Letters)* 67 (6), 1038.
- Durand, G., Gillet-Chaulet, F., Svensson, A., Gagliardini, O., Kipfstuhl, S., Meyssonier, J., Parrenin, F., Duval, P., Dahl-Jensen, D., Azuma, N., 2007. Change of the ice rheology with climatic transitions. Implication on ice flow modelling and dating of the EPICA Dome C core. *Clim. Past* 3, 155–167.
- Durand, G., Persson, A., Samyn, D., Svensson, A., 2008. Relation between neighbouring grains in the upper part of the NorthGRIP ice core – Implications for rotation recrystallization. *Earth and Planet Sci. Lett.* 265, 666–671.
- Duval, P., 1976. Lois du fluage transitoire ou permanent de la glace polycristalline pour divers états de contraintes. *Ann. Geophys.* 32 (4), 335–350.
- Duval, P., 1978. Anelastic behaviour of polycrystalline ice. *J. Glaciol.* 21 (85), 621–628.
- Duval, P., 1981. Creep and fabrics of polycrystalline ice under shear and compression. *J. Glaciol.* 27 (95), 129–140.
- Duval, P., Castelnaud, O., 1995. Dynamic recrystallization of ice in polar ice sheets. *J. Physique IV (suppl. J. Phys. III)*, C3 5, 197–205.
- Duval, P., Le Gac, H., 1980. Does the permanent creep-rate of polycrystalline ice increase with crystal size? *J. Glaciology* 25, 151–157.
- Duval, P., Montagnat, M., 2002. Comment on "Superplastic deformation of ice: experimental observations" by D.L. Goldsby and D.L. Kohlstedt. *J. Geophys. Res.* 107 (2082), 1–4.
- Duval, P., Ashby, M., Anderman, I., 1983. Rate controlling processes in the creep of polycrystalline ice. *J. Phys. Chem.* 87 (21), 4066–4074.
- Duval, P., Arnaud, L., Brissaud, O., Montagnat, M., de La Chapelle, S., 2000. Deformation and recrystallization processes of ice from polar ice sheets. *Ann. Glaciol.* 30, 83–87.
- Duval, P., Montagnat, M., Grennerat, F., Weiss, J., Meyssonier, J., Philip, A., 2010. Creep and plasticity of glacier ice: a material science perspective. *J. Glaciology* 56 (200), 1059–1068.
- Eshelby, J., 1957. The determination of the elastic field of an ellipsoidal inclusion, and related problems. In: *Proc R Soc London Ser A*, vol. 241, pp. 376–396.
- Faria, S.H., 2001. Mixtures with continuous diversity: general theory and application to polymer solutions. *Continuum Mech. Therm.* 13 (2), 91–120.
- Faria, S.H., 2006a. Creep and recrystallization of large polycrystalline masses. I. General continuum theory. In: *Royal Society of London Proceedings Series A*, vol. 462 (2069), pp. 1493–1514.
- Faria, S.H., 2006b. Creep and recrystallization of large polycrystalline masses. III: continuum theory of ice sheets. In: *Royal Society of London Proceedings Series A*, vol. 462, pp. 2797–2816.
- Faria, S.H., 2008. The symmetry group of the CAFFE model. *J. Glaciol.* 54 (187), 643–645.
- Faria, S.H., Hutter, K., 2002. A systematic approach to the thermodynamics of single and mixed flowing media with microstructure. Part I: balance equations and jump conditions. *Continuum Mech. Thermodyn.* 14 (5), 459–481.
- Faria, S.H., Ktitarev, D., Hutter, K., 2002. Modelling evolution of anisotropy in fabric and texture of polar ice. *Ann. Glaciol.* 35, 545–551.
- Faria, S.H., Kremer, G.M., Hutter, K., 2003. On the inclusion of recrystallization processes in the modeling of induced anisotropy in ice sheets: a thermodynamicist's point of view. *Ann. Glaciol.* 37 (1), 29–34.
- Faria, S.H., Kremer, G.M., Hutter, K., 2006. Creep and recrystallization of large polycrystalline masses. II. Constitutive theory for crystalline media with transversely isotropic grains. In: *Royal Society of London Proceedings Series A*, vol. 462 (2070), pp. 1699–1720.
- Faria, S.H., Kipfstuhl, S., Azuma, N., Freitag, J., Hamann, I., Murshed, M.M., Kuhs, W.F., 2009. The multiscale structure of Antarctica. Part I: inland ice. *Low Temp. Sci.* 68, 39–59.
- Faria, S.H., Freitag, J., Kipfstuhl, S., 2010. Polar ice structure and the integrity of ice-core paleoclimate records. *Quat. Sci. Rev.* 29 (1), 338–351.
- Faria, S.H., Weikusat, I., Azuma, N., 2014. The microstructure of polar ice. *J. Struct. Geol.* 61, 2–20.
- Fressengeas, C., 2010. La mécanique des champs de dislocations. Hermès Sci.
- Gagliardini, O., Gillet-Chaulet, F., Montagnat, M., 2009. A review of anisotropic polar ice models: from crystal to ice-sheet flow models. In: *Hondoh, T. (Ed.), 2009. Physics of Ice Core Records II. Supplement Issue of Low Temperature Science*, vol. 68. Hokkaido University, pp. 149–166.
- Gammon, P., Kieffe, H., Clouter, M., 1983. Elastic constants of ice samples by Brillouin spectroscopy. *J. Phys. Chem.* 87, 4025–4029.
- Gao, H., Huang, Y., Nix, W.D., Hutchinson, J.W., 1999. Mechanism-based strain gradient plasticity – I. theory. *J. Mech. Phys. Solids* 47 (6), 1239–1263.
- Gillet, F., Durand, G., 2010. Ice-sheet advance in Antarctica. *Nature* 467, 794–795.
- Gillet-Chaulet, F., Gagliardini, O., Meyssonier, J., Montagnat, M., Castelnaud, O., 2005. A user-friendly anisotropic flow law for ice-sheet modelling. *J. Glaciol.* 41 (172), 3–14.
- Gillet-Chaulet, F., Gagliardini, O., Meyssonier, J., Zwinger, T., Ruokolainen, J., 2006. Flow-induced anisotropy in polar ice and related ice-sheet flow modelling. *J. Non-newtonian Fluid Mech.* 134, 33–43.
- Gillet-Chaulet, F., Hindmarsh, R.C.A., Corr, H.F.J., King, E.C., Jenkins, A., 2011. In-situ quantification of ice rheology and direct measurement of the Raymond effect at Summit, Greenland using a phase-sensitive radar. *Geophys. Res. Lett.* 38 (24).
- Gillet-Chaulet, F., Gagliardini, O., Seddik, H., Nodet, M., Durand, G., Ritz, C., Zwinger, T., Greve, R., Vaughan, D.G., 2012. Greenland ice sheet contribution to sea-level rise from a new-generation ice-sheet model. *The Cryosphere* 6 (6), 1561–1576.
- Gilormini, P., 1995. A critical evaluation for various non-linear extensions of the self-consistent model. In: *Pineau, A., Zaoui, A. (Eds.), IUTAM Symp. on Micromechanics of Plasticity and Damage of Multiphase Materials*. Kluwer Acad. Publ., Sèvres, France, pp. 67–74.
- Glen, J., 1955. The creep of polycrystalline ice. *Proc. R. Soc. London A* 228, 519–538.
- Gödert, G., 2003. A mesoscopic approach for modelling texture evolution of polar ice including recrystallization phenomena. *Ann. Glaciol.* 37, 23–28.
- Goldsby, D.L., Kohlstedt, D.L., 1997. Grain boundary sliding in fine-grained ice I. *Scripta Mat.* 37 (9), 1399–1406.
- Gow, A., 1969. On the rate of growth of grains and crystals in south polar firm. *J. Glaciol.* 8, 241–252.
- Grennerat, F., Montagnat, M., Castelnaud, O., Vacher, P., Moulinec, H., Suquet, P., Duval, P., 2012. Experimental characterization of the intragranular strain field in columnar ice during transient creep. *Acta Mater.* 60 (8), 3655–3666.
- Greve, R., Blatter, H., 2009. *Dynamics of Ice Sheets and Glaciers*. Springer, Berlin.
- Griera, A., Bons, P.D., Jessell, M.W., Lebensohn, R.A., Evans, L., Gomez-Rivas, E., 2011. Strain localization and porphyroblast rotation. *Geology* 39, 275–278.
- Griera, A., Llorens, M.G., Gomez-Rivas, E., Bons, P.D., Jessell, M.W., Evans, L.A., Lebensohn, R.A., 2013. Numerical modelling of porphyroblast and porphyroblast rotation in anisotropic rocks. *Tectonophysics* 587, 4–29.
- Guillopé, M., Poirier, J., 1979. Dynamic recrystallization during creep of single-crystalline halite: an experimental study. *J. Geophys. Res.* 84, 5557–5567.
- Gundestrup, N., Hansen, B.L., 1984. Bore-hole survey at Dye 3, south Greenland. *J. Glaciology* 30, 282–288.
- Hamman, I., Weikusat, C., Azuma, N., Kipfstuhl, S., 2007. Evolution of crystal microstructure during creep experiments. *J. Glaciol.* 53 (182), 479–489.
- Hershey, A.V., 1954. The elasticity of an isotropic aggregate of anisotropic cubic crystals. *J. Appl. Mech.* 21, 236–240.
- Higashi, A., Koizumi, S., Mae, S., 1965. Bending creep of ice single crystals. *Jpn. J. Appl. Phys.* 4, 575–582.
- Hooke, R.L., 2005. *Principles of Glacier Mechanics*, second ed. Cambridge University Press, Cambridge.
- Humphreys, F.J., Hatherly, M., 2004. *Recrystallization and Related Annealing Phenomena*, second ed. Pergamon, Oxford.
- Hutchinson, J., 1977. Creep and plasticity of hexagonal polycrystals as related to single crystal slip. *Metall. Trans.* 8A (9), 1465–1469.
- Idiart, M.I., Moulinec, H., Ponte Castañeda, P., Suquet, P., 2006. Macroscopic behavior and field fluctuations in viscoplastic composites: second-order estimates versus full-field simulations. *J. Mech. Phys. Solids* 54 (5), 1029–1063.

- Jacka, T., 1994. Investigations of discrepancies between laboratory studies on the flow of ice: density, sample shape and size and grain size. *Ann. Glaciol.* 19, 146–154.
- Jacka, T.H., Li, J., 1994. The steady-state crystal size of deforming ice. *Ann. Glaciol.* 20, 13–18.
- Jacka, T.H., Maccagnan, M., 1984. Ice crystallographic and strain rate changes with strain in compression and extension. *Cold Reg. Sci. Technol.* 8, 269–286.
- Jessell, M.W., 1988a. Simulation of fabric development in recrystallizing aggregates. 1. Description of the models. *J. Struct. Geol.* 10, 771–778.
- Jessell, M.W., 1988b. Simulation of fabric development in recrystallizing aggregates. 2. Example model runs. *J. Struct. Geol.* 10, 779–793.
- Jessell, M.W., Bons, P.D., 2002. The numerical simulation of microstructure. In: *Geol Soc. London, Spec Publ.*, vol. 200, pp. 137–147.
- Jessell, M.W., Bons, P.D., Evans, L., Barr, T., Stüwe, K., 2001. Elle: the numerical simulation of metamorphic and deformation microstructures. *Comput. Geosciences* 27, 17–30.
- Jessell, M.W., Siebert, E., Bons, P.D., Evans, L., Piazzolo, S., 2005. A new type of numerical experiment on the spatial and temporal patterns of localization of deformation in a material with a coupling of grain size and rheology. *Earth Planetary Sci. Lett.* 239, 309–326.
- Jessell, M.W., Bons, P.D., Griera, A., Evans, L.A., Wilson, C.J.L., 2009. A tale of two viscosities. *J. Struct. Geol.* 31, 719–736.
- Jones, S., Glen, J., 1969. The mechanical properties of single crystals of pure ice. *J. Glaciol.* 8 (54), 463–473.
- Kanit, T., Forest, S., Galliet, I., Mounoury, V., Jeulin, D., 2003. Determination of the size of the representative volume element for random composites: statistical and numerical approach. *Int. J. Solids Struct.* 40, 3647–3679.
- Ketcham, W.M., Hobbs, P.V., 1969. An experimental determination of the surface energies of ice. *Phil. Mag.* 19, 1161–1173.
- Kipfstuhl, S., Hamann, I., Lambrecht, A., Freitag, J., Faria, S.H., Grigoriev, D., Azuma, N., 2006. Microstructure mapping: a new method for imaging deformation induced microstructural features of ice on the grain scale. *J. Glaciol.* 52 (178), 398–406.
- Kipfstuhl, S., Faria, S.H., Azuma, N., Freitag, J., Hamann, I., Kaufmann, P., Miller, H., Weiler, K., Wilhelms, F., 2009. Evidence of dynamic recrystallization in polar firn. *J. Geophys. Res.* 114, B05204.
- Kreher, W., 1990. Residual stresses and stored elastic energy of composites and polycrystals. *J. Mech. Phys. Solids* 38, 115–128.
- Kröner, E., 1958. Berechnung der elastischen Konstanten des Vielkristalls aus den Konstanten des Einkristalls. *Z. Phys.* 151, 504–518.
- Kröner, E., 1978. Self-consistent scheme and graded disorder in polycrystal elasticity. *J. Phys. F: Metal Phys.* 8, 2261–2267.
- Kitayev, D., Gödert, G., Hutter, K., 2002. Cellular automaton model for recrystallization, fabric, and texture development in polar ice. *J. Geophys. Res. (Solid Earth)* 107 (B8).
- Lahellec, N., Suquet, P., 2006. Effective behavior of linear viscoelastic composites: a time-integration approach. *Int. J. Solids Struct.* 44, 507–529.
- Lahellec, N., Suquet, P., 2007. On the effective behavior of nonlinear inelastic composites: I. Incremental variational principles. *J. Mech. Phys. Solids* 55, 1932–1963.
- Lahellec, N., Michel, J., Moulinec, H., Suquet, P., 2003. Analysis of inhomogeneous materials at large strains using fast fourier transforms. In: *Miehe, C. (Ed.), IUTAM Symposium on Computational Mechanics of Solid Materials at Large Strains.* Kluwer Ac. Pub., Dordrecht, pp. 247–258.
- Laws, N., 1973. Thermoelasticity of composite materials. *J. Mech. Phys. Solids* 21 (9).
- Laws, N., McLaughlin, R., 1978. Self-consistent estimates for the viscoelastic creep compliances of composite materials. *Proc. R Soc. Lond. A353*, 251–273.
- Lebensohn, R.A., 2001. N-site modeling of a 3D viscoplastic polycrystal using fast fourier transform. *Acta Mater.* 49 (14), 2723–2737.
- Lebensohn, R.A., Tomé, C.N., 1993. A self-consistent viscoplastic model: prediction of rolling textures of anisotropic polycrystals. *Mat. Sci. Engin. A* 175, 71–82.
- Lebensohn, R.A., Liu, Y., Ponte-Castañeda, P., 2004a. Macroscopic properties and field fluctuations in model power-law polycrystals: full-field solutions versus self-consistent estimates. In: *Proc Royal Soc Lond A*, vol. 460 (2045), pp. 1381–1405.
- Lebensohn, R.A., Liu, Y., Ponte-Castañeda, P., 2004b. On the accuracy of the self-consistent approximation for polycrystals: comparison with full-field numerical simulations. *Acta Mater.* 52 (18), 5347–5361.
- Lebensohn, R.A., Castelnau, O., Brenner, R., Gilormini, P., 2005. Study of the anti-plane deformation of linear 2-D polycrystals with different microstructures. *Int. J. Solids Struct.* 42 (20), 5441–5459.
- Lebensohn, R.A., Tomé, C.N., Ponte-Castañeda, P., 2007. Self-consistent modelling of the mechanical behaviour of viscoplastic polycrystals incorporating intragranular field fluctuations. *Phil. Mag.* 87 (28), 4287–4322.
- Lebensohn, R.A., Brenner, R., Castelnau, O., Rollett, A.D., 2008. Orientation image-based micromechanical modelling of subgrain texture evolution in polycrystalline copper. *Acta Mater.* 56 (15), 3914–3926.
- Lebensohn, R.A., Montagnat, M., Mansuy, P., Duval, P., Meyssonier, J., Philip, A., 2009. Modeling viscoplastic behavior and heterogeneous intracrystalline deformation of columnar ice polycrystals. *Acta Mater.* 57 (5), 1405–1415.
- Lebensohn, R.A., Kanjarla, A.K., Eisenlohr, P., 2012. An elasto-viscoplastic formulation based on fast Fourier transforms for the prediction of micromechanical fields in polycrystalline materials. *Int. J. Plasticity* 32, 59–69. $\hat{\alpha}^{33}(0)$.
- Letouzé, N., Brenner, R., Castelnau, O., Béchade, J.L., Mathon, M.H., 2002. Residual strain distribution in Zircaloy-4 measured by neutron diffraction and estimated by homogenization techniques. *Scripta Mat.* 47, 595–599.
- Lipenkov, V.Y., Barkov, N.I., Duval, P., Pimienta, P., 1989. Crystalline texture of the 2083m ice core at Vostok Station, Antarctica. *J. Glaciol.* 35 (121), 392–398.
- Lipenkov, V.Y., Salamatin, A.N., Duval, P., 1997. Bubbly-ice densification in ice sheets: II. Applications. *J. Glaciol.* 43 (145), 397–407.
- Liu, Y., Ponte Castañeda, P., 2004. Second-order theory for the effective behavior and field fluctuations in viscoplastic polycrystals. *J. Mechanics Phys. Solids* 52 (2), 467–495.
- Liu, Y., Gilormini, P., Ponte Castañeda, P., 2003. Variational self-consistent estimates for texture evolution in viscoplastic polycrystals. *Acta Mater.* 51, 5425–5437.
- Liboutry, L., Duval, P., 1985. Various isotropic and anisotropic ices found in glacier and polar ice caps and their corresponding rheologies. *Ann. Geophys.* 3 (2), 207–224.
- Llorens, M.G., Bons, P.D., Griera, A., Gomez-Rivas, E., Evans, L.A., 2012. Single layer folding in simple shear. *J. Struct. Geol.* (0):–.
- Logé, R., Bernacki, M., Resk, H., Delannay, L., Dignonnet, H., Chastel, Y., Coupez, T., 2008. Linking plastic deformation to recrystallization in metals using digital microstructures. *Phil. Mag.* 88, 3691–3712.
- Long, M., Becker, T., 2010. Mantle dynamics and seismic anisotropy. *Earth Planetary Sci. Lett.* 297, 341–354.
- Ma, Y., Gagliardini, O., Ritz, C., Gillet-Chaulet, F., Durand, G., Montagnat, M., 2010. Enhancement factors for grounded ice and ice shelves inferred from an anisotropic ice-flow model. *J. Glaciol.* 56 (199), 805–812.
- Mandel, J., 1966. *Mécanique des milieux continus.* Gauthier-Villars, Paris, France.
- Mangeney, A., Califano, F., Castelnau, O., 1996. Isothermal flow of an anisotropic ice sheet in the vicinity of an ice divide. *J. Geophys. Res.* 101 (12), 28,189–28,204.
- Mangeney, A., Califano, F., Hutter, K., 1997. A numerical study of anisotropic, low Reynolds number, free surface flow of ice sheet modeling. *J. Geophys. Res.* 102 (B10), 22,749–22,764.
- Mansuy, P., Philip, A., Meyssonier, J., 2000. Identification of strain heterogeneities arising during deformation of ice. *Ann. Glaciol.* 30, 121–126.
- Mansuy, P., Meyssonier, J., Philip, A., 2002. Localization of deformation in polycrystalline ice: experiments and numerical simulations with a simple grain model. *Comput. Mater. Sci.* 25 (1–2), 142–150.
- Martin, C., Gudmundsson, G.H., Pritchard, H.D., Gagliardini, O., 2009. On the effects of anisotropic rheology on ice flow, internal structure, and the age-depth relationship at ice divides. *J. Geophys. Res.* 114, F04001.
- Masson, R., Zaoui, A., 1999. Self-consistent estimates for the rate-dependent elastoplastic behaviour of polycrystalline materials. *J. Mech. Phys. Solids* 47, 1543–1568.
- Masson, R., Bornert, M., Suquet, P., Zaoui, A., 2000. An affine formulation for the prediction of the effective properties of nonlinear composites and polycrystals. *J. Mechanics Phys. Solids* 48 (6–7), 1203–1227.
- Mathiesen, J., Ferkinghoff-Borg, J., Jensen, M., Levinsen, M., Olesen, P., Dahl-Jensen, D., Svensson, A., 2004. Dynamics of crystal formation in the Greenland NorthGRIP ice cores. *J. Glaciol.* 50, 325–328.
- Mellor, M., Testa, R., 1969. Creep of ice under low stress. *J. Glaciol.* 8, 147–152.
- Michel, J.C., Moulinec, H., Suquet, P., 1999. Effective properties of composite materials with periodic microstructure: a computational approach. *Comp. Meth. Appl. Mech. Eng.* 172, 109–143.
- Michel, J.C., Moulinec, H., Suquet, P., 2000. A computational method based on augmented lagrangians and fast Fourier transforms for composites with high contrast. *Comput. Model. Eng. Sci.* 1, 79–88.
- Michel, J.C., Moulinec, H., Suquet, P., 2001. A computational scheme for linear and non-linear composites with arbitrary phase contrast. *Int. J. Numer. Methods Eng.* 52 (1–2).
- Miguel, M.C., Vespignani, A., Zapperi, S., Weiss, J., Grasso, J.R., 2001. Intermittent dislocation flow in viscoplastic deformation. *Nature* 410, 667–671.
- Miyamoto, A., 1999. *Mechanical Properties and Crystal Textures of Greenland Deep Ice Cores.* Hokkaido University, Sapporo. Ph.D. thesis.
- Molinari, A., Canova, G., Ahzi, S., 1987. A self-consistent approach of the large deformation polycrystal viscoplasticity. *Acta Metal.* 35, 2983–2994.
- Montagnat, M., Duval, P., 2000. Rate controlling processes in the creep of polar ice, influence of grain boundary migration associated with recrystallization. *Earth Planet Sci. Lett.* 183, 179–186.
- Montagnat, M., Weiss, J., Chevy, J., Duval, P., Brunjail, H., Bastie, P., Gil Sevillano, J., 2006. The heterogeneous nature of slip in ice single crystals deformed under torsion. *Phil. Mag.* 86 (27), 4259–4270.
- Montagnat, M., Durand, G., Duval, P., 2009. Recrystallization processes in granular ice. *Suppl. Issue Low Temp. Sci.* 68, 81–90.
- Montagnat, M., Blackford, J.R., Piazzolo, S., Arnaud, L., Lebensohn, R.A., 2011. Measurements and full-field predictions of deformation heterogeneities in ice. *Earth Planetary Sci. Lett.* 305 (1–2), 153–160.
- Montagnat, M., Buiron, D., Arnaud, L., Broquet, A., Schlitz, P., Jacob, R., Kipfstuhl, S., 2012. Measurements and numerical simulation of fabric evolution along the Talos Dome ice core, Antarctica. *Earth Planetary Sci. Lett.* 357–358 (0), 168–178.
- Morgan, V., 1991. High-temperature ice creep tests. *Cold Reg. Sci. Tech.* 19, 295–300.
- Moulinec, H., Suquet, P., 1998. A numerical method for computing the overall response of nonlinear composites with complex microstructure. *Comp. Meth. Appl. Mech. Eng.* 157 (1–2), 69–94.
- Nebozhyn, M., Gilormini, P., Ponte Castañeda, P., 2001. Variational self-consistent estimates for cubic viscoplastic polycrystals: the effects of grain anisotropy and shape. *J. Mech. Phys. Solids* 49, 313–340.

- Nye, J., 1953. Some geometrical relations in dislocated crystals. *Acta Mater.* 1, 153–162.
- Pantleon, W., 2008. Resolving the geometrically necessary dislocation content by conventional electron backscattering diffraction. *Scripta Mater.* 58 (11), 994–997.
- Paterson, W.S.B., 1994. *The Physics of Glaciers*. Pergamon, Oxford.
- Pettit, E.C., Thorsteinsson, T., Jacobson, P., Waddington, E.D., 2007. The role of crystal fabric in flow near an ice divide. *J. Glaciol.* 53 (181), 277–288.
- Pettit, E.C., Waddington, E.D., Harrison, W.D., Thorsteinsson, T., Elsberg, D., Morack, J., Zumberge, M.A., 2011. The crossover stress, anisotropy and the ice flow law at Siple Dome, West Antarctica. *J. Glaciol.* 57 (201), 39–52.
- Piazolo, S., Bons, P.D., Jessell, M.W., Evans, L., Passchier, C.W., 2002. Dominance of microstructural processes and their effect on microstructural development: insights from numerical modelling of dynamic recrystallization. In: *Geol Soc, London, Spec Publ.* vol. 200, pp. 149–170.
- Piazolo, S., Jessell, M.W., Bons, P.D., Evans, L., Becker, J.K., 2010. Numerical simulations of microstructures using the Elle platform: a modern research and teaching tool. *J. Geol. Soc. India* 75, 110–127.
- Piazolo, S., Borthwick, V., Griaera, A., Montagnat, M., Jessell, M.W., Lebensohn, R.A., Evans, L., 2012. Substructure dynamics in crystalline materials: new insight from in situ experiments, detailed EBSD analysis of experimental and natural samples and numerical modelling. *Mater. Sci. Forum* 715–716, 502–507.
- Pimentia, P., Duval, P., Lipenkov, V.Y., 1987. Mechanical behaviour of anisotropic polar ice. In: *International Association of Hydrological Sciences, Publication* 170. *Symposium on The Physical Basis of Ice Sheet Modelling*, pp. 57–66. Vancouver.
- Placidi, L., 2004. Thermodynamically Consistent Formulation of Induced Anisotropy in Polar Ice Accounting for Grain Rotation, Grain-size Evolution and Recrystallization. Ph.D. thesis. Darmstadt University of Technology, Darmstadt. Available at: <http://elib.tu-darmstadt.de/diss/000614/>.
- Placidi, L., 2005. *Microstructured Continua Treated by the Theory of Mixtures*. University of Rome, La Sapienza; Rome. Ph.D. thesis.
- Placidi, L., Hutter, K., 2005. An anisotropic flow law for incompressible polycrystalline materials. *Z. für Angew. Mathematik Physik (ZAMP)* 57, 160–181. <http://dx.doi.org/10.1007/s00033-005-0008-7>.
- Placidi, L., Hutter, K., 2006. Thermodynamics of polycrystalline materials treated by the theory of mixtures with continuous diversity. *Continuum Mech. Thermodyn.* 17 (6), 409–451.
- Placidi, L., Faria, S.H., Hutter, K., 2004. On the role of grain growth, recrystallization, and polygonization in a continuum theory for anisotropic ice sheets. *Ann. Glaciol.* 39, 49–52.
- Placidi, L., Greve, R., Seddik, H., Faria, S.H., 2010. Continuum-mechanical, anisotropic flow model, based on an anisotropic flow enhancement factor (CAFFE). *Continuum Mech. Thermodyn.* 22 (3), 221–237.
- Ponte Castañeda, P., 1991. The effective mechanical properties of nonlinear isotropic composites. *J. Mech. Phys. Solids* 39, 45–71.
- Ponte Castañeda, P., 1996. Exact second-order estimates for the effective mechanical properties of nonlinear composite materials. *J. Mech. Phys. Solids* 44, 827–862.
- Ponte Castañeda, P., 2002. Second-order homogenization estimates for nonlinear composites incorporating field fluctuations. I – Theory. *J. Mech. Phys. Solids* 50, 737–757.
- Ponte-Castañeda, P., Suquet, P., 1998. Nonlinear composites. *Adv. Appl. Mech.* 34, 171–302.
- Raabe, D., Becker, R.C., 2000. Coupling of a crystal plasticity finite-element model with a probabilistic cellular automaton for simulating primary static recrystallization in aluminium. *Model. Simul. Mater. Sci. Eng.* 8 (4), 445.
- Raabe, D., Roters, F., 2004. Using texture components in crystal plasticity finite element simulations. *Int. J. Plasticity* 20, 339–361.
- Ricaud, J.M., Masson, R., 2009. Effective properties of linear viscoelastic heterogeneous media: Internal variables formulation and extension to ageing behaviours. *Int. J. Solids Struct.* 46, 1599–1606.
- Roessiger, J., Bons, P.D., Griaera, A., Jessell, M.W., Evans, L., Montagnat, M., Kipfstuhl, S., Faria, S.H., Weikusat, I., 2011. Competition between grain growth and grain size reduction in polar ice. *J. Glaciol.* 57, 942–948.
- Rolland du Roscoat, S., King, A., Philip, A., Reischig, P., Ludwig, W., Flin, F., Meyssonier, J., 2011. Analysis of snow microstructure by means of X-ray diffraction contrast tomography. *Adv. Engineering Mater.* 13, 128–135.
- Russell-Head, D.S., Wilson, C.J.L., 2001. Automated fabric analyser system for quartz and ice. *J. Glaciol.* 24 (90), 117–130.
- Sanchez-Hubert, J., Sanchez-Palencia, E., 1978. Sur certains problèmes physiques d'homogénéisation donnant lieu à des phénomènes de relaxation. *Comptes Rendus Acad. Sc Paris A286*, 903–906.
- Sauter, F., Leclercq, S., 2003. Modeling of the non-monotonous viscoplastic behavior of uranium dioxide. *J. Nucl. Mater.* 322, 1–14.
- Schmatz, J., 2010. Grain Boundary – Fluid Inclusion Interaction in Rocks and Analogues. RWTH-Aachen, Germany. Ph.D. thesis.
- Schulson, E.M., Duval, P., 2009. *Creep and Fracture of Ice*. Cambridge University Press.
- Seddik, H., Greeve, R., Placidi, L., Hamann, I., Gagliardini, O., 2008. Application of a continuum-mechanical model for the flow of anisotropic polar ice to the EDML core, Antarctica. *J. Glaciol.* 54 (187), 631–642.
- Seddik, H., Greve, R., Zwinger, T., Placidi, L., 2011. A full Stokes ice flow model for the vicinity of Dome Fuji, Antarctica, with induced anisotropy and fabric evolution. *The Cryosphere* 5 (2), 495–508.
- Seddik, H., Greve, R., Zwinger, T., Gillet-Chaulet, F., Gagliardini, O., 2012. Simulations of the Greenland ice sheet 100 years into the future with the full Stokes model Elmer/Ice. *J. Glaciol.* 58 (209), 427–440.
- Solas, D., Gerber, P., Baudin, T., Penelle, R., 2004. Monte Carlo method for simulating grain growth in 3D. influence of lattice site arrangements. *Mater. Sci. Forum* 467–470, 1117–1122.
- Sotin, C., Tobie, G.J.W., 2009. *Europa after Galileo*. The University of Arizona Press, Tucson, AZ, p. 85–118.
- Suquet, P., 1987. In: Sanchez-Palencia, E., Zaoui, A. (Eds.), *Homogenization Techniques for Composite Media*. Lecture Notes in Physics, vol. 272. Springer, Berlin/Heidelberg, pp. 193–198.
- Suquet, P., Moulinec, H., Castelnau, O., Montagnat, M., Lahelec, N., Grennerat, F., Duval, P., Gerber, P., Baudin, T., Penelle, R., 2011. Multi-scale modeling of the mechanical behavior of polycrystalline ice under transient creep. *Proceida IUTAM* (in press).
- Taupin, V., Varadhan, S., Chevy, J., Fressengeas, C., Beaudoin, A.J., Montagnat, M., Duval, P., 2007. Effects of size on the dynamics of dislocations in ice single crystals. *Phys. Rev. Lett.* 99 (15), 155507.
- Taupin, V., Richeton, T., Chevy, J., Fressengeas, C., Weiss, J., Louchet, F., Miguel, M., 2008. Rearrangement of dislocation structures in the aging of ice single crystals. *Acta Mater.* 56 (7), 1555–1563.
- Taylor, G., 1938. Plastic strain in metals. *J. Inst. Met.* 62, 307–324.
- Thorsteinsson, T., 2002. Fabric development with nearest-neighbor interaction and dynamic recrystallization. *J. Geophys. Res.* 107 (B1).
- Thorsteinsson, T., Kipfstuhl, J., Miller, H., 1997. Textures and fabrics in the GRIP ice core. *J. Geophys. Res.* 102 (C12), 26,583–26,600.
- Tommasi, A., Knoll, M., Vauchez, A., Signorelli, J., Thoraval, C., Logé, R., 2009. Structural reactivation in plate tectonics controlled by olivine crystal anisotropy. *Nat. Geosci.* 2 (6), 423–427.
- Urai, J., Means, W., Lister, G., 1986. Dynamic recrystallization of minerals. In: Hobbs, B.E., Heard, H.C. (Eds.), *Mineral and Rock Deformation: Laboratory Studies*. Geophysical Monograph, pp. 161–200.
- Vacher, P., Dumoulin, S., Morestin, F., Mguil-Touchal, S., 1999. Bidimensional strain measurement using digital images. In: *Proceedings of the Institution of Mechanical Engineers, Part C: Journal of Mechanical Engineering Science*, vol. 213 (8), pp. 811–817.
- Van der Veen, C.J., Whillans, I.M., 1990. Flow law for glacier ice: comparison of numerical predictions and field measurements. *J. Glaciol.* 36, 324–339.
- Van der Veen, C.J., Whillans, I.M., 1994. Development of fabric in ice. *Cold Reg. Sci. Technol.* 22 (2), 171–195.
- Varadhan, S., Beaudoin, A., Fressengeas, C., 2006. Coupling the dynamic of statistically distributed and excess dislocations. *Proc. Sci.* vol. 004, 1–11. SMPRI2005.
- Verdier, M., Fivel, M., Groma, I., 1998. Mesoscopic scale simulation of dislocation dynamics in fcc metals: principles and applications. *Model. Simul. Mat. Sci. Eng.* 6, 755–770.
- Vu, Q.H., Brenner, R., Castelnau, O., Moulinec, H., Suquet, P., 2012. A self-consistent estimate for linear viscoelastic polycrystals with internal variables inferred from the collocation method. *Model. Simul. Mater. Sci. Eng.* 20 (2), 024003.
- Weertman, J., 1973. Creep of ice. In: Whalley, E., Jones, S., Gold, L. (Eds.), *Physics and Chemistry of Ice*. Roy. Soc. Canada, Ottawa, pp. 320–337.
- Weikusat, I., Kipfstuhl, S., Faria, S.H., Azuma, N., Miyamoto, A., 2009. Subgrain boundaries and related microstructural features in EDML (Antarctica) deep ice cores. *J. Glaciol.* 55 (191), 461–472.
- Weiss, J., Grasso, J.R., 1997. Acoustic emission in single crystals of ice. *J. Phys. Chem. B* 101 (32), 6113–6117.
- Weiss, J., Marsan, D., 2003. Three-dimensional mapping of dislocation avalanches: clustering and space/time coupling. *Science* 299 (5603), 89–92.
- Weiss, J., Miguel, M.C., 2004. Dislocation avalanche correlations. *Mater. Sci. Eng. A* 387–389, 292–296, 13th International Conference on the Strength of Materials.
- Weiss, J., Montagnat, M., 2007. Long-range spatial correlations and scaling in dislocation and slip patterns. *Phil. Magazine* 87 (8–9), 1161–1174.
- Weiss, J., Grasso, J.R., Miguel, M.C., Vespignani, A., Zapperi, S., 2001. Complexity in dislocation dynamics: experiments. *Mater. Sci. Eng. A* 309–310 (0), 360–364. *Dislocations 2000: An International Conference on the Fundamentals of Plastic Deformation*.
- Wenk, H.R., Canova, G., Bréchet, Y., Flandin, L., 1997. A deformation-based model for recrystallization of anisotropic materials. *Acta Mater.* 45 (8), 3283–3296.
- Willis, J.R., 1981. Variational and related methods for the overall properties of composites. *Adv. Appl. Mech.* 21, 2–78.
- Wilson, C., Zhang, Y., 1994. Comparison between experiment and computer modeling of plane strain simple shear ice deformation. *J. Glaciol.* 40 (134), 46–55.
- Wilson, C., Burg, J., Mitchell, J., 1986. The origin of kinks in polycrystalline ice. *Tectonophysics* 127, 27–48.
- Zhang, Y., Jenkins, J.T., 1993. The evolution of the anisotropy of a polycrystalline aggregate. *J. Mech. Phys. Solids* 41, 1213–1243.